THE UNIVERSITY OF CHICAGO

ROLE OF THE UNFOLDED PROTEIN RESPONSE IN TYPE I CALR-MUTANT MYELOPROLIFERATIVE NEOPLASMS

A DISSERTATION SUBMITTED TO

THE FACULTY OF THE DIVISION OF THE BIOLOGICAL SCIENCES

AND THE PRITZKER SCHOOL OF MEDICINE

IN CANDIDACY FOR THE DEGREE OF

DOCTOR OF PHILOSOPHY

COMMITTEE ON CANCER BIOLOGY

BY

JUAN M. IBARRA

CHICAGO, ILLINOIS

JUNE 2023

DEDICATION

To my mother, Otilia Hernández-Muñoz, you have taught me more in life with actions than you could ever do with words – no prize will ever compensate you braving the untamed waters of the Rio Bravo border as a young, anguished mother back in 1976.

In your name, having endured cervical cancer, I dedicate every bit of my intellect, hard work, and discipline to you. Witnessing your strength, courage, humility, and compassion towards others has been my greatest lesson.

For our sacrifices.

……

A mi madre, Otilia Hernández-Muñoz, quien me a enseñado más en la vida con acciones, que con lo que pudiese en palabras – ningún galardón compensara el que allá desafiado las aguas salvajes del Río Bravo, en la frontera, siendo una madre joven angustiada en el año de 1976.

En su nombre, después de haber lidiado con cáncer cervicouterino, le dedico todo mi intelecto, arduo trabajo, y disciplina. Ser testigo de su fuerza, coraje, humildad, y compasión hacia los demás ha sido mi mayor lección.

Por nuestros sacrificios.

TABLE OF CONTENTS

LIST OF FIGURES

LIST OF TABLES

LIST OF ABBREVIATIONS

AML	Acute myeloid leukemia
ASCT	Autologous stem cell transplant
BCL2	B-cell lymphoma 2
BM	Bone marrow
BMF	Bone marrow fibrosis
BMT	Bone marrow transplant
bZIP	Basic leucine zipper
CALR	Calreticulin
CBC	Complete blood count
CEL	Chronic eosinophilic leukemia
CLP	Common lymphoid progenitor
CML	Chronic myeloid leukemia
CMP	Common myeloid progenitor
CNL	Chronic neutrophilic leukemia
DAPI	4′,6-diamidino-2-phenylindole
DMSO	Dimethyl sulfoxide
ECM	Extracellular matrix
ELISA	Enzyme-linked immunosorbent assay
EPO	Erythropoietin
ER	Endoplasmic reticulum
ERAD	ER-associated degradation
ERN1	Endoplasmic reticulum to nucleus signaling 1

ET	Essential thrombocythemia
EtBr	Ethidium bromide
GFP	Green fluorescent protein
GM-CSF	Granulocyte-macrophage colony-stimulating factor
GRP78	Glucose-regulated protein 78
H&E	Hematoxylin and eosin
HCT	Hematocrit
HD	Healthy donor
HM	Hematological malignancy
HSC	Hematopoietic stem cell
HSPA5	Heat shock 70 protein 5
HU	Hydroxyurea
IHC	Immunohistochemistry
IL-3	Interleukin 3
IP3R	Inositol 1,4,5-trisphosphate receptor
IRE1α	Inositol-requiring enzyme 1 alpha
KIRA8	Kinase inhibiting RNase attenuator 8
LB	Luria broth
MDS	Myelodysplastic syndrome
MF	Myelofibrosis
MOMP	Mitochondrial outer membrane permeabilization
MPNs	Myeloproliferative neoplasms
MPN-U	Myeloproliferative neoplasm unclassifiable

NT	Nucleotide
PBMC	Peripheral blood mononuclear cell
PERK	Protein kinase R-like ER kinase
PLT	Platelet
PV	Polycythemia vera
qPCR	Quantitative polymerase chain reaction
RIDD	IRE1α-dependent decay
SCF	Stem cell factor
SD	Standard deviation
SERCA	Sarcoendoplasmic reticular Ca2+ ATPases
shRNA	Short hairpin ribonucleic acid
SOCE	Store-operated Ca2+ entry
STIM1	Stromal interaction molecule 1
STR	Short tandem repeat
TBST	Tris buffered saline buffer + tween 20
TPO	Thrombopoietin
tRNA	Transfer ribonucleic acid
TSEN	tRNA splicing endonuclease
UPR	Unfolded protein response
WBC	White blood cell
WHO	World health organization
XBP1	X-box binding protein 1
2-APB	2-Aminoethoxydiphenyl borate

ACKNOWLEDGMENTS

I would like to express my gratitude to my advisors Dr. Shannon Elf and Dr. Scott Oakes. You both have been a source of scientific training, teaching, and opportunities to grow as scientist and researcher – I am very thankful for your time and effort. To my thesis committee, Dr. Marsha Rosner, Dr. Lucy Godley, and Dr. David Pincus, your guidance has been vital to advance my research and scientific maturity. I also appreciate the times you all have offered me support and encouragement. Dr. Lucy Godley, I am further grateful for your support and dedication to my growth, and for constantly emphasizing the patients, and the clinical considerations of my research.

To Yassmin Elbanna, who has shared this treasurable journey with me. I am grateful for having worked and learned next to you. Witnessing your transformation from mentee to a mentor to me has been an enjoyable experience. I seek to continue learning from your tenancy, creativity, cleverness, and the warm spirit you bring to life and science, I am happy to call you a esteemed friend. To all former and current lab members who have enriched my training and contributed to this work – for your sacrifices, talent, and constant investment – particularly, Kasia Kurylowicz, Diane Silva, Harrison Greenbaum, Deborah Rodriguez, and Dr. Michele Cibbodo. To all my funding sources, the CCB program, and Dr. Kay Macleod for giving the opportunity to join the program despite of my 2.9 undergraduate GPA, thank you.

To those who have also expanded my graduate experience – Dr. Victoria Prince, your profound dedication to the needs of students, and your placement of Equity and Inclusion at the front and center of graduate education deserves to be recognized. I appreciate learning from your measured maneuvering and intentional vision while serving in the BDC. To Dr. Eileen Dolan, your continued support does not go unnoticed. Throughout our extended work together you have allowed me to absorb much from your selfless leadership and good karma – I seek to carry this

into my future work. To Dr. Basia Galinski, for serving as mentor for my DEIship, I thank you for your commitment to my professional development. Dr. Megan Mekinda, Dr. Sonia Hernández, Dr. Raquel Castellanos, and Ms. Dustielyn Savage, this gratitude also extends to you.

To the UC-SACNAS chapter, thank you for your exemplary leadership and hard work, you are a source of inspiration and a reflection of the times ahead – Angel Salazar, Anna Martinez, Keishla Colón Montañez, Diana Acuña, Margot Bolaños, and Belle Lomeli.

To my BSD friends – Jorden Lane, Joash Lake, Isaac Magallanes, Armun Liaghat, Kirsten Webster, Julian Bertini, Indya Weathers, and particularly Bridget Chak, thank you all for your company – being there for each other has made grad school much bearable. Briana Banks, my close companion, I cherish all this time we have journey and grown together. To my friends across other divisions – Emmanuel, Clarke, Mauro, Jose, Olga, Judit, Alex, Joseph, and those outside, Mitchell, Stevie, Chris, Gabriel, Uriel, and Ali, thank you for the brightness you have brought to my days. To my dearest friends Ximena, Karen, Nana, and Kim, thank you for the sustenance you have offered me throughout all the stages of my career that have led me to where I am at today.

Elena Cortés and Victor Mendoza – in the name of the low-income and disadvantaged Latino students who deserved opportunity, but opportunity never served them – thank you for being a source of comfort and encouragement in navigating this path. Your lifelong friendship is one of the greatest gifts I could ever receive – thank you for carrying me safe to the finish line. *Para mi familia*, for your patience, refuge, and love – *gracias por rezar y cuidar de mi, y sobre todo gracias por darme tanto con tan poco.*

ABSTRACT

Approximately 20% of patients with myeloproliferative neoplasms (MPNs) harbor mutations in the gene calreticulin (*CALR*), with 80% of those mutations classified as either type 1 or type 2. Current targeted therapies for *CALR* mutated MPNs are not curative and fail to differentiate between type 1 versus type 2 mutant *CALR*-driven disease, despite the different phenotypic and prognostic outcomes in these patients. To improve treatment strategies for *CALR* mutated MPN patients, it is critical to identify specific dependencies unique to each *CALR* mutation type that can be exploited for therapeutic gain. Molecularly, type 2 *CALR* mutant proteins retain many of the calcium binding sites present in the wild type protein, while type 1 *CALR* mutant proteins lose these residues. The functional consequences of this differential loss of calcium binding sites remain yet unexplored. Here, we show that the loss of calcium binding residues in the type 1 mutant *CALR* protein directly impairs its calcium binding ability, which in turn leads to depleted endoplasmic reticulum (ER) calcium and subsequent activation of the IRE1α/XBP1 pathway of the unfolded protein response (UPR). Genetic or pharmacological inhibition of IRE1α/XBP1 signaling induces cell death only in type 1 mutant but not type 2 mutant or wild type *CALR*-expressing cells and abrogates type 1 mutant *CALR*-driven MPNs disease progression *in vivo*. In a continued line of research, we aim to define the role of the RNA 2', 3'- cyclic phosphate and 5'-OH ligase (*RTCB*) in CALR mutant MPNs. RTCB is the primary ligase responsible for the re-joining of XBP1 mRNA exons upon IRE1α splicing. Given our previous findings showing that the IRE1α-XBP1 pathway is critical in type 1 mutant CALR-driven MPNs, we aim at dissecting its XBP1-dependent vs independent functions and whether *RTCB* targeting represents a novel target in this disease. Separately, given the need to dissect the molecular players and mechanisms involved in myelofibrosis, this work aims to develop a cell-based system that mimics the

pathological features of myelofibrosis in vitro. Overall, this work is the first to demonstrate that type 1 and type 2 mutant *CALR*-expressing cells display differential molecular dependencies that can be targeted for therapeutic gain. Moreover, this study answers an enduring question regarding the functional consequence of the loss of calcium binding sites on the type 1 mutant CALR protein and demonstrates how type 1 *CALR* mutant-expressing cells rewire the UPR, downstream calcium signaling, and apoptotic pathways to drive MPNs.

PUBLICATIONS

The following chapters consist in part of the following published manuscript:

Ibarra J, Elbanna YA, Kurylowicz K, Ciboddo M, Greenbaum HS, Arellano NS, Rodriguez D, Evers M, Bock-Hughes A, Liu C, Smith Q, Lutze J, Baumeister J, Kalmer M, Olschok K, Nicholson B, Silva D, Maxwell L, Dowgielewicz J, Rumi E, Pietra D, Casetti IC, Catricala S, Koschmieder S, Gurbuxani S, Schneider RK, Oakes SA, Elf SE. Type I but Not Type II calreticulin Mutations Activate the IRE1α/XBP1 Pathway of the Unfolded Protein Response to Drive Myeloproliferative Neoplasms. *Blood Cancer Discov*. 2022 Jul 6;3(4):298-315. doi: 10.1158/2643-3230.BCD-21-0144. PMID: 35405004; PMCID: PMC9338758.

CHAPTER 1: INTRODUCTION

Chapter 1 consist in part of the introduction section from Ibarra and Elbanna et al., *Blood Cancer Discovery* (2022); see publications section.

1.1 Hematopoiesis and blood cell formation:

Hematopoiesis is a multi-step orderly process responsible for blood cell formation (1,5,6). This process starts in the bone marrow (BM) and is tightly regulated by a complex network of cell-intrinsic and environmental factors (1). As a lifelong process, hematopoiesis starts in the early embryo and continues to be replenished throughout adulthood (8). In the human body hematopoiesis supplies with >100 billion mature blood cells per day involved in a variety of functions including oxygen delivery, immunity, and tissue remodeling (3,7,8). Given the ongoing production of a vast and wide variety of blood cell types, this process is highly regulated and requires a highly responsive control system (6). Hematopoietic stem cells (HSCs), which are small, rare (1 per 10^5 bone marrow cells), mononuclear noncycling or extended cycling cells, sit at the top of hierarchy in the mammalian hematopoietic system (8, 39,40). HSCs are capable of self-renewal as well as differentiation to give rise to all mature functional hematopoietic cell types through the production of lymphoid or myeloid progenitor cell lineages (common lymphoid progenitors, CLPs, and common myeloid progenitors, CMPs, respectively) (4,9) (**Figure 1.1**)

To achieve mature cell status, HSCs undergo differentiation, which is influenced by a variety of regulatory pathways largely controlled by cytokines. For instance, HSC to CLP has shown to be dependent on interleukin 7 (IL-7), while CMP differentiation relies on stem cell factor (*SCF*) and thrombopoietin (*TPO*) (10,11). Both CMP and CLP lineages can further differentiate into downstream progenitors, further giving rise to mature cells. In the case of CLP differentiation, this can result in functional T-cells, NK cells, and B cells. On the other hand, CMP differentiation

can give rise to megakaryocytes, platelets (thrombocytes), red blood cells (erythrocytes), monocytes, and neutrophils, eosinophils, which are involved in process including oxygen transport, wound repair, innate and acquired immunity, inflammation, and homeostasis. (10, 11). Notably, TPO is required for CMPs to differentiate into megakaryocytes and platelets, while red blood cell maturation is regulated by erythropoietin (*EPO*) signaling (12, 13, 14) (**Figure 1.1**).

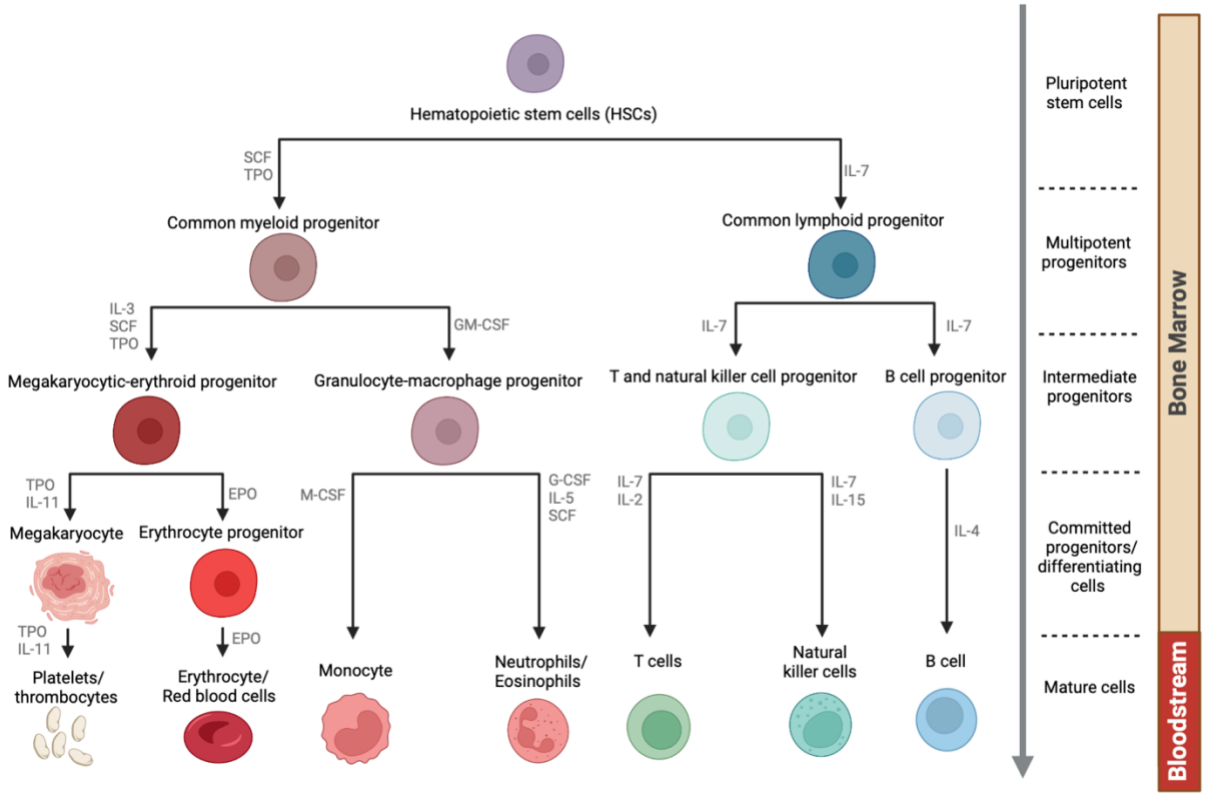

Figure 1.1 Human hematopoiesis and differentiation. Hematopoietic stem cells (HSCs) and giving rise to common myeloid progenitors (CMP) and common lymphoid progenitors (CLP) and their respective mature functional lineages. Key cytokines and growth signals involved in differentiation and cell identity maintenance are shown. SCF, stem cell factor; TPO, thrombopoietin; IL-3, interleukin 3; GM-CSF, granulocyte-macrophage colony-stimulating factor; IL-11, interleukin 11; EPO, erythropoietin; M-CSF, Macrophage colony-stimulating factor; G-CSF, granulocyte colony-stimulating factor; IL-5, interleukin 5; IL-7, interleukin 7; IL-2, interleukin 2; IL-15, interleukin 15; IL-4, interleukin 4. Legend and column on the right indicates cell state, and location, respectively. (Figure adapted from Metcalf, 2008., Robb 2007) (10, 11). (Generated in BioRender)

Hematological malignancies and myeloid cancers:

Hematological malignancies (HMs) are a group of diverse diseases connected to the bone marrow, blood, and lymphatic systems, characterized by uncontrolled cell growth (15, 16). HMs encompass plasma cell cancer or myeloma, lymphomas, and leukemias (15). Myelomas result from the abnormal production of mature plasma B-cells, which are involved in the production of monoclonal and heavy-chain proteins (18). Lymphoma develops in immune cells known as lymphocytes (T or B lymphocytes) found in the lymph nodes, spleen, thymus, and bone marrow, as well as in other body organs (17, 19). Leukemias (whether lymphoid or myeloid), arise in blood-forming cells and are characterized by the excess production of abnormal white blood cells in the bloodstream and hematopoietic organs (e.g., BM, spleen, tonsils) (17, 27). Worldwide, HMs account for 1.2 million new cases of cancer each year and around 7% of all malignancies that are diagnosed for the first time, while leukemia accounts for 2.5% of all cancer diagnoses with more than 400,000 new diagnosed each year (17).

A further form of hematological malignancies are myeloid malignancies, which are clonal disorders of myeloid progenitor cells. These develop as result of genetic and epigenetic changes that interfere with crucial myeloid cell-lineage processes, including self-renewal, proliferation, and differentiation. These malignancies include both chronic stages, such as myeloproliferative neoplasms (MPNs) and myelodysplastic syndromes (MDS), as well as acute stages such as acute myeloid leukemia (AML). Notably, AML can occur *de novo* (~80% of the cases) or evolve from a chronic stage (e.g., secondary AML) (20).

1.3 Myeloproliferative neoplasms:

MPNs are a heterogenous collection of bone marrow-derived malignancies, which result in the increased proliferation of mature myeloid blood cells. The cumulative yearly incidence of these illnesses is 1–5 cases/100,000 patients, with most of these patients being adult to elderly (21, 22). Given the extensive clinical-pathological and molecular understanding of MPNs, which dates to 1951 when William Damashek first recognized these group of malignancies, the world health organization (WHO) currently classifies MPNs into four major sub-groups based on their shared pathological, clinical, and molecular features. These four groups include (a) Chronic Myeloid Leukemia (CML); (b) classical Philadelphia-negative MPNs; (c) non-classical Philadelphia-negative MPNs (Chronic Neutrophilic Leukemia, CNL; Chronic Eosinophilic Leukemia, CEL); and (d) MPNs, unclassifiable (MPNs-U) (23). This final group accounts for MPNs that have aberrant molecular characteristics or clinical-pathological mismatches that are poorly defined (22, 23, 37).

1.4 BRC-ABL-negative myeloproliferative neoplasms:

The BCR–ABL-negative MPNs comprise three distinct mature myeloid cell proliferative diseases defined cytogenetically by the lack of the Philadelphia chromone or bcr/abl fusion gene, as found in other forms of myeloid malignancies such as acute myeloid leukemia (AML) or chronic myeloid leukemia (CML) (24, 38). These three forms of MPNs are classified as: polycythemia vera (PV), essential thrombocythemia (ET), and myelofibrosis (MF). PV is characterized by over proliferation of red blood cells, which can result in blood thickening and increased risk of hemorrhage, thrombosis, and splenomegaly (41, 42, 242-244) (**Figure 1.2**). Treatment for PV commonly involves the use of phlebotomy (blood removal) and blood thinner medications such as low-dose aspirin (43, 44). ET is defined by megakaryocytic hyperplasia and thrombocytosis,

which can lead to an increased risk of blood clots (242-244). ET treatment commonly involves cytoreductive therapy or aims at reducing the platelets and number of thrombotic events, such as through the administration of hydroxyurea (45, 46). MF is a third form of MPNs, which is defined by megakaryocytic hyperplasia, abnormal collagen deposition, and fibrotic remodeling of the bone marrow stromal cells (242-244). There is no cure for MF outside of allogenic stem cell transplantation, and existing treatments are mainly palliative (47, 48, 49).

In addition, pre-fibrotic myelofibrosis (pre-PMF), which separates a subset of patients with slight phenotypic changes from ET and a greater rate of progression to myelofibrosis, has been included in the new WHO classification of MPNs (27). Notably, some of the shared clinical characteristics of these forms of MPNs include the presence of malignant transformed cells that do not require growth factors for proliferation, hypercellularity of the bone marrow, an elevated risk of thrombotic events and bleeding, and spontaneous progression to AML (26).

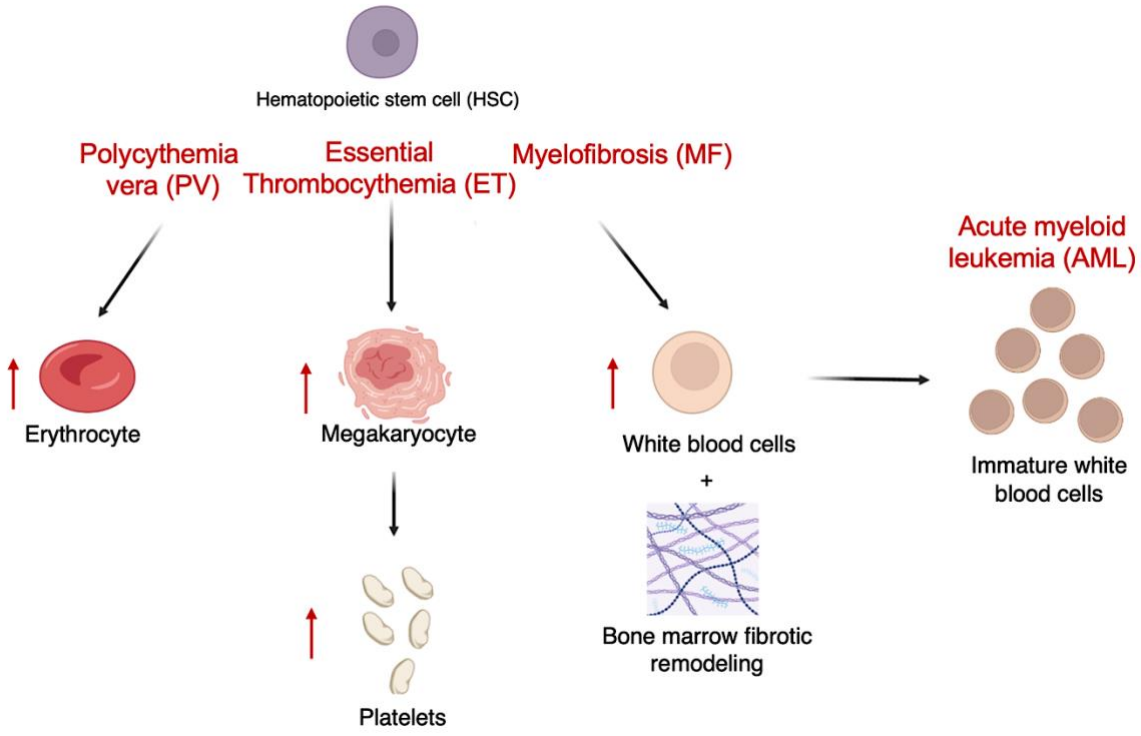

Figure 1.2 BRC-ABL-negative myeloproliferative neoplasms. Development and pathobiological features of the three different types of MPNs; polycythemia vera (PV), essential thrombocythemia (ET), and myelofibrosis (MF). Red arrows indicate the type of mature myeloid cell over proliferation that defines each MPNs. In addition, MPNs can transform to acute myeloid leukemia (AML), with MF carrying the highest transformation risk. (Generated in BioRender)

AML is a heterogeneous disease marked by the clonal growth of myeloid progenitors (blasts) in the bone marrow and peripheral circulation (71). As an aggressive malignancy, that leads to symptoms related to bone marrow failure and organ infiltration, if untreated, AML is a universally fatal condition and life-threatening complications can quickly develop in asymptomatic patients (72). If untreated, AML median survival is average 2-months and a 2-year survival of 6% (73, 74).

Although AML typically manifest as *de novo* it is important to highlight that AML can result in patients with underling hematological disorders such as MPNs and/or as a direct result of mutations acquired through earlier treatment such as chemotherapy or radiation therapy (75, 76,

77). When it comes to clinical outcomes, PV and ET are indolent MPN forms, with overall survival (OS) rates of ~15 and ~18 years, respectively. However, MF has the worst prognosis with a median survival of ~4 years (28, 29). In addition, patients with MF have the highest risk of transformation (8-23%) to AML within the first 10 years post diagnosis (30, 31,35). Patients with post-MF AML transformation have very poor outcomes with OS from 3 to 8 months and a 1-year survival rate sitting between 5-10%, and with this disease stage being refractory to chemotherapy treatment (32, 33, 34,35, 36).

When it comes to MPNs presentation and symptoms, the International Consensus Classification (ICC) of myeloid neoplasms and acute leukemias has recently updated several criteria components for the diagnosis of MPNs (**Table 1.1**). These criteria build from the World Health Organization (WHO) classification and encompass further understanding of the biology and clinical-pathological characteristics of myeloid malignancies. This diagnostic criterion also encompasses genetic, mutational, and molecular understanding of MPNs, which will be covered in the next section.

Table 1.1 International consensus classification of myeloid neoplasms

Diagnostic criteria for MPNs			
PV	**ET**	**Post-ET MF**	**PMF, overt fibrotic stage**
Major criteria **1.** Elevated hemoglobin concentration or elevated hematocrit or increased red blood cell mass* **2.** Presence of JAK2 V617F or JAK2 exon 12 mutation† **3.** Bone marrow biopsy showing age-adjusted hypercellularity with trilineage proliferation (panmyelosis), including prominent erythroid, granulocytic, and increase in pleomorphic, mature megakaryocytes without atypia Minor criterion • Subnormal serum erythropoietin level	Major criteria **1.** Platelet count ≥ 450 × 109/L **2.** Bone marrow biopsy showing proliferation mainly of the megakaryocytic lineage, with increased numbers of enlarged, mature megakaryocytes with hyperlobulated staghorn-like nuclei, infrequently dense clusters*; no significant increase or left shift in neutrophil granulopoiesis or erythropoiesis; no relevant BM fibrosis† **3.** Diagnostic criteria for BCR::ABL1-positive CML, PV, PMF, or other myeloid neoplasms are not met **4.** JAK2, CALR, or MPL mutation‡ Minor criteria • Presence of a clonal marker§ or absence of evidence of reactive thrombocytosis‖	Required criteria **1.** Previous established diagnosis of ET **2.** Bone marrow fibrosis of grade 2 or 3 Additional criteria **1.** Anemia (ie, below the reference range given age, sex, and altitude considerations) and a >2 g/dL decrease from baseline hemoglobin concentration **2.** Leukoerythroblastosis **3.** Increase in palpable splenomegaly of >5 cm from baseline or the development of a newly palpable splenomegaly **4.** Elevated LDH level above the reference range **5.** Development of any 2 (or all 3) of the following constitutional symptoms: >10% weight loss in 6 mo, night sweats, unexplained fever (>37.5°C)	Major criteria **1.** Bone marrow biopsy showing megakaryocytic proliferation and atypia,* accompanied by reticulin and/or collagen fibrosis grades 2 or 3 **2.** JAK2, CALR, or MPL mutation† or presence of another clonal marker‡ or absence of reactive myelofibrosis§ **3.** Diagnostic criteria for ET, PV, BCR::ABL1-positive CML, myelodysplastic syndrome, or other myeloid neoplasms‖ are not met
The diagnosis of PV requires either all 3 major criteria or the first 2 major criteria plus the minor criterion‡	The diagnosis of ET requires either all major criteria or the first 3 major criteria plus the minor criteria	The diagnosis of post-ET MF is established by all required criteria and at least 2 additional criteria	The diagnosis of overt PMF requires all 3 major criteria and at least 1 minor criterion confirmed in 2 consecutive determinations
Adapted from Arber DA, Orazi A, Hasserjian RP, et al. International Consensus Classification of Myeloid Neoplasms and Acute Leukemias: integrating morphologic, clinical, and genomic data. Blood. 2022;140(11):1200-1228. doi:10.1182/blood.2022015850 Ref. 239.			

1.5 Myeloproliferative neoplasms mutational landscape:

Somatic mutations that develop in the hematopoietic stem cell (HSC) compartment and activate the JAK2-STAT signaling pathway are sufficient and the primary cause of *BCR-ABL*-negative MPNs in most cases (36,55,56) (**Figure 1.3**). In 2005, the discovery of a mutation in the non-receptor tyrosine kinase *JAK2* gain-of-function mutation (*JAK2V617F*; a G to T somatic mutation at nucleotide 1849, in exon 14, resulting in the substitution of valine to phenylalanine at codon 617) provided an underling mutational genetic basis for MPNs malignancy entities (36, 50-54). JAK2 mutation results in the JAK2-STAT driven signaling pathway being activated continuously even when EPOR, MPL, and G-CSFR ligand binding are absent (54, 52). Currently, activating mutations in the JAK2 account for 95% of PV and ~50% of ET and PMF cases (5-8).

Located on chromosome 1p34, activating mutations in MPL, the gene encoding the thrombopoietin receptor, occur in ~3% to 5% of ET patients and 5% to 10% of PMF patients (57, 250-253) (**Figure 1.4**). MPL and its ligand TPO are essential for hematopoietic stem cell self-renewal, and platelet and megakaryocyte development. (58, 59, 60). There are a number of known MPL mutations, however the two most common types are W515L and W515K within exon 10 (61, 57, 62, 63). Importantly, the generation of mature platelets is negatively impacted by MPL's role as a regulator of TPO levels. TPO is not eliminated in MPL mutant instances, which results in high plasma TPO levels. This unregulated stimulation fuels the observed excessive megakaryopoiesis (64, 56). Upon the discovery of JAK2 and MPL mutations, it became evident that a percentage of MPNs patients were negative for mutations in either of these two genes, this then led to the finding of a third major driver mutation (65,66).

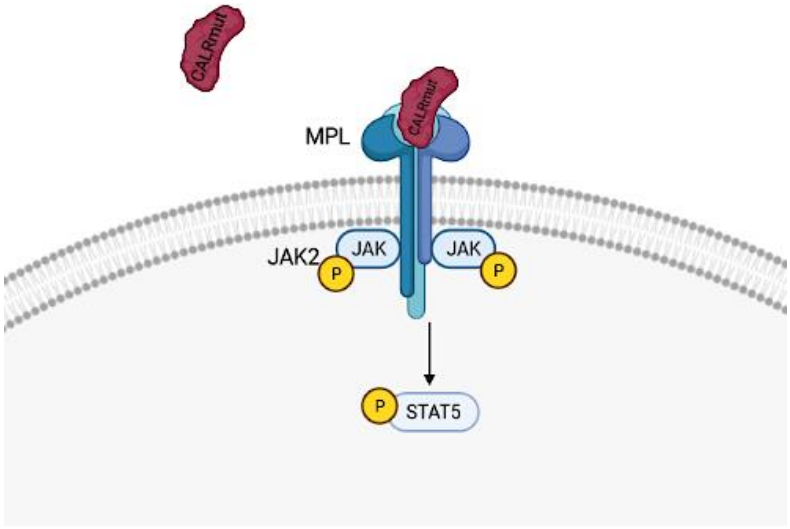

Figure 1.3 JAK-STAT signaling in myeloproliferative neoplasms malignancy. Mutations in either MPL receptor or JAK2 can lead to constitutive activation of the JAK-STAT pathway in the hematopoietic stem cell compartment. *CALR* mutation can also result in JAK-STAT activation through its interaction with MPL. As result of any of these events, aberrant JAK-STAT pathway arises to drive MPNs malignancy. (Generated in BioRender)

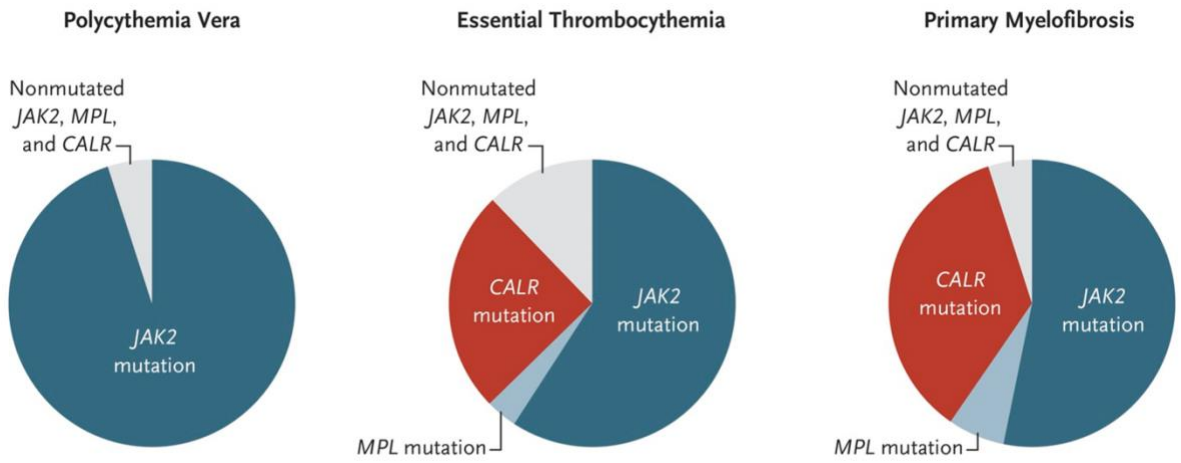

Figure 1.4 Myeloproliferative neoplasms mutational landscape. Breakdown of mutations in *BCR-ABL* negative MPNs; mutations in the *JAK2* account for 95% of PV and ~50% of ET and PMF cases, while MPL mutations present in ~3% to 5% of ET patients and 5% to 10% of PMF patients. Around 40% of ET and PMF patients harbor CALR mutations. There is also a group across, PV, ET and PMF that do not carry mutations in any of these three genes and are termed as JAK2, MPL, CALR negative. Adapted from: Klampfl T, Gisslinger H, Harutyunyan AS, et al. Somatic mutations of calreticulin in myeloproliferative neoplasms. *N Engl J Med*. 2013;369(25):2379-2390. doi:10.1056/NEJMoa1311347 (Ref. 240).

1.6 Calreticulin mutations in myeloproliferative neoplasms:

In 2013, two independent research teams independently discovered calreticulin (*CALR*) mutations in *JAK2* and *MPL* mutations negative MPNs by using whole exon sequencing (67,68). Approximately 40% of ET and MF patients harbor somatic, heterozygous *CALR* mutations (**Figure 1.4**). This gene encodes a encodes a calcium (Ca2+)-binding chaperone protein that primarily resides in the endoplasmic reticulum (ER) and is involved in the folding of glycoprotein in the ER lumen as they move through the secretory pathway (60,70, 245, 246) CALR contains three distinct domains: the globular N-domain and proline-rich P-domain are responsible for the chaperone function of the protein, though the P domain also contains one high affinity calcium binding site; the highly disordered C-terminal domain binds Ca2+ with a series of acidic amino acids, and terminates at an ER retention signal (KDEL) (247) (**Figure 1.5**).

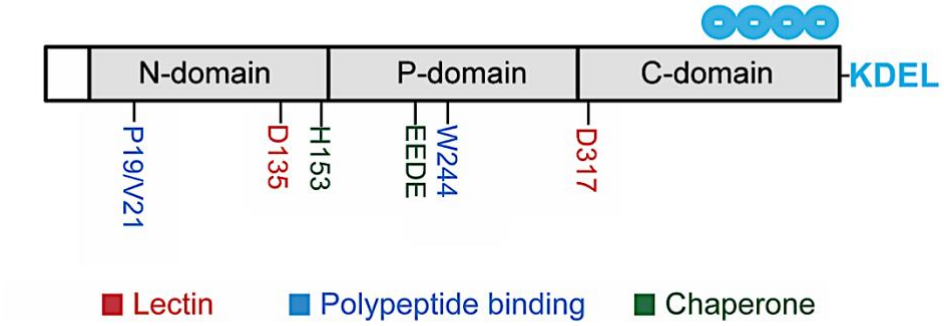

Figure 1.5 Calreticulin protein structure. Calreticulin protein contains a globular N-domain, a proline-rich P domain, and a disordered, negatively charged C-domain that contains an endoplasmic reticulum retention signal or KDEL. Calreticulin also contains lectin sites that interact with monoglucosylated oligosaccharides on newly synthesized glycoproteins in the ER. Additionally, calreticulin contains polypeptide binding sites, which function to bind and release nascent polypeptides to suppress the aggregation of unfolded substrates in the ER.

All *CALR* mutations occur as +1 base pair frameshift-induced indels in exon 9 of the gene, which encodes the C-terminal calcium binding domain, and produce an identical 36 amino acid mutant C-terminal tail. The mutant C-terminus is characterized by the replacement of the acidic calcium binding residues with positively charged arginine and lysine residues, and loss of the KDEL sequence (**Figure 1.6**). This neomorphic sequence is required for the oncogenic activity of mutant CALR, wherein the mutant protein aberrantly binds to the thrombopoietin receptor MPL to constitutively activate pathogenic JAK-STAT signaling and drive the disease (248-250).

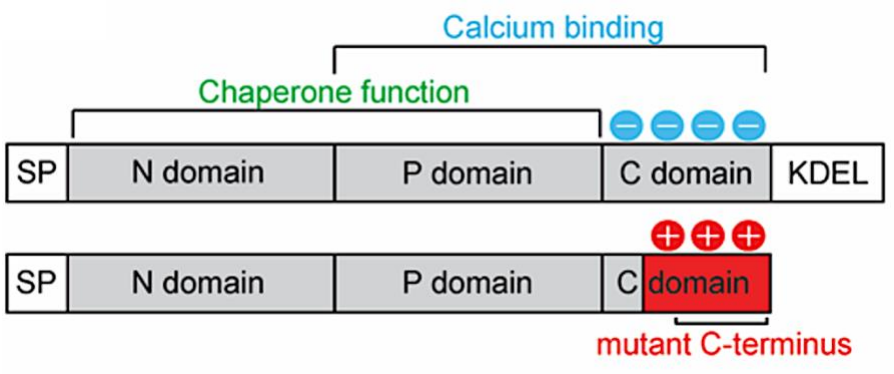

Figure 1.6. Structural comparison of wild type and CALR mutant proteins. CALR contains three distinct domains: the N-domain and P-domain are responsible for the chaperone function of the protein, though the P domain also contains one high affinity calcium binding site; the C-terminal domain binds Ca2+ with a series of acidic amino acids (denoted by blue circles), and terminates at an ER retention signal (KDEL). SP = ER signal peptide. CALR mutations occur in the C-terminal calcium binding domain, and produce an identical 36 amino acid mutant C-terminal tail (red shaded region). The mutant C-terminus is characterized by the replacement of the acidic calcium binding residues with positively charged residues (denoted by red circles), and loss of the KDEL sequence. SP = ER signal peptide.

1.7 Type 1 and type 2 calreticulin mutations in myeloproliferative neoplasms

80% of CALR mutations are classified as either type 1 (52 bp deletion; CALRdel52) or type 2 (5 bp insertion; CALRins5). Molecularly, type 1 and type 2 *CALR* mutations are classified based on the extent of amino acid homology with the wild-type protein. While type 2 CALR mutant proteins retain many of the calcium binding sites present in the wild type protein, type 1 CALR mutant proteins lose these residues (**Figure 1.7**).

Figure 1.7 C-terminal amino acid sequence of CALRwt versus type 1 CALRdel52 and type 2 CALRins5. CALRins5 retains many of the Ca2+ binding residues present in the wild type protein, which are lost in the del52 mutant protein (highlighted in blue). 36 amino acid mutant C-terminal tail shared between all CALR mutant proteins is depicted in red.

Importantly, it had not yet been shown that type 1 mutations directly result in a loss of calcium binding ability. It has however been demonstrated that patients with type 1 CALR mutations, but not those with type 2, exhibit abnormal intracellular Ca2+ signals, characterized by significantly increased store-operated Ca2+ entry (SOCE) activity, a regulator of calcium flux into the cell (252). A subsequent study reported that this abnormal SOCE activity is a result of diminished interaction between mutant CALR and stromal interaction molecule 1 (STIM1) (261), a protein of SOCE machinery that functions as a calcium sensor in the ER (262). However, in contrast to its predecessor (252), this study did not identify any significant differences in SOCE activation between type 1 and type 2 mutant CALR megakaryocytes, despite the fact that type 1 mutant proteins lose the calcium binding residues present in the type 2 proteins. This suggests that there may be other regulatory mechanisms at play that mediate intracellular Ca2+ signaling in type 1 versus type 2 mutant CALR-expressing cells outside of SOCE machinery. Moreover, in addition to understanding how Ca2+ signaling differs in type 1 versus type 2 mutant CALR cellular contexts, and whether differential signaling is a direct result of the loss of calcium binding sites on the type 1 mutant protein, it is critical to understand the functional consequences of these differences. Ca2+ affects myriad cellular pathways, but which are differentially regulated by abnormal Ca2+ signaling in type 1 versus type 2 mutant CALR has yet to be explored.

1.8 Type 1 and type 2 calreticulin mutations clinical and prognostic differences in myeloproliferative neoplasms

Despite their shared mutant C-termini and mutual ability to bind and activate MPL, patients with type 1 and type 2 *CALR* mutations display significant clinical and prognostic differences. Type 1 mutations are primarily associated with an MF phenotype and a higher risk of fibrotic transformation in ET, while type 2 mutations are more common in ET (251, 251). Within ET, type

2 CALR patients exhibit higher platelet counts and a lower thrombotic risk, and within MF, type 1 patients have a better prognosis than type 2 patients. The mechanisms underlying these divergent clinical phenotypes remain unknown but suggest that the molecular pathogenesis is not limited to activation of the MPL-JAK-STAT signaling axis. To date, however, there has been no identification of differentially activated pathways or dependencies in type 1 versus type 2 mutant CALR-driven disease.

1.9 Current myeloproliferative neoplasms treatment therapies

Allogenic stem cell transplant (ASCT) is the only potentially curative therapy for MPNs; however, this carries high-therapy related morbidity and mortality (approximately 30%) and given the median age at diagnosis of 65 years, this is only practical to a limited percentage of patients (81, 82, 83, 84, 85, 86, 88, 89, 90). Beyond transplant success, donor availability, and the possibility of life-threatening infections and graft versus host disease are among limiting concerns for transplants beyond late age (87, 85). Given its inhered risk, the need for ASCT is often a debated consideration for patients (91, 92). Alternative therapies that are currently on the market are non-curable and only can provide palliative treatment, with no disease-modifying ability (85). Notably, these treatments focus at reducing symptom burden underlying MPNs pathological and clinical presentation (78, 79, 85).

For patients with conventional *BCR-ABL*-negative myeloproliferative neoplasms, hydroxycarbamide also known as hydroxyurea (HU) continues to be the first-line therapy, most often utilized, and well-tolerated cytoreductive medication for MPNs (93, 94, 95, 103). As an anti-metabolite HU prevents DNA synthesis, leading to control in erythrocytosis and thrombocytosis as well as reduction thrombotic tendency in PV and ET patients (95, 79). Improvement in splenomegaly, bone pain, constitutional symptoms, and pruritus are also seen after HU treatment

(94, 96). Yet, HU only temporarily relieves symptoms, and it has demonstrated to have side effects such as myelosuppression, particularly granulocytes, while other non-hematological side effects include pneumonitis, mucocutaneous ulcers, fever, and different gastrointestinal symptoms (99, 100, 95). In addition, among these adverse side-effects HU treatment in MPNs patients has also been associated with malignant manifestations such as squamous cell carcinoma (101). It is also important to note that PV and ET patients are also oftentimes managed by a combination of phlebotomy, aspirin, along with HU (102, 104, 95).

With a better understanding of the critical role of the JAK-STAT pathway in the pathogenesis of MPNs, in 2011 the arrival of the JAK 1/2 inhibitor ruxolitinib—the first targeted therapy in this field—was a turning point in the treatment of MPNs (105, 106, 107, 108). As a potent and selective ATP competitive (cyclopentylpropionitrile derivative) kinase inhibitor of JAK1/2, Ruxolitinib has been approved for the treatment of intermediate to high-risk MF, and hydroxyurea resistant PV (107,108, 109). Ruxolitinib has demonstrated efficacy in lowering levels of inflammatory cytokines, the excess generation of mature myeloid cells, and the associated clinical symptoms in MPNs, and although effective at reducing symptom burden, these drugs are not curative (110, 111, 112, 113). Importantly, Ruxolitinib has demonstrated only minor reduction in MPNs stem cell pool (110, 114, 295). Consequently, persistent administration of these drugs will probably be necessary for long-term illness management by targeted JAK2 inhibition, which can be impractical due to the adverse effects can present such as dose-limiting cytopenia and infectious complications (110, 115, 116, 117). Furthermore, although *CALR* mutation positive patients can be treated with JAK2 inhibitors, these drugs are not curative and primarily alleviate symptom burden without altering the natural course of the disease due to an inability to eradicate the malignant clone (110, 111, 112, 113, 114, 118, 119, 120, 253-260). Thus, in order to improve

treatment strategies for *CALR* mutation positive MPNs patients, it is critical to identify specific dependencies unique to *CALR* mutation type that can be exploited for therapeutic gain.

1.10 Endoplasmic reticulum stress and improperly folded proteins

The endoplasmic reticulum (ER) is a large and dynamic intracellular organelle with a membrane that serves as the initial compartment in the secretory route (121, 122). The ER is engaged in a wide range of biological processes. It functions as a factory for protein synthesis, aids in calcium storage and regulation, lipid synthesis and storage, and glucose metabolism (122-129). A major function of the ER is to serve as a site for the synthesis, folding, maturation, quality control, and destruction of secretory and transmembrane proteins (122, 130). It also makes sure that only properly folded proteins are transported to their sites of action (122, 130). A protein intended for secretion must undergo correct folding and modifications with the help of chaperones and folding enzymes after protein synthesis and translocation into the ER lumen. N-linked glycosylation, the creation of disulfide bonds, and oligomerization are some of these alterations (125, 135, 136). Notably, nearly a 1/3 of all proteins, are co-translationally targeted to the ER, where they are exposed to a wealth of chaperones and foldases that aid in their folding, assembly, and post-translational modification before they are exported from the ER (134). Proteins that do not fold correctly within a particular amount of time are targeted for ER-associated degradation (ERAD), which effectively retro-translocate them from the ER into the cytosol for degradation using the ubiquitin-proteasome system (131, 132, 133). Even though protein misfolding happens all the time, it might get worse under unfavorable intrinsic and environmental circumstances, hence, to prevent cellular function from being impacted, recognition of misfolded proteins and removal of these aggregates through the ERAD pathway must be closely regulated (137, 121, 122).

A cellular state known as "ER stress" is brought on by circumstances that interfere with ER homeostasis and protein folding quality control which in turn lead to accumulation of misfolded proteins (138, 139). A number of cell intrinsic and extrinsic insults can perturb protein folding and quality control, including variations in nutrient levels, increased demands on protein secretion, hypoxia, mutations in client proteins of the secretory pathway that stabilize or promote aggregation of intermediate folding forms, and decreases in calcium levels with inhibitory effects on calcium-dependent chaperones (140, 141, 143). To alleviate ER stress, adaptive ER stress responses are activated to deal with the load of improperly folded proteins resulting in cell survival or apoptosis (144, 145, 146).

1.11 Endoplasmic reticulum and Ca2+ regulation

A number of proteins are primarily synthesized and transported in the ER; however, this organelle also serves as a significant intracellular Ca2+ storage site (212, 213, 214). Ca2+ typically has a cytosolic concentration of 100 nM or less, an ER lumen concentration of 100-800 nM, and an extracellular Ca2+ concentration of 2 mM (215, 216). The ER contains Ca2+ channels that respond to the needs and fluctuations of Ca2+ in the cell, importantly, in response to low intracellular Ca2+ levels, a number of calcium channels, ryanodine receptors, and inositol 1,4,5-trisphosphate (IP3R) receptors release Ca2+ into the cytosol from the ER (215). Ca2+ can enter the cell from the extracellular medium or leak out of the ER into the cytoplasm before being pumped back into the ER by sarcoendoplasmic reticular Ca2+ ATPases (SERCAs), which adds to the levels of regulation (215). A method for Ca2+ entrance into the cell is activated when ER Ca2+ stores are quickly depleted through IP3 receptor (IP3R)-mediated release. This process is referred to as store-operated Ca2+ entry (SOCE) (215, 217). Therefore, the localization, function, and interaction of proteins—whether they are associated with other proteins, organelles, or nucleic

acids—can all be influenced by Ca2+ (122). Of relevance, one such pathway that is heavily influenced by Ca2+ signaling is the unfolded protein response (UPR). There are several forms in which Ca2+ can influence ER stress, for instance, most ER-localized chaperones and folding enzyme are Ca2+ dependent and rely on Ca2+ activity (218, 219). These ER resident Ca2+ binding proteins and folding enzymes influence protein folding integrity and UPR signaling through interactions with stress signaling sensors (218, 219, 220).

1.12 The unfolded protein response and endoplasmic reticulum stress

In response to ER stress, cells activate a signaling mechanism known as the UPR, which reduces protein synthesis, eliminates unfolded or misfolded proteins, and promotes ER's ability to fold proteins (121, 139) Through this response, the UPR coordinates the activation of three stress sensors (inositol-requiring enzyme 1 alpha (IRE1α), protein kinase R-like ER kinase (*PERK*), and activating transcription factor 6 (*ATF6*)), which activate genes that work to restore ER function and drive adaptation to microenvironmental changes through downstream transcriptional activation (155, 156, 157, 140). If ER stress load becomes unresolved, the UPR forces the cell into apoptosis (147,263). When the ER is in a homeostatic state, binding Ig protein [BiP; also known as glucose-regulated protein, 78kD (GRP78) and heat shock 70 kDa protein 5 (HSPA5)] interacts with the luminal domains of IRE1, PERK, and ATF6 to maintain them in a monomeric and inactive form (140, 148, 149, 121). BiP/GRP78 is titrated off the ER stress sensors and onto misfolded proteins as they start to accumulate within the ER lumen, priming the UPR stress sensors to be ready to signal. This is due to BiP/higher GRP78's affinity for the exposed hydrophobic polypeptide domains contained within misfolded proteins. The ER luminal domains of the unrestrained UPR sensors can then directly bind to misfolded proteins, causing their oligomerization and activation (140, 148). The early effects of the UPR, known as homeostatic

UPR, aim to restore ER homeostasis by reducing demand and boosting capacity on the machinery for folding proteins in an effort to maintain cell function (139, 140). However, if these corrective actions fail to adequately restore homeostasis, the ER sensors then start a different program called the terminal UPR, which promotes cell death (140, 151, 152, 153, 154). Importantly, chronic ER stress has been linked to numerous cancer types, and certain tumor cells use the UPR as an essential survival mechanism to tolerate stress (264, 265).

1.13 The IRE1α/XBP1 axis of the unfolded protein response

In humans, inositol requiring enzyme 1 α (IRE1α) is encoded by the endoplasmic reticulum to nucleus signaling 1 (*ERN1*) gene (155, 162, 163). IRE1α is a type I transmembrane protein kinase receptor, which has site-specific endoribonuclease (RNase) activity in its cytosolic domain (164-166, 155) Notably, *Ern1* deletion (KO) in mice causes growth retardation, flaws in hepatic organogenesis, and problems in placental development, all of which cause embryonic lethality (169). When ER stress is present, BiP dissociation, which is brought on by a buildup of unfolded proteins, causes IRE1α to oligomerize and activate its cytosolic kinase domain. Trans-autophosphorylation is made possible by the oligomers' face-to-face positioning and proximity to one another (167, 168, 121). Remediable ER stress results in low-level, transitory dimerization/tetramerization and kinase autophosphorylation, which limits IRE1α's RNase activity to a single adaptive task: removing a 26-nucleotide unconventional intron from the mRNA for XBP1 (X-box binding protein 1) (140, 160, 161, 170, 155). Upon this event, the tRNA ligase RNA 2′,3′-cyclic phosphate and 5′-OH ligase (*RTCB*) re-ligates the spliced XBP1 via phosphodiester bond formation, changing the open reading frame, and resulting in the translation of the basic leucine zipper (bZIP) transcription factor XBP1 spliced (XBP1s) (160, 161, 171-176). In turn, to alleviate ER stress and reestablish homeostasis, XBP1s regulates transcription of a

variety of gene targets, such as the expression of chaperones, foldases, and elements of the ERAD pathway (177, 178, 179) (**Figure 1.8**). On the other hand, a sustained, high-level IRE1α autophosphorylation triggers higher-order IRE1α oligomerization in response to ongoing and unresolved ER stress. In addition to increasing XBP1 splicing activity when IRE1α's RNase is oligomerized, it also lessens its specificity such that it targets hundreds of mRNA species as they attempt translation at the ER membrane by degrading them endonucleolytically – through a mechanism know as regulated IRE1α-dependent decay (RIDD) (180, 181, 182, 183). Notably, this unselective mRNA RIDD-driven destruction can induce cell death (140, 184, 185, 186). Hence, overall IRE1α can induce divergent outcomes (pro-survival/pro-apoptotic) based on the ER stress input prolongation.

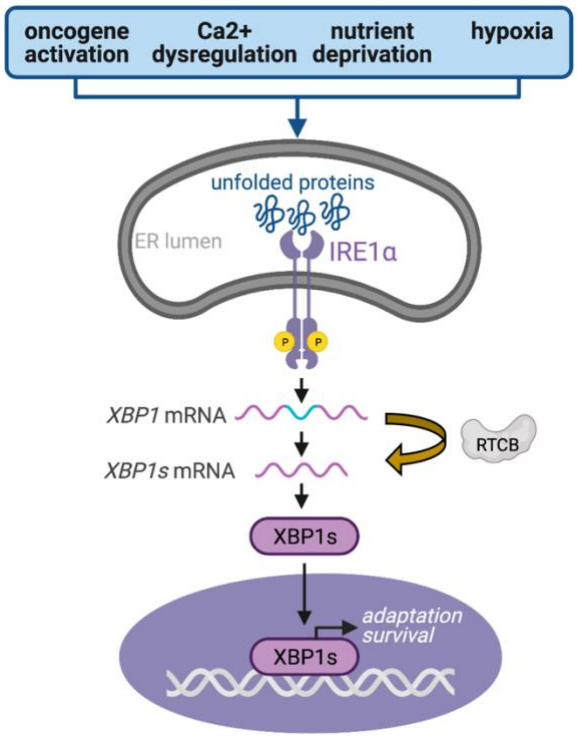

Figure 1.8 IRE1α-XBP1 arm of the unfolded protein response. A number of cellular and environmental insults such as ca2+ dysregulation can disrupt protein folding integrity in the ER and result in the accumulation of unfolded proteins in the ER lumen. The IRE1α -XBP1 axis is the most conserved and well-characterized UPR pathway. IRE1a is a transmembrane kinase and RNAse that becomes activated upon binding of unfolded proteins. Upon activation, IRE1a oligomerizes and transphosphorylates, which activates its RNAse activity. The RNAse then splices XBP1 RNA, removing a 26-nucleotide intron. The spliced XBP1 exons are then ligated back via RTCB ligase through phosphodiester bonds. Upon splicing, XBP1 translates into an active transcription factor that then translocates to the nucleus to execute various transcriptional programs involved in adaptation to cellular stress. Adapted from: Oakes SA. Endoplasmic Reticulum Stress Signaling in Cancer Cells. *Am J Pathol*. 2020;190(5):934-946. doi:10.1016/j.ajpath.2020.01.010 (Ref. 140) (Generated in BioRender)

1.14 The TSEN complex and tRNA splicing:

As the ligase responsible for catalyzing the splicing of XBP1 mRNA upon IRE1α cleavage, mammalian RTCB functions as part of what is known as the tRNA splicing endonuclease (TSEN) complex to catalyze the ejection of tRNA introns (187-192, 208) (**Figure 1.9**). Transfer RNAs (tRNAs) are crucial for the conversion of messenger RNA (mRNA) into proteins. Prior to reaching their mature and functional state, eukaryotic tRNA genes go through a number of post-

transcriptional processing and modification stages, which are carried out by RNA Pol III (187, 192, 193, 197). All known domains of life contain a conserved subset of tRNA genes with introns, which must be removed during tRNA maturation (198-200). Notably, to catalyze the elimination of tRNA introns, eukaryotes employ the TSEN complex, which is composed of four separate subunits (TSEN2, TSEN 25, TSEN34, TSEN54) (187-192, 201, 202) (**Figure 1.9**). While TSEN15 and TSEN54 are non-catalytic structural proteins with yet unknown role in tRNA splicing, TSEN2 and TSEN34 are metal ion independent nucleases that cleave the 5' and 3' splice sites, respectively. They produce the 3′ exon using a 5′-hydroxyl group and the 5′ exon using a 2′3′-cyclic phosphate (201, 203, 192). Upon cleavage, the tRNA exons are linked together by ligation via RTCB through nucleotidyl transfer steps, concluding with phosphodiester bond establishment between the exon ends (204-207, 209, 210). Overall, aside from its specific role in XBP1 ligation, RTCB also functions as part of the tRNA ligation process, which is involved in a number of cellular activities such as mRNA transport, DNA double-strand break repair, and microRNA maturation (212).

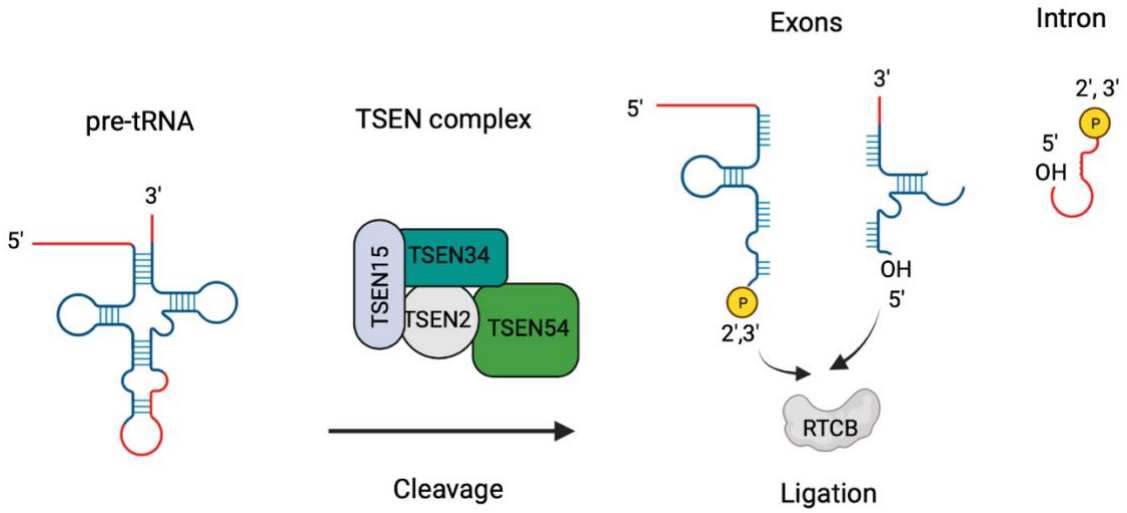

Figure 1.9 TSEN complex and RTCB ligation. In humans tRNA-splicing proceeds via the tRNA splicing endonuclease (TSEN) complex containing four subunits including two endonucleases (TSEN2 and TSEN34) and two structural components (TSEN15 and TSEN54). Following cleavage by the TSEN complex, RTCB ligase proceeds ligation through nucleotidyl transfer steps, culminating with phosphodiester bond formation between the 2'3' phosphate and 5' OH group in the exon ends. Adapted from: Hayne CK, Schmidt CA, Haque MI, Matera AG, Stanley RE. Reconstitution of the human tRNA splicing endonuclease complex: insight into the regulation of pre-tRNA cleavage. *Nucleic Acids Res*. 2020;48(14):7609-7622. doi:10.1093/nar/gkaa438 (Ref. 192). (Generated in BioRender)

1.15 BCL2 family of proteins and apoptosis modulation

When there is short-term or long-term ER stress, the UPR initiates a complicated cell death pathway that is mediated by a number of cell fate components, where the B-cell lymphoma 2 (*BCL2*) family of proteins plays a central role (221, 222). By studying the t (14;18) chromosomal translocation in B cell lymphoma, molecular investigation led to the discovery of Bcl-2, the first member of the BCL-2 protein family (224, 226) Since that time, at least 20 BCL-2 family members have been identified. At least one of the four conserved -helical motifs known as Bcl-2 homology (BH1-4) domains is present in all BCL-2 family proteins (225, 226). BCL2 family of proteins can be divided into 2 groups; a) the antiapoptotic family members, which consist of BCL-2, BCL-XL, BCL-w, MCL-1, and A1, have all four BH domains, and b) pro-apoptotic family members

including the multidomain proteins (Bax, Bak, and Bok) and the BH3-only proteins (Bad, Bid, Bik/Nbk, Bim, Bmf, Nix/BNIP3, Hrk, Noxa, and Puma) (226).

As the intrinsic apoptotic pathway's "point of no return," mitochondrial outer membrane permeabilization (MOMP) is regarded as a crucial checkpoint for the management of cell death. Cytochrome *c* and numerous other proapoptotic molecules are released as a result of MOMP, which causes the apoptosome to form in the cytoplasm and the caspase cascade to be activated (227, 228). Notably, MOMP is positively and negatively regulated via these groups of BCL-2 family pro-and anti-apoptotic proteins (229). Furthermore, although the BCL-2 family of proteins has a well-defined role in apoptosis control, their function in ER stress-induced apoptosis is complex (223). Yet, it is well recognized that the transcriptional and posttranslational regulation of proapoptotic BH3-only proteins is one mechanism by which the unfolded protein response initiates apoptosis under prolonged endoplasmic reticulum stress conditions (222, 223).

1.16 Modeling myelofibrosis in an *in vitro* cell system

Myelofibrosis (MF) is a slowly developing malignancy characterized by an increase in myeloid cells and structural abnormalities of the bone marrow matrix. At its end-stage manifestations, the disease suppresses normal hematopoiesis, results in bone marrow failure, and has excessive reticulin fiber and cross-linked collagen deposition in the bone marrow (230, 231).

According to studies, the degree of bone marrow fibrosis (BMF) and the prognosis of MPNs are related, with more fibrosis being associated with a worse prognosis (232, 233). ASCT is the only therapy thought to be curative for myelofibrosis, although its usage is constrained by substantial treatment-related morbidity and death (234).

Fibrosis is a pathologic process characterized by abnormal myofibroblast accumulation and excessive deposition of reticulin and collagen fibers, as well as other elements of the extracellular

matrix (ECM) (235). It has been proposed that BMF in MPNs results from abnormal growth factor and cytokine production from mutant hematopoietic progenitors (236). For instance, transforming growth factor beta (TGF- β) and platelet-derived growth factor can drive fibrosis by influencing bone marrow surrounding stromal cells (237, 238). Therefore, given the importance of cell-cell crosstalk between mutant hematopoietic progenitors and the bone marrow stroma cell populations in myelofibrosis development, it is critical to develop cell systems that recapitulate and yet facilitate the study of such cellular interactions and dynamics, to pinpoint the mechanisms driving such fibrotic processes and enable molecular target discovery.

1.17 Hypothesis and Specific Aims

The **objective** of my research is to define the contributions of IRE1α/XBP1 signaling to type 1 CALR mutant MPN. Based on my preliminary data, my **central hypothesis is that hyperactivation of IRE1α/XBP1 signaling contributes to cell survival and disease progression in type 1 CALR MPN.** I further predict that additional components of the IRE1α/XBP1 axis could also impact disease progression, particularly, the RTCB ligase responsible for XBP1 mRNA ligation. In addition, I also predict that CALR mutant myelofibrosis could be modeled *in vitro* through cell crosstalk between the transformed malignant cell clone expressing CALR mutant and the bone marrow stromal cells. I therefore propose to dissect the role of IRE1α/XBP1 arm of the UPR in type 1 CALR mutant MPN and establish myelofibrosis *in vitro* modeling through the following three aims:

Aim 1: To define whether IRE1α/XBP1 pathway is required for type 1 CALR-driven disease. My preliminary data indicate that the IRE1α/XBP1 pathway of the unfolded protein response is activated in type 1 CALR mutant MPN cells. However, whether this is required for type 1 CALR mutant cell survival and MPN disease progression remains to be defined. I hypothesize that IRE1α-XBP1 activation represent a dependency for type 1 CALR mutant MPN disease. To test this, I will use CALR mutant MPN cell models, and an MPN transplant mouse model, to assess XBP1 activation via RNA sequencing, qPCR, western blot, and IHC. Further to determine the necessity of the IRE1α/XBP1 pathway for cell survival and disease progression, I will perform IRE1α and XBP1 knockdown in our cell lines expressing CALR mutant variants, alongside drug treatment with KIRA8 (IRE1α specific inhibitor) in both our CALR mutant cell line models and BMT mouse model. In addition, to dissect the specific XBP1 downstream targets playing a role in disease progression, I will assess differentially activated pathways and determine

their relevance to IRE1α/XBP1 pathway via our knockdown cells. Overall, these results will inform whether IRE1α/XBP1s represents a dependency in type 1 CALR mutant MPN.

Aim 2: Define the role of RTCB in type 1 CALR mutant MPN. As the ligase responsible for XBP1 ligation, I hypothesize that RTCB is also required for the survival of type 1 CALR mutant MPN given our observation on IRE1α/XBP1 pathway activation in type 1 CALR mutant cells. In addition, I further predict that if XBP1 is necessary for type 1 CALR mutant cell survival, RTCB depletion might provide an even improved therapeutic gain, given IRE1α inhibition (via currently available drugs: KIRA8) also targets IRE1α functions independent of XBP1. Hence, to ask whether RTCB is relevant to CALR mutant MPN, I will first measure *RTCB* mRNA and protein levels via q-PCR and western blotting in our cell line system expressing CALR mutant variants. Further, to interrogate whether RTCB is dependent for the survival of CALR mutant cells, I will perform RTCB knockdown followed by proliferation studies in our CALR mutant cell line models. These results will define the significance of RTCB in type 1 CALR MPNs and whether it represents a plausible therapeutic target.

Aim 3: Develop *in vitro* model system to study myelofibrosis

We know that in the context of myelofibrosis, there is a major interplay between malignant transformed clones and the bone marrow stromal cells (BMSCs) that promote fibrotic transformation. However, whether this phenotype can be recapitulated *in vitro* to facilitate its study remains undetermined. Therefore, I hypothesize that a fibrotic phenotype can be recapitulated through the *in vitro* cell crosstalk between *CALR* mutant MPN transformed cells and BMSCs. Further, I also predict that cytokines and growth factors, particularly, transforming growth factor beta (TGF-β), contribute to this crosstalk fibrotic transformation. To test this, I will take MPN CALR mutant variants cells' conditioned media and treat BMSCs followed by assessment of

fibrotic markers expression (Fibronectin and *COL1A1*) on BMSCs via western blot and immunofluorescence. To assess TGF-β secretion by CALR mutant cells I will then perform TGF-β quantification in the conditioned media of CALR mutant cells via enzyme-linked immunosorbent assay (ELISA). Finally, to validate the impact of TGF-β secretion on fibrosis phenotype development, I will then treat BMSCs with recombinant human TGF-β and measure fibrotic marker expression. Overall, these experiments will allow me to test whether I can recapitulate a fibrotic phenotype as observed in myelofibrosis via *in vitro*, and whether TGF-β represents a plausible driver in fibrotic transformation.

CHAPTER 2: METHODS

Chapter 2 consist in part of the methods section from Ibarra and Elbanna et al., *Blood Cancer Discovery* (2022); see publications section.

2.1 Cell lines and cell culture

293T, U2OS, and HS-5 cells were obtained from American Type Culture Collection (ATCC) and their identity was authenticated by Short Tandem Repeat (STR) profiling. Ba/F3 cells and UT-7 cells were purchased from German Collection of Microorganisms and Cell Cultures (DSMZ) and were not further authenticated. All cell lines were tested for mycoplasma bi-monthly. 293T and U2OS cells were cultured in Dulbecco's modified eagle medium (DMEM; Corning) medium with 10% fetal bovine serum (FBS; Corning) and 1% penicillin/streptomycin (Corning). When passed, media was removed from cell culture plates, and cells underwent trypsinization with warm (37°C) 0.05% Trypsin EDTA (Trypsin 2.21mM EDTA 1x Sodium Bicarbonate; Corning). Cells were then incubated at 37°C for 3-5 minutes, trypsin was then washed off and media was further added to deactivate any trypsin left. Cells were then plated under fresh media. Ba/F3 and UT-7 cells were cultured in RPMI 1640 medium with 10% (Ba/F3) 20% (UT7) and 1% penicillin/streptomycin. Ba/F3 cells were supplemented with 2 ng/mL (1:10,000 dilution) murine interleukin-3 (IL-3; R&D Systems); UT-7 cells were supplemented with 10 ng/mL (1:1000 dilution) human granulocyte-macrophage colony-stimulating factor (GM-CSF; R&D Systems). When it came to cytokine starve either Ba/F3 or UT-7 cells, these were collected and spun down for 1 minute at 1500 rpm, supernatant was then aspirated and pellet was resuspended in 5 mL phosphate-buffered saline buffer (Fisher), followed again for a spin of 1-minute 1500 rpm, supernatant was then aspirated (this wash process was done 3x). Cells were then resuspended in complete media without cytokines. All cell lines were grown at 37°C, 5% CO2, 95% humidity.

2.2 Retro and lentivirus generation

For each retrovirus construct transfected (MSCV-IRES-GFP-CALRwt, -CALRdel52 or -CALRins5), one 10cm dish of 293T cells ($3x10^6$) in 5mL media were plated one day 1. After 24hrs, the constructs were prepared (10 μg expression plasmid + 5 μg EcoPak). Each construct mix was placed in 1.5ml Eppendorf tube and 500 μL of OptiMEM (Gibco) was added to each tube, followed by through mix. 45 μL of TransIT LT-1 Reagent (Mirus Bio) was then added to each tube mix and incubated for 30 minutes at room temperature. Upon incubation this mixture was added dropwise to 293T media in their respective plate and cells were incubated for 24hrs. For lentivirus pLKO.1-based lentiviral vector shRNA constructs targeting mouse IRE1α (sh-1 5' CCG GGC TCG TGA ATT GAT AGA GAA ACT CGA GTT TCT CTA TCA ATT CAC GAG CTT TTT 3', sh-2 CCG GCC CAC TTC TCT TTC TTT CTA ACT CGA GTT AGA AAG AAA GAG AAG TGG GTT TTT 3') or mouse XBP1 (sh-1 5' CCG GAG ATA GAA AGA AAG CCC GGA TCT CGA GAT CCG GGC TTT CTT TCT ATC TTT TTT 3', sh-2 5' CCG GCC AGG AGT TAA GAA CAC GCT TCT CGA GAA GCG TGT TCT TAA CTC CTG GTT TTT 3') or human *RTCB* (sh-1 5' CCT TGG TTG TTC CAC AGA GTT 3', sh-2 5' AGA GGC TCC TGA GTC CTA TAA 3') the same described steps were followed except the following amounts of construct and packaging plasmids were used; 7 μg expression plasmid + 4 μg VSVG + 4 μg PSPAX2 packaging plasmids. On day 3, upon 24hrs, supernatant media containing the virus was collected with a 10 mL syringe, which was then filtered through 0.2 μm pore size filters into 15 mL conical tubes. Upon virus collection, plates were replenished with 5 mL of fresh media and incubated for additional 24 hrs, then a second round of virus following the same steps described. Virus was stored at -80°C until ready to use, and the 24 and 48hrs batches of virus collected were combined.

2.3 Stable over-expression cell line generation

Ba/F3 and UT-7 cell lines stably expressing the thrombopoietin receptor (MPL) were generated by retroviral transduction (as described in the retro and lentivirus generation section). However, in this case retroviral supernatants were generated by co-transfection of pMSCV-hygro-hMPL with the packaging plasmids. Viral supernatants were collected at 24- and 48-hours post-transfection. Ba/F3 or UT-7 cells were subjected to spin infection with viral supernatants as follows: cells to be transduced were counted and concentration was adjusted to 3 x 10^6 cells / mL, follow by seeding 500 µL cells per well (in a 6 well plate). 1.5 mL of the virus was then added into each well and leaving one well without virus as untransduced control. Cells were then supplemented with the appropriate cytokines as previously described and 1 µL of polybrene (Millipore sigma) was added into to each well. In a pre-heated centrifuge, plates were spun at 2000 rpm for 2 hours at 37°C. Plates were then removed from centrifuge and placed in incubator overnight. The following day, media was switched culture media and appropriate cytokines. In the other hand, stable expression of CALR variants was achieved by co-transfecting pMSCV-neo-FLAG-tagged-CALR variants (pMSCV-neo-signal peptide-FLAG-CALRwt, -CALRdel52, -CALRins5), pMSCV-IRES-GFP-CALR variants, or pMSCV-puro-P+C with packaging plasmids in 293T cells. Retroviral supernatants were collected at 24- and 48-hours post-transfection. Ba/F3, UT-7, or U2OS cells were subjected to spin infection (as described) with viral supernatants, followed by 7 days of antibiotic selection (neomycin 1 mg/mL; puromycin 2 µg/mL), and cell sorting for GFP positivity.

2.4 Generation of shRNA stable knockdown cell lines

Stable knockdown of endogenous IRE1α or XBP1 or RTCB was achieved using pLKO.1-based lentiviral vector shRNA constructs targeting mouse IRE1α or XBP1 or RTCB (see retro and lenti virus generation for details on virus generation and constructs used). A scrambled shRNA was used as a control. From the lentivirus generated Ba/F3-MPL-CALR cells growing in IL-3 were spin transduced (as previously described) with lentiviral supernatant in the presence of 8 μg/mL polybrene (Sigma). Cell selection began 48 hours post-transduction with 2 μg/ml puromycin (Gibco), or neomycin (G418) 1 mg/ml (Sigma) based on the selection backbone of the vector. Selected cells were then expanded and validated by qPCR and western blot.

2.5 Animal models and bone marrow transplant

All animal use and experiments performed were approved by Institutional Animal Care and Use Committee (ACUP#72596) at the University of Chicago. 6–8-week-old C57BL/6 female mice were purchased from The Jackson Laboratory. For mouse bone marrow transplants, leg bones and spines are removed from CO2 inhalation euthanized healthy mice, and mortar and pestle crushed in PBS (Fisher) + 1% penicillin/streptomycin (Corning). Crushed bone marrows were filtered through 3x rounds of filtration in the following filter size order 100, 70, and 40 μm. Cells filtered were spun down for 5 minutes at 1800 rpm, followed by supernatant removal. Cell pellet was lysed for red blood cells by adding 5 mL of 1x red cell lysis buffer (Invitrogen) and incubated on ice for 5 minutes, then spun down for 5 minutes at 1800 rpm. For c-KIT enrichment, cells were then then resuspended in 500 μL MACS wash buffer (Miltenyi Biotec) and 100 μL murine CD117 Kit (c-KIT) MicroBeads (Miltenyi Biotec) were added, followed by incubation in ice for 20 minutes, with frequent mixing to ensure all cells were stained. Upon incubation, 5 mL of MACS

buffer (Miltenyi Biotec) was added, and cells were spun down for 5 minutes at 1800 rpm. Supernatant was then removed, and cell pellet was resuspended in 4 mL MACS buffer (Miltenyi Biotec) and subjected to positive selection using an autoMACS Pro Separator (Miltenyi Biotec). c-KIT-enriched cells were plated in 10 cm petri dish (non-TC treated) then cultured overnight in SFEM medium (supplemented with 50 ng/mL recombinant murine TPO, 50 ng/mL recombinant murine SCF, 10 ng/mL recombinant murine IL-3, and 10 ng/mL recombinant murine IL-6 (cytokines obtained from R&D Systems). For transduction, 5 mL of the each of the retrovirus generated as previously described for MSCV-IRES-GFP-CALRwt, -CALRdel52 or -CALRins5 constructs was placed into their respective well in a 6 well RetroNectin (Takara Bio) treated plate and c-KIT positive cells were infected via spin infection (30 min at 3000 rpm). Cells were then cultured overnight in SFEM media + cytokine cocktail as formerly described. The following day, each of the cKIT+ cell groups transduced with the given retrovirus CALR variants (1×10^6 per mouse) were resuspended in Hank's Balanced Salt Solution and injected retro-orbitally into lethally irradiated (900 cGy) C57 BL/6 recipient mice. 75 µL of peripheral blood was collected in heparinized capillary tubes retro-orbitally and transfer to EDTA collection tubes to measure complete blood counts (CBC) at 4 weeks post-transplant and at the indicated timepoints. CBCs were obtained by running the blood on the Hemavet 950 FS Auto Blood Analyzer (Drew Scientific).

2.6 RNA sequencing

The sequencing procedure was carried out using the NovaSeq 6000 sequencing (Illumina) at the University of Chicago Genomics Facility (Chicago, IL). RNA extracted from Ba/F3-MPL cells was prepared following the standard protocols recommended by the RNeasy Mini Kit

(Qiagen) and sequenced in two runs to generate paired-end 100bp reads. For each sample, the raw FASTQ files from two flow cells were combined before downstream processing. RNA-Seq data were processed using a local Galaxy 20.05 instance for the following steps: quality and adapter trimming were performed on the raw sequencing reads using Trim Galore! 0.6.3 (288, 289). The reads were mapped to the mouse genome (GRCm38.p4 with GENCODE annotation) using RNA STAR 2.7.5b (290). The resulting mapped reads from each sample were counted by Feature Counts 1.6.4 for per gene read counts (291).

2.7 Statistical analysis for RNA sequencing

The raw counts were analyzed for differential expression between experimental conditions using DESeq2 1.22.1 which also generated a normalized gene expression matrix (292). Gene expression data normalized by DESeq2 were used for gene set enrichment analyses and heat mapping using Morpheus from the Broad Institute (293). For calculation of percent spliced XBP1, mapped reads for XBP1 gene were used from RNA-Seq replicates 1 and 3 to calculate the extent of alternative splicing for each genotype. Specifically, the percentage of spliced reads for a sample was calculated by diving the number of alternatively spliced reads over the total number of XBP1 reads for that sample. Splicing data was analyzed and plotted using Prism. Accession Number: gene expression data are available in the GEO database with the accession number GSE173805.

2.8 Quantitative real-time PCR

Total RNA was extracted from cells using the PureLink RNA Mini Kit as directed by their protocol (Invitrogen). cDNA was synthesized from 1 μg of RNA template using the iScript cDNA Synthesis Kit (BioRad) as follows: for each sample the following was combined, 4μl of 5x iScript

reaction mix, 1 µl of iScript reverse transcriptase, and 15 µl of the following: 1 µg of the RNA template and as much as nuclease-free water needed to make 15 µl total. Samples were then incubated in the thermocycler under the following protocol sequence, 5 minutes at 25°C > 20 minutes at 46 °C > 1 minute at 95 °C and final hold at 4°C. Upon cycle completion, cDNA concentration was measured via nanodrop. For qPCR the following was performed, the employed primers were diluted to 25 uM. For each primer pair the following master mix was made: 0.2 µl forward primer, 0.2 µl reverse primer, 5.0 µl SYBR green (Applied Biosystems) and 3.6 µl H2O. cDNA was then diluted 10 ng/µl and into each well of a 96-well plate (performed as triplicate with 3 H2O controls, the following was added: 1 µl of the diluted cDNA and 9 µl of the master mix. Samples were run under standard thermal cycling program for qPCR in the QuantStudio Real-Time qPCR system (Fisher). Primers used for qPCR are listed below (**Table 2.1**). Beta-actin was used for normalization.

Table 2.1 qPCR primers information		
Gene	**Forward (5' to 3')**	**Reverse (5' to 3')**
Beta-actin (mouse)	CATTGCTGACAGGATGCAGAAGG	TGCTGGAAGGTGGACAGTGAGG
ITPR1 (mouse)	CTCTGTATGCGGAGGGATCTAC	GCGGAGTATCGATTCATAGGAC
ADAM10 (mouse)	GAAGATGGTGTTGCCGACAG	ATTTCCATACTGACCTCCCAG
DNAJB9 (mouse)	TCGGGGCGCACAGGTTATTAG	ATCCTGGCGTGTGTGGAAG
XBP1 (mouse)	ACATCTTCCCATGGACTCTG	TAGGTCCTTCTGGGTAGACC
BCL-2 (mouse)	GGATAACGGAGGCTGGGATGC	ACTTGTGGCCCAGGTATGC
Beta-actin (human)	CACCATTGGCAATGAGCGGTTC	AGGTCTTTGCGGATGTCCACGT
ITPR1 (human)	GTGACAGGAAACATGCAGACTCG	CAGCAGTTGCACAAAGACAGGC

Table 2.1 qPCR primers information (Continuation)		
ITPR2 (human)	CTTCCTCTATGGGGACATC	GGCAGAGTATCGATTCATAGGG
ADAM10 (human)	CTGGCCAACCTATTTGTGGAA	GACCTTGACTTGGACTGCACTG
SERP1 (human)	AAATCTAGGGCGACGCTTGACAGA	AAGAGGAAGGAAACGCAACGCAAC
BCL-2 (human)	ATCGCCCTGTGGATGACTGAGT	GCCAGGAGAAATCAAACAGAGGC
IRE1α (human)	GCCGAAGTTCAGATGGAATC	ATCTGCAAAGGCCGATGA
RTCB (human)	GAAGGAGCAACTTGCCCAAGCT	AGTGCTCCTTGTCTTCAGCCCA

2.9 Protein purification

CALR variants were cloned into the pBAD-DEST49 expression vector, then transformed into One Shot BL21 (DE3) chemically competent *E. coli* cells. Transformed cells were grown in Luria broth (LB) under ampicillin selection followed by the addition of 0.02% L-arabinose for induction of CALR expression. After 4 hours, cells were harvested and lysed via sonication. Proteins were purified using ProBond resin (Invitrogen). Purification was performed as directed by the ProBond purification system protocol (Invitrogen). The eluted proteins were validated via western blot.

2.10 Western blotting

To make cell lysates from each of the samples described, cells were spun down for 1 minute in a 15 mL conical tube at 1500 rpm, cell pellets were then transferred to a 2 mL Eppendorf tube using ice cold 1x PBS. Tubes were spun down for 30 seconds at 13k rmp, and PBS was removed from the cell pellet. Cell pallets were then resuspended in Nonidet P-40 (Fisher) lysis buffer supplemented with protease inhibitors (PI) (Fisher). Samples were then rotated in cold room (4°C)

for 20 minutes, followed by spun down for 20 minutes (4°C) at 13k rmp. Supernatant was then removed and placed into a 1.5 mL Eppendorf tube. To determine protein concentration a standard Bradford assay was performed. Based on the protein concentration determined for each of the samples, the final protein concentration was adjusted to 2 μg/μL using lysis buffer + PI.2x SDS (sodium dodecyl sulfate) sample buffer (Invitrogen) was added to each sample (1:1 ratio SDS: total volume). Samples were then boiled for 10 minutes in 95°C heat block. Samples were then either frozen or loaded (20 μg/well) and resolved on pre-made SDS-PAGE (polyacrylamide gel electrophoresis) (Invitrogen Novex Tris-Glycine) using Tris-Glycine SDS running buffer. 5 μL of protein standard ladder were loaded into each gel (BioRad Precision Plus Protein). Samples ran at 225 V until separated. Gels were then transferred into transferred to nitrocellulose membranes utilizing the iBlot 2 Gel Transfer Device (Fisher) following its given transfer protocol. For primary antibody incubation, membranes were incubated for 1 hour in 5% powder milk in Tris Buffered Saline Buffer + Tween 20 (TBST) buffer at room temperature. Following blocking, membranes were incubated with respective antibodies (see **Table 2.2** below for information on antibodies used) at dilution of 1:1000 (antibody: TBST buffer) for 1 hour at room temperature or overnight at 4°C on a rocker. For secondary antibody incubation, membranes were washed twice with TBST buffer for 30min each on a rocker at room temperature. Upon washes, membranes were incubated with HRP-conjugated secondary antibody (see see table below for information on antibodies used) for 1 hour at room temperature. Membranes were then washed twice, 30 minutes each with TBST buffer on a rocker at room temperature. For membrane development, 1:1 SuperSignal West Dura (Fisher) and pipetted on membrane until fully covered, followed by incubation in the dark for 2 minutes. Membrane was then placed in iBright Imagining Analysis Software (fisher) and analyzed via its chemifluorescence detection input.

Table 2.2 Antibodies information		
Antibody target	**Source**	**Identifier (catalog number)**
p-IRE1α (human + mouse)	ABclonal	Cat# AP1146
IRE1α (human + mouse)	Cell signaling	Cat# 3294
XBP1s (human + mouse)	Cell signaling	Cat# 40435
XBP1s (human + mouse)	Abcam	Cat# ab37152
β-actin (human + mouse)	Cell signaling	Cat# 12620
LSD1 (human + mouse)	Cell signaling	Cat# 2139
MEK1 (human + mouse)	Cell signaling	Cat# 2352
CALR (human + mouse)	Cell signaling	Cat# 12238
CALR mutant c-terminus (human)	HistoBiotech	Cat# HG-CAL2-250
BCL-2 (human)	Cell signaling	Cat# 4223
BCL-2 (human + mouse)	Cell signaling	Cat# 3498
p-IP3R (human + mouse)	Cell signaling	Cat# 3760
IP3R (human + mouse)	Cell signaling	Cat# 8568
COL1A1 (human)	Cell signaling	Cat# 39952
Fibronectin (human)	Cell signaling	Cat# 26836
RTCB (human)	Thermofisher	Cat# PA5-44610

2.11 Stains-all assay

For this assay, 25 mL of 10mM Tris Base, pH 8.8, were aliquoted in a 50ml conical tube**.** 0.1% formamide (25 µl) and 0.025% stains-All dye (6.25 mg) (Sigma) were then added. This was followed by vortex and mix until stain-all powder was completely dissolved (until final color was strong violet). CALR recombinant variant proteins were normalized to a concentration of 0.5 µg/ µl. 20 µg of each recombinant protein were incubated in the stains-all complete solution made at a 1:1 ratio (in this case 40 µl of protein + 40 µl of stains all solution). Samples were incubated for 30 min in the dark, followed by spectral absorbance reading at wavelength ranging from 610-650 nm. Acquired spectral data was then analyzed.

2.12 Immunofluorescence and conditioned media preparation

For immunofluorescence in U2OS, cells were grown onto 13 mM Deckgläser Cover Glasses. After transient transfection using FLAG-tagged CALR variants or P+C constructs, cells were washed twice with PBS and fixed with 4% paraformaldehyde for 10 minutes at room temperature. Cells were permeabilized with 0.1% triton X-100 and blocked in normal donkey serum for 1 hour at room temperature. Cells were then incubated with the corresponding primary antibodies overnight in 4 degrees C. Cells were washed twice and incubated with secondary antibody for 1 hour at room temperature. The cells were then washed twice and mounted onto slides using ProLong Gold Antifade Reagent with 4′,6-diamidino-2-phenylindole (DAPI). For immunofluorescence in HS-5 cells, coverslips were coated in poly-L-lysine for 1 h at room temperature followed by rinsing with sterile H_2O (three times 1 h each). These were then placed in ultraviolet (UV) light overnight to dry and sterilize. HS-5 cells were then plated and grown in the coated slides in a 6-well plate under required growth conditions. 24 hrs post seeding, cells were treated with either conditioned media from UT7-MPL cells expressing CALR variants (72hrs or 7 days) or recombinant TGF-β1((2.5 ng/ml) for 48 hours). Conditioned media was obtained from UT-7-MPL cells expressing CALR variants by seeding 3.0×10^6 in 3 mL of growth media (minus cytokines) in 6-well plate and collecting the cell conditioned media after 24 hrs via centrifugation at 4k rpm. Upon HS-5 incubation under the given conditions, media was removed, and cells were incubated in 100% methanol (chilled at -20°C) at room temperature for 5 min for fixation. Upon fixation, cell slides were washed three times with ice-cold PBS. Cells were then blocked via incubation with 1% BSA, 22.52 mg/mL glycine in PBST (PBS+ 0.1% Tween 20) for 30 min. Following this, cells were incubated in the described antibodies (1:100) in 1% BSA in PBST 1 h

at room temperature. Upon incubation cells were washed three times with PBS, 5 min each wash. Cells were then incubated with fluorescence dye-conjugated secondary antibody in 1% BSA for 1 h at room temperature in the dark. The secondary antibody solution was then washed three times with PBS for 5 min each in the dark. Finally, a drop of mounting medium (ProLong Gold Antifade Reagent) was applied to each of the slides, and the coverslip was mounted. Nail polish was applied to seal coverslip and stored in the dark until imaged via fluorescence microscopy.

2.13 Intracellular calcium imaging

U2OS cells were seeded at 0.5×10^6 cells per 1 mL of DMEM. After 24 hours, cells were transiently co-transfected with venus fluorescent iV2-CALR variant plasmids and red fluorescent pCMV-R-CEPIAer, which was a gift from Masamitsu Iino (Addgene plasmid # 58216; http://n2t.net/addgene:58216 ; RRID:Addgene_58216). Cells were imaged on the Leica Stellaris 8 Laser Scanning Confocal the following day.

2.14 Calcium imaging analysis

Venus expressing cells were segmented using the ROI manager on ImageJ. The intensity of the red fluorescent expression for each cell (5 cells per condition) was calculated then averaged.

2.15 ELISA assay

Enzyme-linked immunosorbent assay (ELISA) was performed in conditioned media of UT7-MPL cells expressing CALR mutant variants. Conditioned media was collected from cells plated $1.5x10^6$ cells per well in a 6-well plate and 3 mL of growth media after 24hrs. ELISA assay

was performed and followed as indicated by the manufacturers protocol (R&D systems, Cat# DB100B).

2.16 Cell Proliferation Assay

Cultured Ba/F3-MPL or UT-7-MPL cells were washed 4 times with PBS to starve them of cytokines, then grown in RPMI-1640 supplemented with 10% FBS (Ba/F3) or 20% FBS (UT-7) and 5% penicillin/streptomycin. Cells were then seeded in triplicate with the indicated treatments at 1.25×10^5 cells/mL in the presence or absence of cytokines for the indicated time points. Living cells were counted at each time point using a Vi-CELL automated cell counter (Beckman Coulter).

2.17 Annexin V/Propidium Iodide stain flow cytometry

Ba/F3-MPL or UT7-MPL cells were harvested, washed 3 times with PBS and stained with FITC-Annexin V (BD) and propidium iodide, and incubated in the dark at room temperature for 20 minutes. Cells were then re-suspended in 1X Annexin V Binding Buffer (BD), and the percentage of apoptotic and dead cells was measured on the Beckman CytoFLEX S flow cytometer.

2.18 Drug preparation and treatments

KIRA8 was a gift from Scott Oakes. For cell use purposes KIRA8 was given as a stock concentration of 20mM, which was then further diluted in Dimethylsulfoxide (DMSO) to 10,000 uM. From this concentration, KIRA8 was diluted in the respective cell growth to the desired dose (in our case 5 uM) while DMSO was used a vehicle control. For mouse *in vivo* experiments, KIRA8 was dissolved in the following vehicle is 3% Ethanol, 1.2% sterile water, 7% Tween 80, and 88.8% of 0.85% NaCl and prepared as follows based on the amount of drug necessary (we did

50 mg/kg/day per mice): 100 mg of KIRA8 was added to 300 uL of 200 proof ethanol. This was then mixed in 120 uL of Milli Q water and briefly pulsed mixed in a 90°C heat block. Tubes were removed from heath block every few seconds, followed by vortex, and repulse until drug was dissolved completely (without over heating). 700 uL of Tween 80 were added followed by thorough mix and vortex. Drug mix was diluted to 10 mL with 0.85% NaCl followed by vortex/invert to mix thoroughly. The full solution was passed through a 0.22-micron syringe filter and then aliquot as desired. Drug aliquots were prepared 2-3 days before injections and stored at 4°C and maintained in ice during injections. 2-Aminoethoxydiphenyl borate (2-APB) was purchased from Santa Cruz Biotechnology. For use, 2-APB was diluted in DMSO at 10 mM and then further diluted in growth media at the use treatment concentration of 100 uM. Venetoclax (ABT-199) was purchased from Abcam and diluted in DMSO at 50 mM. This concentration was further diluted in growth media at the use treatment concentration of 1 μM. Venetoclax was administered in mice at a dose of 25 mg/kg by oral gavage. Venetoclax treatment in mice was delivered in the following vehicle 60% phosal 50 propylene glycol, 30% polyethylene glycol (PEG) 400, 10% ethanol, and this same vehicle solution was used a control. 2-Aminoethoxydiphenyl borate (2-APB) was purchased from Santa Cruz Biotechnology. For use, 2-APB was diluted in DMSO at 10 mM and then further diluted in growth media at the use concentration of 100 uM.

2.19 Immunohistochemistry

Spleens and bone marrow were resected, fixed in formalin, and embedded in paraffin before being mounted onto Vectabond-coated Superfrost Plus Slides. Slides were baked at 60 degrees C overnight, deparaffinized by 5-minute washes three times in xylene, hydrated in a graded

series of ethanol washes, and rinsed with distilled water. Epitopes were retrieved by heating samples in 10 mM Tris-EDTA buffer, pH 9 on high until boiling followed by 10 minutes on low. For XPB1 staining, sections were incubated in an XBP1 antibody (Abcam), diluted 1:500 using RTU horse serum overnight at 4 degrees C. After incubation in the primary antibody, sections were washed and incubated in ImmPRESS secondary antibody for one hour at room temperature. Sections were then washed three times and nuclear stained with Hematoxylin before two graded series of ethanol washes and one xylene wash for 30 minutes prior to mounting using Permount. Images were captured using the Zeiss Axioskop upright histology microscope at 40X magnification and analyzed using ImageJ software and 3D hisTECH.

2.20 Histopathology

Mouse tissues (bone marrow and spleen) were fixed in 10% neutral buffered formalin, embedded in paraffin, and stained with hematoxylin and eosin (H&E). Images of histologic slides were obtained on the CRi Pannoramic MIDI scanner (Cambridge Research and Instrumentation). Bone marrow megakaryocytes were analyzed and quantified by two independent pathologists who were blinded to mouse genotype and represent an average megakaryocyte count from 10 high-power fields assessed.

2.21 Statistical analysis

All comparisons represent two-tailed unpaired Student's t test analysis unless otherwise specified. $p < 0.05$ = *; $p < 0.01$ = **; $p < 0.001$ = **

CHAPTER 3: TYPE 1 CALR MUTATIONS ACTIVATE THE IRE1α /XBP1 ARM OF THE UNFOLDED PROTEIN RESPONSE TO DRIVE MYELOPROLIFERATIVE NEOPLASMS

Chapter 3 consist in part of the results section from Ibarra and Elbanna et al., *Blood Cancer Discovery* (2022); see publications section.

Sustained ER stress has been documented in many cancer types, and some tumor cells exploit the UPR as a critical mechanism by which to withstand stress and promote survival (264, 265). Although CALR, as an ER chaperone, is an important UPR effector, the role of the UPR in mutant CALR-driven MPNs remains unclear. One study showed that both type 1 and type 2 CALR mutations impair the UPR, but this work was shown in an artificial cell system co-expressing BCR-ABL (266). Other studies have indicated that CALR mutations activate the UPR. One such study showed that CALR mutated CD34+ cells from MPNs patients exhibit transcriptional up-regulation of UPR genes (267), while another performed unbiased proteomics to identify the mutant CALR interactome and found that type 1 and type 2 mutant CALR proteins show enriched binding to UPR proteins compared to wild type CALR (268). Despite these advances in our understanding of calcium signaling and UPR activation in the context of CALR mutations, many outstanding questions remain. Here, we sought to first functionally validate whether the UPR is indeed activated by CALR mutations. Further, given the differences in both amino acid composition and clinical phenotype between type 1 and type 2 CALR mutants, we examined whether the UPR is differentially activated between mutation types, and in so doing provide the first evidence for unique molecular dependencies in type 1 versus type 2 mutant CALR-driven MPNs. In addition, though traditionally considered gain-of-function mutations, we sought to directly answer the

enduring question of whether type 1 CALR mutations serve as loss-of-function mutations in the context of calcium binding ability. Finally, we show that the functional consequence of the differential loss of calcium binding sites induced by type 1 versus type 2 CALR mutations is the activation of and dependency on the UPR, and that this pathway can be targeted for therapeutic intervention in type 1 mutant CALR-driven disease.

3.1.1 Type 1 CALRdel52 mutations differentially activate the IRE1α/XBP1 pathway of the unfolded protein response

To identify whether the UPR is differentially regulated in mutant versus wild type CALR (CALRwt)-expressing cells, and in type 1 CALRdel52 versus type 2 CALRins5-expressing cells, we performed whole-transcriptome RNA sequencing (**Figure 3.2**) using the Ba/F3 cell line model system in which we previously dissected the molecular mechanisms underlying mutant CALR-mediated hematopoietic transformation (**Figure 3.1**) (250, 269). We found that CALRdel52 cells display strong enrichment of IRE1α−mediated UPR as compared to both CALRwt and CALRins5-expressing cells (**Figure 3.3; Table 3.1**).

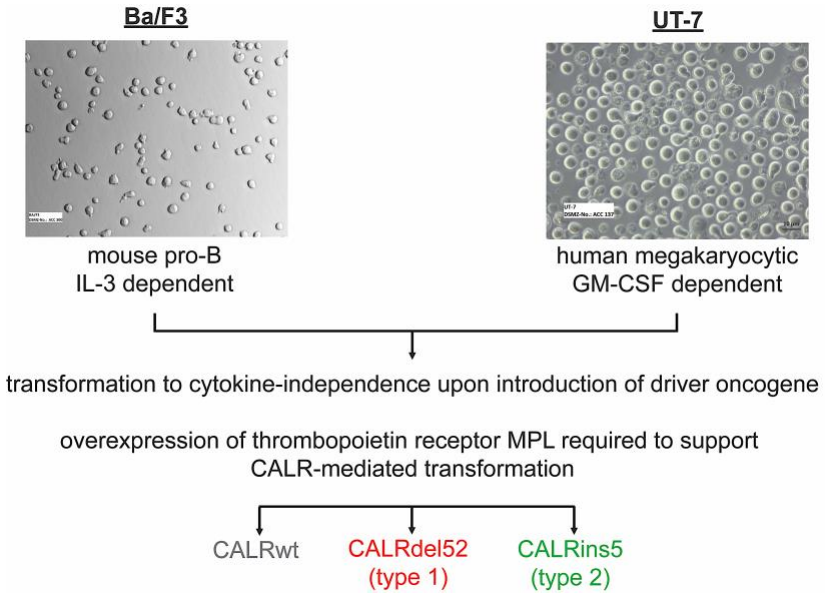

Figure 3.1 CALR mutant myeloproliferative neoplasms *in vitro* cell line models. Workflow for the generation of Ba/F3 (mouse pro-B cell line) and UT-7 MPL (human megakaryocytic) as cell line *in vitro* models for CALR mutant MPN.

In addition to its ER sensor domain, IRE1α possesses two enzymatic domains, an endonuclease (RNase) and a serine-threonine kinase domain, within its C-terminal cytoplasmic tail. Upon sensing misfolded proteins in the ER, IRE1α oligomerizes and trans-autophosphorylates, which activates its endonuclease activity. The RNase domain then initiates an unconventional RNA splicing activity, removing a 26 nucleotide (nt) intron from the X-box binding protein 1 (*XBP1*) mRNA. Rejoining of the remaining mRNA fragments by the RTCB ligase results in translational a frameshift in XBP1 that produces a highly active transcription factor. XBP1 then translocates to the nucleus to execute various transcriptional programs involved in adaptation to cellular stress (270, 271).

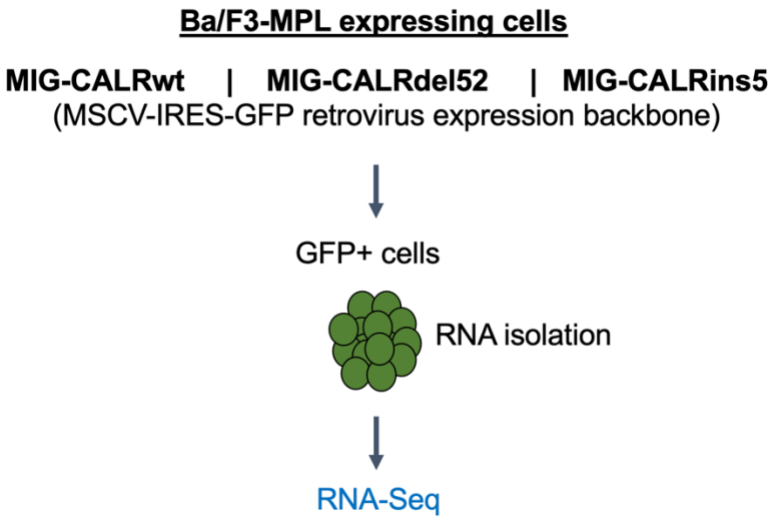

Figure 3.2 Workflow for RNA-Seq experiment in Ba/F3-MPL cells expressing CALR variants in MSCV-IRES-GFP (MIG) backbone. Upon CALR variants expression, cells were sorted for GFP positivity. RNA was isolated and sent to UChicago Genomics facility for RNA-sequencing.

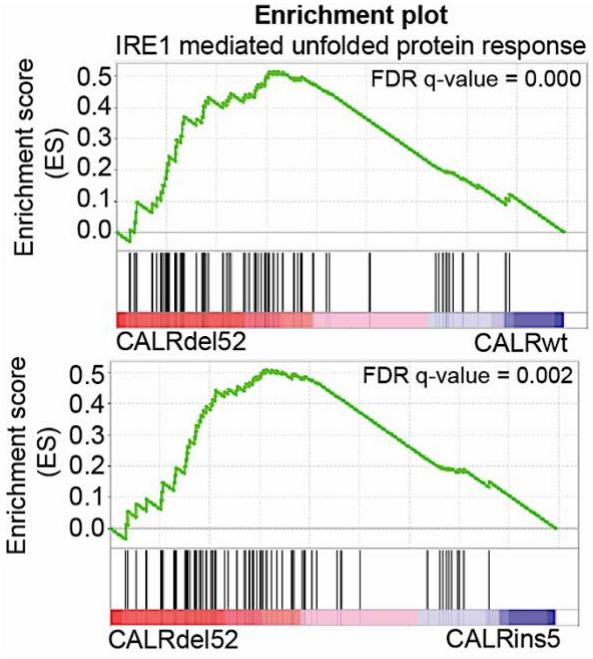

Figure 3.3 GSEA plots for IRE1α mediated unfolded protein response in Ba/F3-MPL-CALRdel52 cells versus Ba/F3-MPL-CALRwt cells and Ba/F3-MPL-CALRins5 cells. (Contributions: J.I., H.G., Q.S.).

Table 3.1 GSEA information

Gene set	# of genes	Comparison	Direction of enrichment	ES	NES	FDR q-value	Nominal p-value	FWER p-value	Reference
GO_IRE1_MEDIATED_UNFOLDED_PROTEIN_RESPONSE	67	CALRdel52 v CALRwt	Up in CALRdel52	0.51554465	1.7148542	0	0	0	1, 2
		CALRdel52 v CALRins5	Up in CALRdel52	0.511103	1.5929528	0.001	0.0018018018	0.001	
KEGG_CALCIUM_SIGNALING_PATHWAY	178	CALRdel52 v CALRwt	Down in CALRdel52	-0.41716456	-1.6352867	0	0	0	3, 4
		CALRdel52 v CALRins5	Down in CALRdel52	-0.43079248	-1.5916203	0	0	0	
GO_BH_DOMAIN_BINDING	11	CALRdel52 v CALRwt	Up in CALRdel52	0.68182033	1.5257971	0.027	0.027826088	0.016	5, 6
		CALRdel52 v CALRins5	Up in CALRdel52	0.5055993	1.1025407	0.367	0.36734694	0.198	

1 http://amigo.geneontology.org/amigo/term/GO:0036498
2 https://www.gsea-msigdb.org/gsea/msigdb/cards/GOBP_IRE1_MEDIATED_UNFOLDED_PROTEIN_RESPONSE.html
3 https://www.gsea-msigdb.org/gsea/msigdb/cards/KEGG_CALCIUM_SIGNALING_PATHWAY.html
4 https://www.genome.jp/kegg/pathway/hsa/hsa04020.html
5 https://www.gsea-msigdb.org/gsea/msigdb/cards/GOMF_BH_DOMAIN_BINDING.html
6 http://amigo.geneontology.org/amigo/term/GO:0051400

Given the enrichment of IRE1α-mediated UPR genes in CALRdel52 compared to CALRwt and CALRins5-expressing cells, we next assessed spliced XBP1 in CALRdel52 versus CALRwt and CALRins5 cells at the protein level. Indeed, consistent with our RNA-Seq results, we found that CALRdel52-expressing Ba/F3-MPL, human megakaryocytic UT-7-MPL demonstrate

increased levels of spliced XBP1 (XBP1s) protein compared to CALRwt- and CALRins5-expressing cells, this was accompanied with increased IRE1α phosphorylation (**Figure 3. 4).** Lastly, we examined XBP1s transcriptional activity by performing quantitative PCR (qPCR) of canonical XBP1s target genes in UT-7-MPL cells. In accordance with our previous results, we found significantly increased expression of XBP1 target genes DNAJB9, ADAM10, and SERP1 (**Figure 3.5**), in type 1 CALRdel52- compared to CALRwt and type 2 CALRins5-expressing cells. Together, these results confirm that the IRE1α/XBP1 pathway of the UPR is differentially activated in CALRdel52 compared to CALRwt and CALRins5 cells.

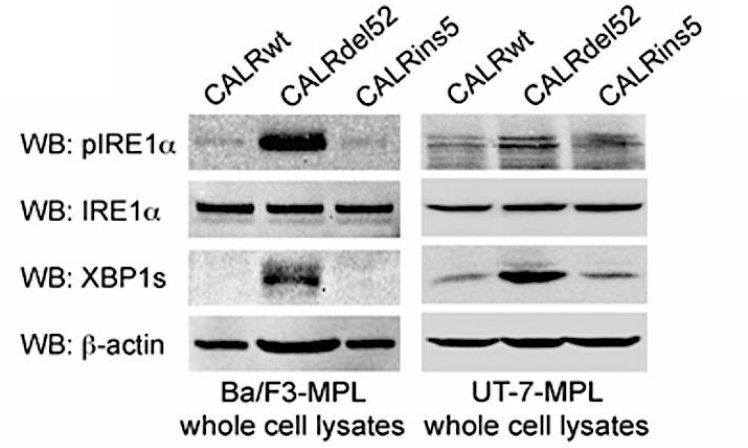

Figure 3.4 Expression of IRE1α/ XBP1 pathway components and canonical gene targets in B a/F3-MPL and UT-7-MPL cells expressing CALR variants. Western blot for phospho-IRE1α, total IRE1α and spliced XBP1 (XBP1s) in Ba/F3-MPL and UT-7-MPL cells expressing CALR variants (Contributors; J.I.).

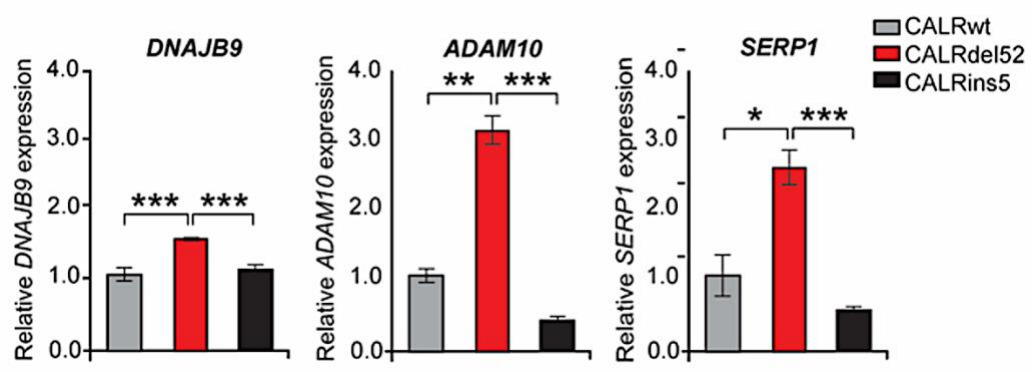

Figure 3.5 qPCR for XBP1 targets *DNAJB9*, *ADAM10*, and *SERP1* in UT-7-MPL cells. Each bar represents the average of three 3 replicates. Error bars denote standard deviation (SD). Significance was determined by 2-tailed Student's t-test (* $p<0.05$; ** $p<0.01$; *** $p<0.001$). (Contributors: J.I., K.K.).

3.2.2 Type 1 CALRdel52 mutations lead to loss of calcium binding function, resulting in ER calcium depletion

Given the differential activation of IRE1α/XBP1 by CALRdel52 compared to CALRins5, we hypothesized that the molecular mechanism underlying this activation may be related to the loss of calcium binding residues unique to the type 1 protein (**Figure 1.7**). We first analyzed our RNA-Seq data for global transcriptomic changes in Ca2+ signaling pathways between CALRdel52 versus CALRwt or CALRins5-expressing cells. We found that Ca2+ signaling pathway genes were significantly enriched in CALRdel52- as compared to CALRwt and CALRins5-expressing cells (**Figure 3.6: Left**). This suggests that there are indeed differences in calcium regulation unique to CALRdel52 cells.

Next, we asked whether the CALRdel52 protein does in fact lose its ability to bind Ca2+ as a result of the loss of Ca2+ binding residues in the C-terminus. In order to examine this, we performed a Stains-All assay as a metric of Ca2+ binding ability. Stains-All is a cationic carbocyanine dye which, upon interaction with acidic Ca2+-binding residues, produces a dye-

protein complex that increases the absorbance spectrum of the dye (273). We found that incubation of purified, recombinant CALR proteins (rCALR) (**Figure 3.6: Right**) with Stains-All dye led to similar increases in absorbance in CALRwt and CALRins5 protein-dye complexes compared to Stains-All alone, suggesting similar Ca2+ binding capabilities between the two proteins. However, CALRdel52 protein-dye complexes resulted in a significantly decreased absorbance compared to CALRwt and CALRins5, and no significant increase in absorbance compared to Stains-All alone (**Figure 3.6: Center**). Together, this suggests that CALRdel52 mutations, but not CALRins5 mutations, lead to loss of Ca2+ binding function.

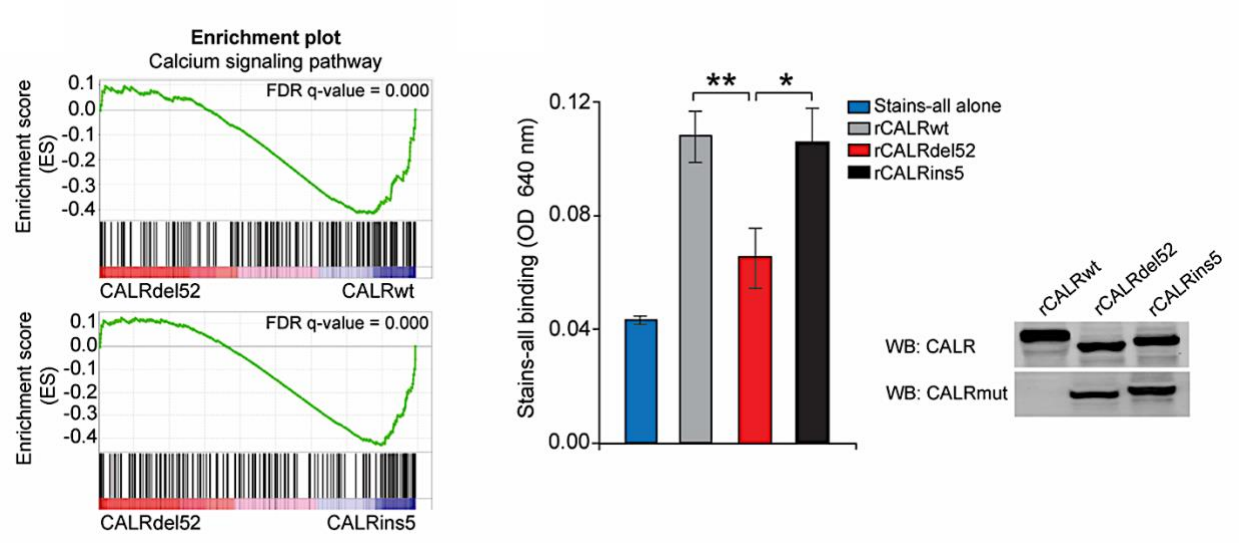

Figure 3.6 Left: GSEA plots for Calcium signaling pathway in Ba/F3-MPL-CALRdel52 cells versus Ba/F3-MPL-CALRwt cells (left top) and Ba/F3-MPL-CALRins5 cells (left bottom). Center: Absorbance (640 nm) of 20 µg of recombinant CALRwt, CALRdel52, CALRins5 incubated with 0.025% stains-all solution to indirectly measure the calcium binding ability of each rCALR protein. Each bar represents the average of 3 independent replicates. Error bars denote standard deviation (SD). Significance was determined by 2-tailed Student's t-test (* $p<0.05$; ** $p<0.01$). Right: Western blot for CALR (which detects both wild type and mutant CALR) and mutant CALR (which only detects the mutant C-terminus) for rCALR proteins used in Stains-all assay (Contributions: J.I., H.G., Q.S.).

To next assess the functional effects of the loss of CALRdel52 Ca2+ binding ability, we performed Ca2+ imaging studies using a genetically encoded ER-targeted red fluorescent Ca2+ indicator, R-CEPIA1er (274). This sensor is designed to bind free intraluminal ER Ca2+ that is not bound by other proteins, and thus serves to qualitatively measure ER calcium concentration. Here, we used the human bone osteosarcoma cell line U2OS, an adherent cell line with abundant ER that has been shown to be optimal for live imaging studies. Cells were transiently co-transfected with plasmids encoding CALRwt, CALRdel52, and CALRins5 in a backbone expressing Venus fluorescent protein (iV2) (275) and the plasmid encoding the R-CEPIA1er Ca2+ sensor 48 hours prior to imaging. Cell imaging studies revealed that cells transfected with CALRdel52 plasmid demonstrated significantly decreased fluorescence of the ER Ca2+ sensor, indicating decreased ER Ca2+ concentration, compared to cells expressing CALRwt or CALRins5 Notably, this was not due to an inability of CALRdel52 to localize to the ER, as immunofluorescence studies demonstrated similar ER localization of FLAG-tagged CALRwt, CALRdel52, and CALRins5, evidenced by the overlap of staining for ER marker calnexin (red) with anti-FLAG (green). We thus conclude that loss of Ca2+ binding sites on the CALRdel52 protein leads to a loss of Ca2+ binding function, resulting in diminished ER Ca2+ storage capacity and depleted ER calcium levels. Further, to get to the mechanism, we show that depletion of ER Ca2+ by CALRdel52 mediates activation of the IRE1α/XBP1 pathway, and that this activation can be rescued by introduction of a functional CALR Ca2+ binding construct. (This data was work from Elbanna Y. and is shown in Ibarra and Elbanna., et al *Blood Cancer Discovery* (2022) Figures 2 & 3) (294).

3.2.3 Type 1 mutant CALRdel52-expressing cells are dependent on depleted ER calcium to activate IRE1α/XBP1, which promotes cell survival via up-regulation of BCL-2

Early outputs of UPR activation attempt to restore protein homeostasis by increasing protein-folding capacity so the cell continues to survive and function. However, if these adaptive responses are inadequate, the UPR ER stress sensors, including the IRE1α/XBP1 arm, can initiate an alternative response called the terminal UPR, which in turn promotes cell death. Several studies have found that not only is IRE1α/XBP1 activated across different cancers, but that it might be necessary for the survival and growth of cancer cells under conditions of ER stress (277). Having discerned the mechanism of ER stress underlying activation of the IRE1α/XBP1 pathway in CALRdel52 cells, we next asked whether this pathway represents a unique molecular dependency that promotes CALRdel52 cell survival.

To further interrogate the specific requirement of IRE1α and XBP1s for CALRdel52 cell survival, we generated shRNA knockdowns against IRE1α and XBP1 in Ba/F3-MPL cells. Knockdown efficiency of the top scoring shRNAs against IRE1α (**Figure 3.7: Top**) and XBP1 (**Figure 3.7: Center**) were validated by western blot. Trypan blue exclusion cell counting assays demonstrated that cell viability was significantly decreased only in CALRdel52 cells upon knockdown of IRE1α and XBP1 (**Figure 3.7: Bottom**), suggesting that this pathway is required by CALRdel52 cells, but not CALRwt or CALRins5 cells for survival.

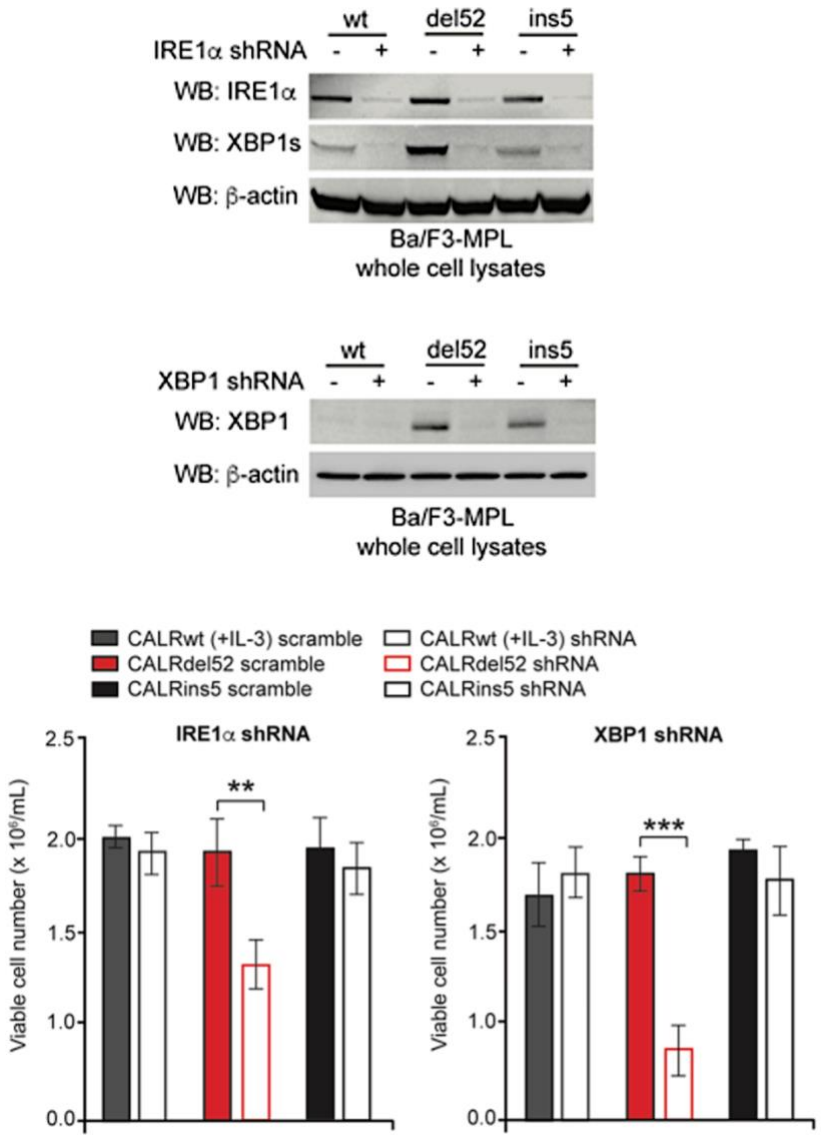

Figure 3.7 Top: Western blot for IRE1α and XBP1s in Ba/F3-MPL cells expressing CALR variants and either a scrambled shRNA or shRNA against IRE1α. Center: Western blot for XBP1 in Ba/F3-MPL cells expressing CALR variants and either a scrambled shRNA or shRNA against XBP1. Bottom: Total viable cell number at 48 hours post IL-3 withdrawal in Ba/F3-MPL cells expressing CALR variants and either a scrambled shRNA or shRNA against IRE1α (left) or XBP1 (right). Ba/F3-MPL-CALRwt cells grown in the presence of IL-3 was included as a control. Each bar represents the average of 3 independent replicates. Error bars denote standard deviation (SD). Significance was determined by 2-tailed Student's t-test (** $p<0.01$; ***$p<0.001$). (Contributors, J.I.)

We next sought to further dissect the mechanism by which IRE1α/XBP1 promotes cell survival, with a particular focus on the anti-apoptotic protein BCL-2. Although its function is best characterized in mitochondria, BCL-2 has also been shown to localize to the ER (278), where it plays a role in the control of Ca2+ homeostasis. Interestingly, BCL-2 over-expression has been shown to inhibit apoptosis in the face of depleted ER Ca2+ (279-281). Given the CALRdel52-driven phenotype of ER Ca2+ depletion and consequential IRE1α/XBP1 activation we observed, we asked whether BCL-2 may act downstream of IRE1α/XBP1 to promote continued cell survival. Notably, BCL-2 has been shown to regulate the IRE1α/XBP1 pathway, whereby BCL-2 enhances IRE1α endonuclease activity to promote sustained production of XBP1s (282). However, whether BCL-2 can also act downstream of IRE1α/XBP1 to promote cell survival remains unclear.

To address this question, we first analyzed our RNA-Seq for BH (BCL-2 homology) domain binding signatures in CALRwt, CALRdel52 and CALRins5-expressing cells. We found significant enrichment of BH domain binding genes in CALRdel52 compared to CALRwt (**Figure 3.8**). Among the anti-apoptotic genes, we found to be up-regulated specifically in CALRdel52 compared to CALRwt and CALRins5, we chose to focus on BCL-2 given its role in modulating the apoptotic response to ER Ca2+ depletion.

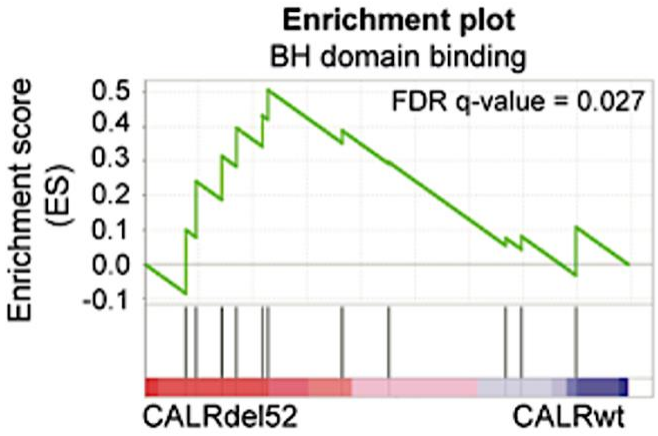

Figure 3.8 GSEA plots for BH domain binding in Ba/F3-MPL-CALRdel52 cells versus Ba/F3-MPL-CALRwt cells (Contributors: JI, Q.S., P.Y.,)

To validate BCL-2 up-regulation in CALRdel52 cells, we performed qPCR for BCL-2 in Ba/F3-MPL cells and UT-7-MPL cells (**Figure 3.9: Top**). In each cell type, we found significant up-regulation of BCL-2 mRNA expression in CALRdel52 cells compared to both CALRwt and CALRins5-expressing cells. We further confirmed this finding at the protein level by western blot in UT-7-MPL cells (**Figure 3.9: Bottom**).

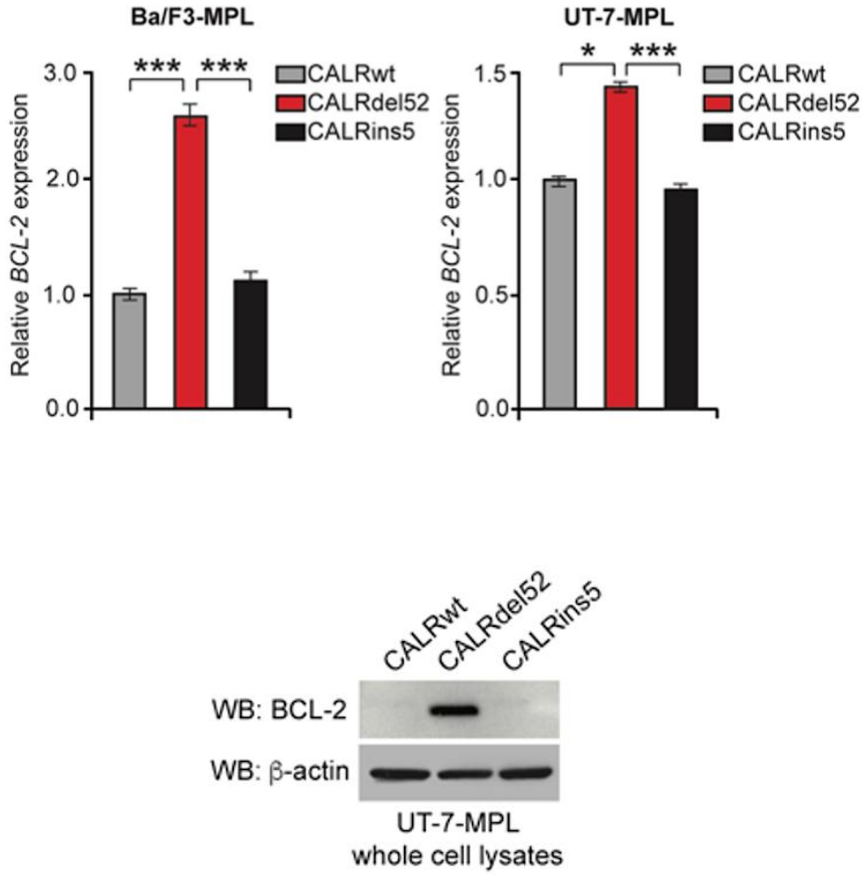

Figure 3.9 qPCR for BCL2 expression in Ba/F3-MPL cells (top left) and UT-7-MPL cells (top right) expressing CALRwt, CALRdel52 and CALRins5. Each bar represents the average of 3 independent replicates. Error bars denote standard deviation (SD). Significance was determined by 2-tailed Student's t-test (* $p<0.05$; ***$p<0.001$). BCL-2 expression in UT7-MPL cells expressing CALR variants (bottom right). (Contributors: J.I., K.K.,)

To determine if the observed BCL-2 up-regulation is mediated by the IRE1α/XBP1 pathway, we performed qPCR (**Figure 3.10: Top)** and western blot (**Figure 3.10: Bottom left)** for BCL-2 in XBP1 knockdown cells, which both display downregulation of XBP1. In all cases, we saw significantly decreased BCL-2 expression in CALRdel52 cells when XBP1 levels were down-regulated. Having validated that BCL-2 is downstream of XBP1 in CALRdel52 cells, we next sought to confirm that XBP1 up-regulates BCL-2 to promote cell survival in CALRdel52 cells. To do this, we treated cells with BCL-2 inhibitor Venetoclax and performed Annexin V/PI staining to assay for apoptosis (**Figure 3.10: Bottom right**). We found that while neither CALRwt nor CALRins5 cells exhibited a significant increase in apoptosis upon Venetoclax treatment, CALRdel52 cells underwent significant apoptotic cell death upon treatment. This suggests that the IRE1α/XBP1 pathway mediates up-regulation of BCL-2 specifically in CALRdel52 cells to promote cell survival in the face of CALRdel52-driven ER Ca2+ depletion.

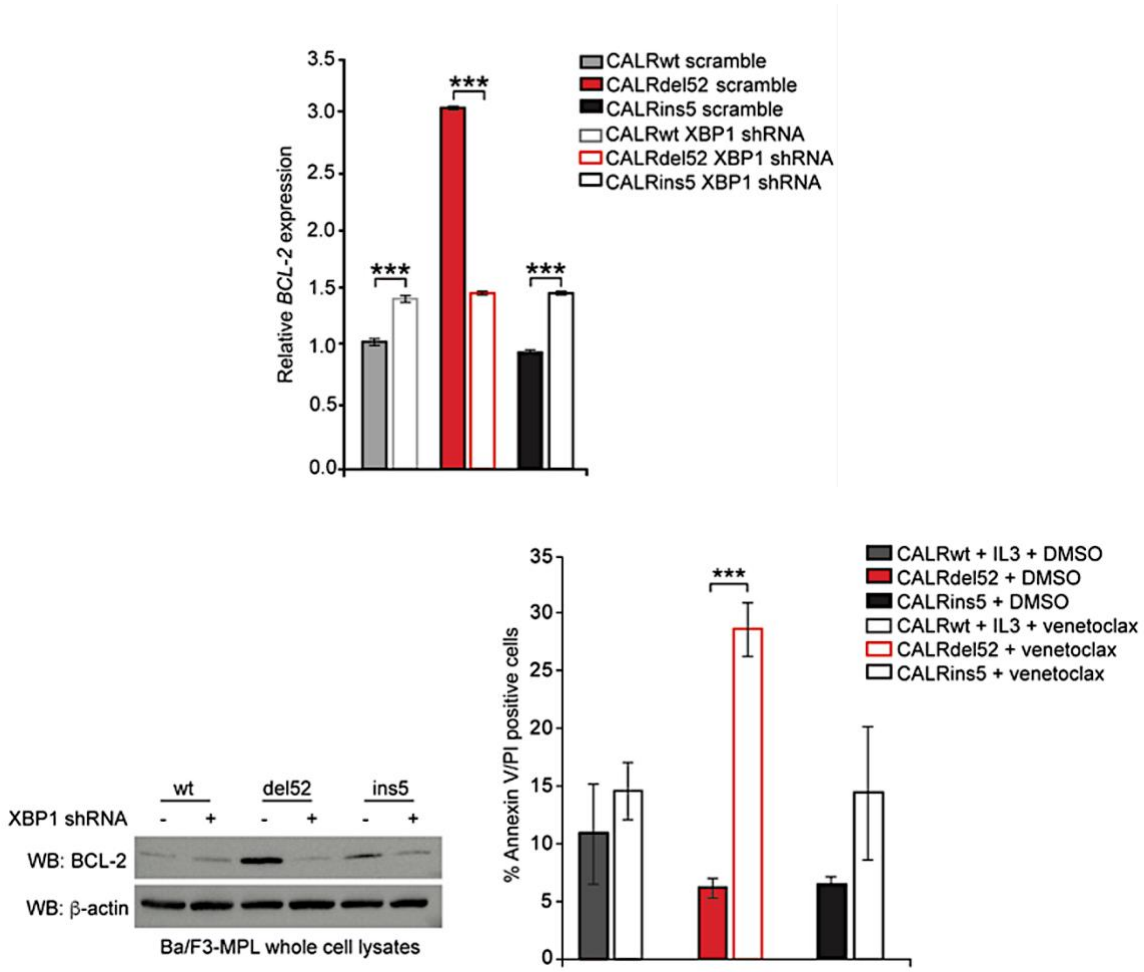

Figure 3.10 Top: qPCR for BCL2 expression in Ba/F3-MPL cells expressing CALR variants and a scramble shRNA or shRNA against XBP1. Each bar represents the average of 3 independent replicates. Error bars denote standard deviation (SD). Significance was determined by 2-tailed Student's t-test (*** $p<0.001$). Bottom left: Western blot for BCL-2 in Ba/F3-MPL cells expressing CALR variants and a scramble shRNA (-) or shRNA against XBP1 (+). Bottom right: Quantification of flow cytometric analysis for Annexin V/PI double positivity in Ba/F3-MPL cells expressing CALR variants and treated with or without Venetoclax (1 μM for 24 hours). Each bar represents the average of 3 independent replicates. Error bars denote standard deviation (SD). Significance was determined by 2-tailed Student's t-test (*** $p<0.001$). (Contributors: J.I., K.K.,)

3.2.4 XBP1 up-regulates the IP3 receptor to induce a positive feedback loop of sustained depleted ER calcium and IRE1α/XBP1 pathway activation in type 1 CALRdel52-expressing cells

Having dissected the requirement for IRE1α/XBP1 signaling in promoting survival of CALRdel52 cells, we next turned our focus to how CALRdel52 cells sustain depleted ER Ca2+ in order to promote continued activation of IRE1α/XBP1 survival signaling. Inositol 1,4,5-trisphosphate (IP3) receptors (IP3Rs) the main Ca2+-release channels in the ER and play a key role in the control of Ca2+ signaling (238). Notably, IP3Rs initiate SOCE, which has been shown to be differentially regulated in mutant versus wild type-CALR expressing cells (252, 261). Interestingly, BCL-2 has been shown to bind IP3R in order to inhibit Ca2+ release from the ER, which in turn prevents apoptosis (284). Here, we hypothesized that because CALRdel52 mutations engender dependency on depletion of ER Ca2+, this mechanism is re-wired to promote IP3R-regulated Ca2+ release from the ER and sustain IRE1α/XBP1 activation, which up-regulates BCL-2 to promote cell survival independent of IP3R inhibition.

To first assess whether IP3R is up-regulated in CALRdel52-expressing cells, we performed qPCR for the IP3R gene ITPR1 in Ba/F3-MPL cells and UT-7-MPL cells (**Figure 3.11: Top**). In each cell type, we found significant up-regulation of ITPR1 mRNA expression in CALRdel52 cells compared to CALRwt and CALRins5-expressing cells. We confirmed this finding at the protein level by western blot in Ba/F3-MPL and UT-7-MPL cells (**Figure 3.211: Bottom**).

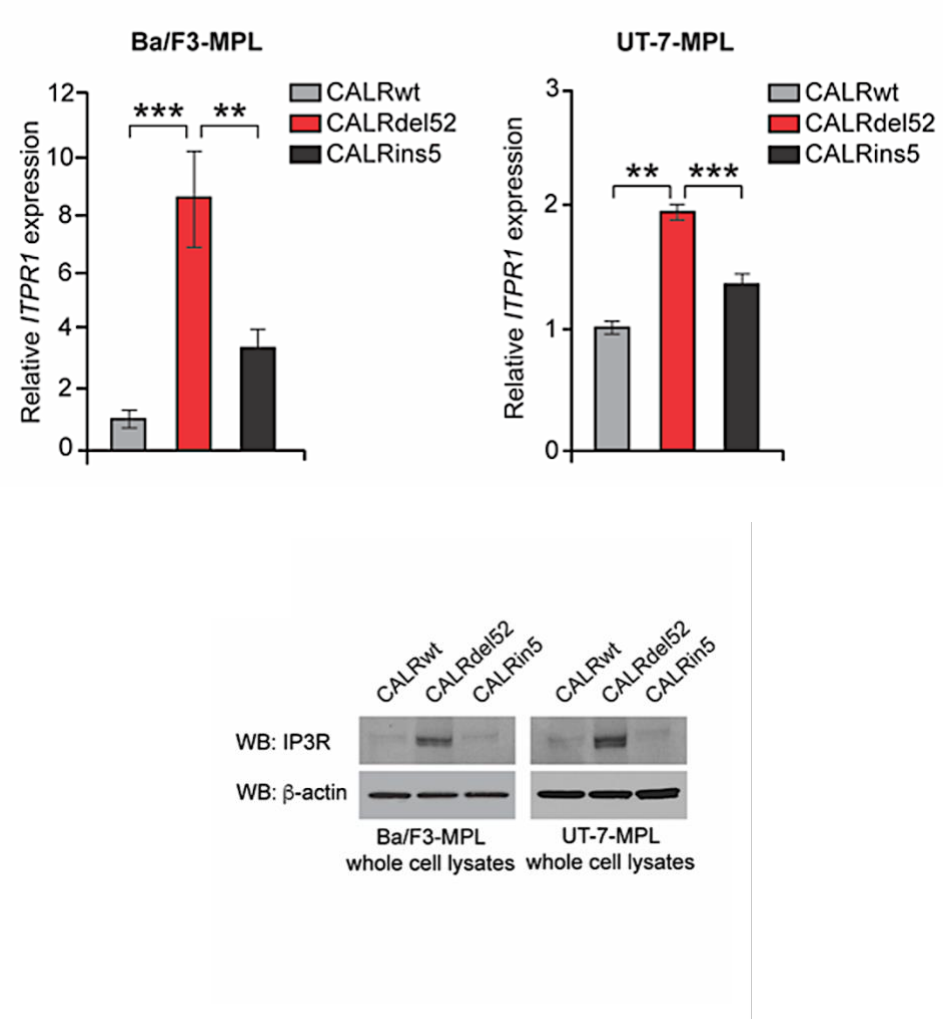

Figure 3.11 qPCR for ITPR1 in Ba/F3-MPL cells (top left) and UT-7-MPL cells (top right) expressing CALRwt, CALRdel52 and CALRins5. Each bar represents the average of 3 independent replicates. Error bars denote standard deviation (SD). Significance was determined by 2-tailed Student's t-test (** $p<0.01$; ***$p<0.001$).Western blot for IP3R in Ba/F3-MPL and UT-7-MPL cells expressing CALR variants. β-actin was used as a loading control (bottom right). (Contributors: J.I., K.K.,)

To determine if this up-regulation is mediated by the IRE1α/XBP1 pathway, we performed qPCR and western blot (**Figure 3.12)** for ITPR1 in XBP1 knockdown cells. We saw significantly decreased ITPR1 mRNA (**Figure 3:12 Top**) and IP3R protein (**Figure 3:12 Bottom**) expression only in CALRdel52 cells in response to XBP1 down-regulation. This suggests that CALRdel52 cells mediate up-regulation of IP3R at least in part via the IRE1α/XBP1 pathway.

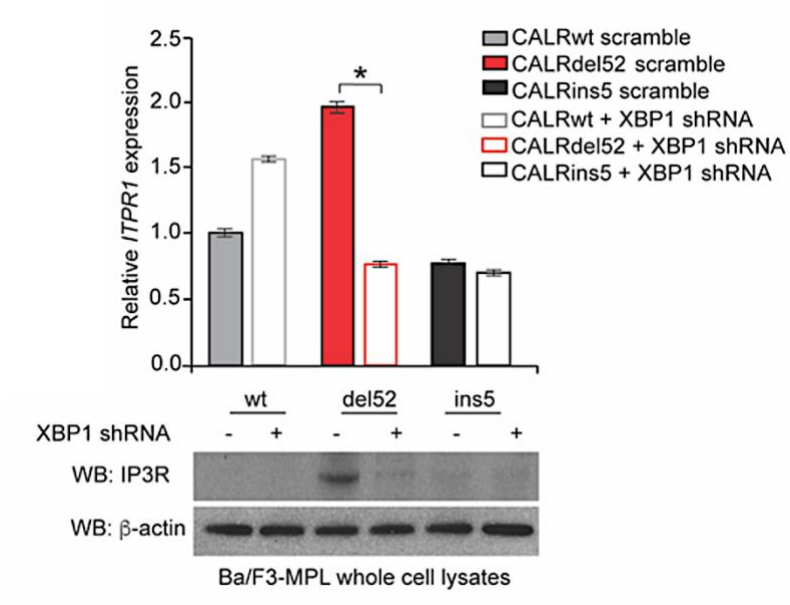

Figure 3.12 Top: qPCR for ITPR1 expression in Ba/F3-MPL cells expressing CALR variants and a scramble shRNA or shRNA against XBP1. Each bar represents the average of 3 independent replicates. Error bars denote standard deviation (SD). Significance was determined by 2-tailed Student's t-test (* $p<0.05$). bottom: Western blot for IP3R in Ba/F3-MPL cells expressing CALR variants and a scramble shRNA (-) or shRNA against XBP1 (+) (Contributors: J.I., K.K.,).

Next, we tested whether IP3R is the channel by which CALRdel52-expressing cells mediate efflux of ER Ca2+ to sustain ER Ca2+ depletion. To do so, we utilized the allosteric IP3R inhibitor, 2-aminoethoxydiphenyl borate (2-APB), which inhibits IP3R Ca2+ release (285). U2OS cells transiently co-transfected with CALR variants and the CEPIA1er Ca2+ sensor was treated with vehicle or 2-ABP for 90 seconds and imaged as previously described in Figures 2 and 3. We found that CALRdel52-expressing cells treated with 2-APB demonstrated significantly increased

ER Ca2+ levels compared to CALRdel52 cells treated with vehicle, as measured by fluorescence of the ER Ca2+ sensor (**Figure 3.13)**. This suggests that IP3R is at least partially responsible for the depleted ER Ca2+ stores in CALRdel52 cells.

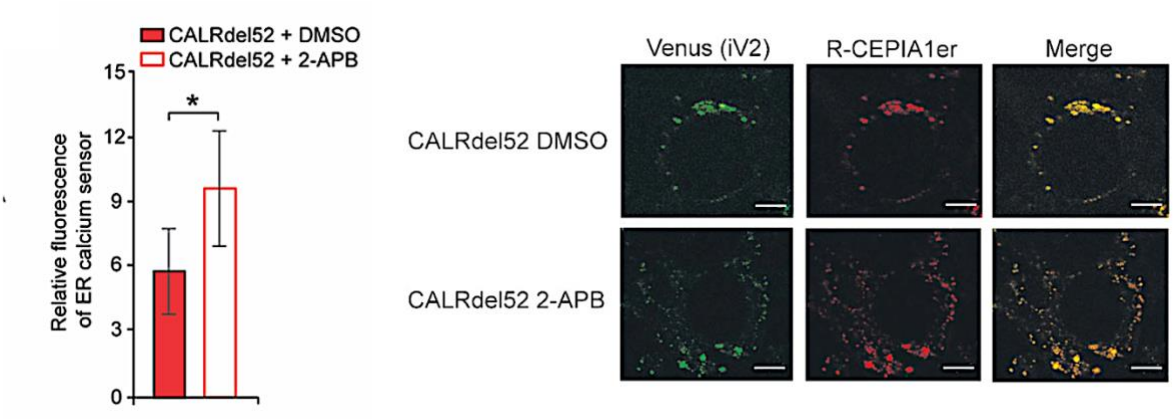

Figure 3.13 Left: quantification of relative fluorescence of Ca2+ sensor in U2OS cells expressing iV2-CALRdel52 treated with or without 2-APB (100 μM for 1.5 minutes). Each bar represents the average of 3 independent replicates. Error bars denote standard deviation (SD). Significance was determined by 2-tailed Student's t-test (* $p<0.05$). Right: Representative images of Ca2+ sensor expression (red) in U2OS cells transiently transfected with iV2-CALRwt, CALRdel52, and CALRin5 (green) in the presence or absence of treatment with IP3R inhibitor 2-ABP (100 μM, 5 minutes). White scale bars = 10 μm. (Contributors: J.I., Y.E.).

Finally, we tested the hypothesis that XBP1 up-regulates IP3R to produce a positive feedback loop whereby IP3R sustains ER Ca2+ depletion to promote continued activation of IRE1α/XBP1 in CALRdel52 cells. To do this, we interrogate the effects of IP3R inhibition on XBP1 transcriptional activity, we performed qPCR for XBP1 targets ADAM10 and SERP1, and found that 2-APB treatment led to significantly decreased expression of both genes in CALRdel52 cells (**Figure 3.14: Top**). Finally, to determine whether IP3R activity is important for the survival of CALRdel52 cells, we treated UT-7-MPL cells with 2-APB and performed Annexin V/PI staining to measure apoptosis. We found that while 2-APB had no significant pro-apoptotic effect

on CALRwt or CALRins5-expressing cells, CALRdel52 cells displayed significantly increased annexin V-PI positivity in response to 2-APB treatment (**Figure 3.14: Bottom**).

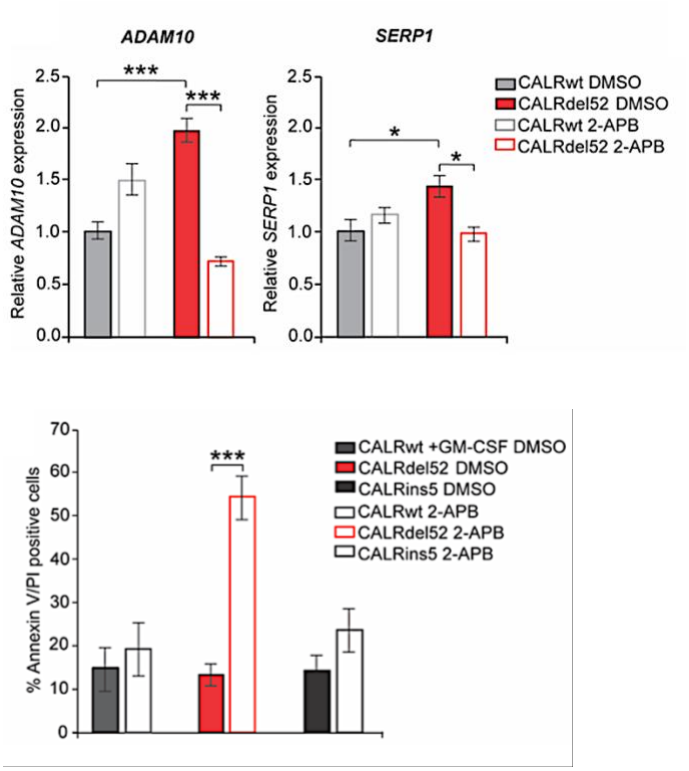

Figure 3.14 Top: qPCR for ADAM10 and SERP1 expression in UT-7-MPL cells expressing CALR variants treated with or without 2-APB (100 μM for 24 hours). Each bar represents the average of 3 independent replicates. Error bars denote standard deviation (SD). Significance was determined by 2-tailed Student's t-test (** $p<0.01$). Bottom: quantification of flow cytometric analysis for Annexin V/PI double positivity in Ba/F3-MPL cells expressing CALR variants and treated with or without 2-ABP (100 μM for 72 hours). Each bar represents the average of 3 independent replicates. Error bars denote standard deviation (SD). Significance was determined by 2-tailed Student's t-test (*** $p<0.01$) (Contributors, J.I., D.R.).

To determine whether this increased cell death is mediated through down-regulation of BCL-2, we performed a western blot for BCL-2 in 2-ABP treated UT-7-MPL cells. Indeed, we found that BCL-2 expression is decreased in CALRdel52 cells upon 2-ABP treatment (**Figure 3.15**). Together, these results indicated that CALRdel52 cells promote ER Ca2+ depletion via

XBP1-mediated up-regulation of IP3R, which in turn leads to continued activation of IRE1α/XBP1 to promote cell survival through BCL-2.

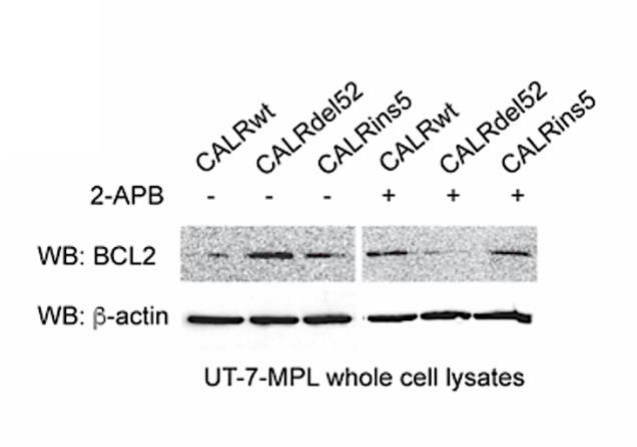

Figure 3.15 Western blot for BCL-2 in Ba/F3-MPL cells expressing CALR variants and treated with or without 2-ABP (100 μM for 24 hours). β-actin was used as a loading control. (B) Quantification of BCL-2 band relative to β-actin control from Figure 5I. Analysis was performed using Thermo Fisher Scientific iBright Analysis Software. (Contributors: J.I).

3.1.5 The IRE1α/XBP1 pathway represents a novel target for therapy in CALRdel52-driven MPNs

Given the dependence of CALRdel52 cells on the IRE1α/XBP1 pathway, we reasoned that IRE1α may represent a novel target for therapy in CALRdel52-driven MPNs. To test this, we employed the highly selective IRE1α inhibitor, KIRA8, that binds to the kinase domain of IRE1α and allosterically inhibits its RNase activity (286).

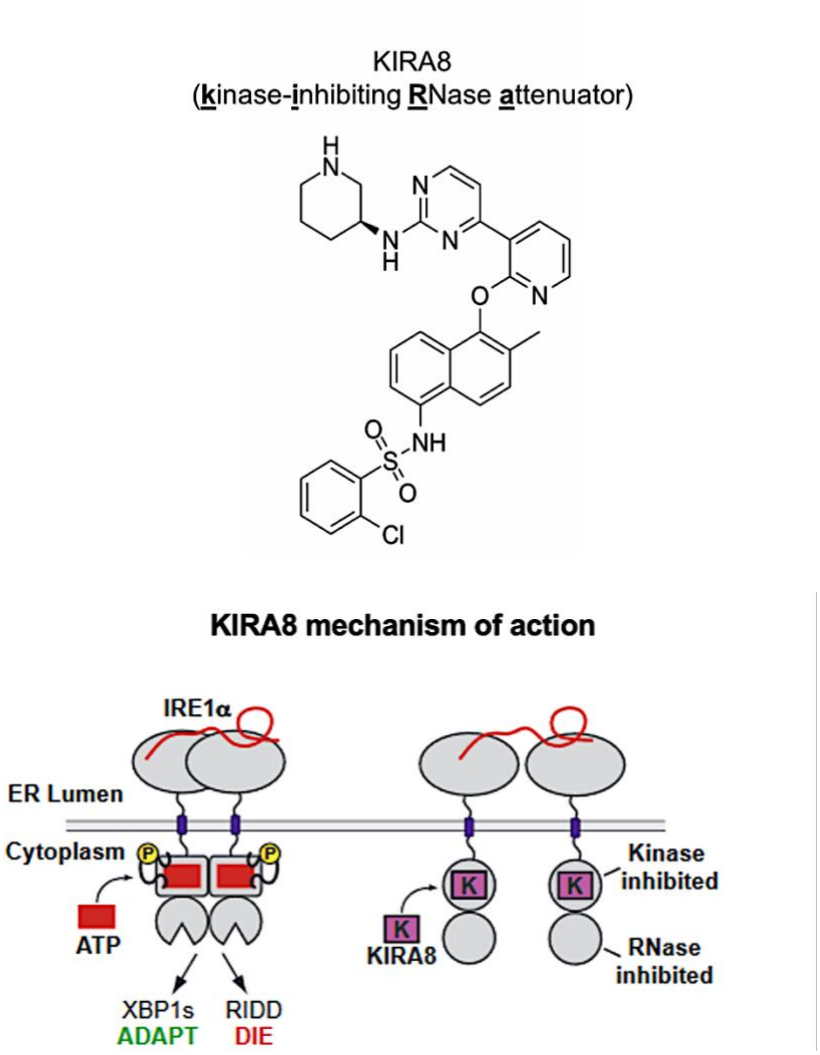

Figure 3.16 KIRA8 molecular structure (top) and mechanism of action (bottom). Figure adapted from Moore PC, Qi JY, Thamsen M, et al. Parallel Signaling through IRE1α and PERK Regulates Pancreatic Neuroendocrine Tumor Growth and Survival. *Cancer Res*. 2019;79(24):6190-6203. doi:10.1158/0008-5472.CAN-19-1116 (Ref. 241)

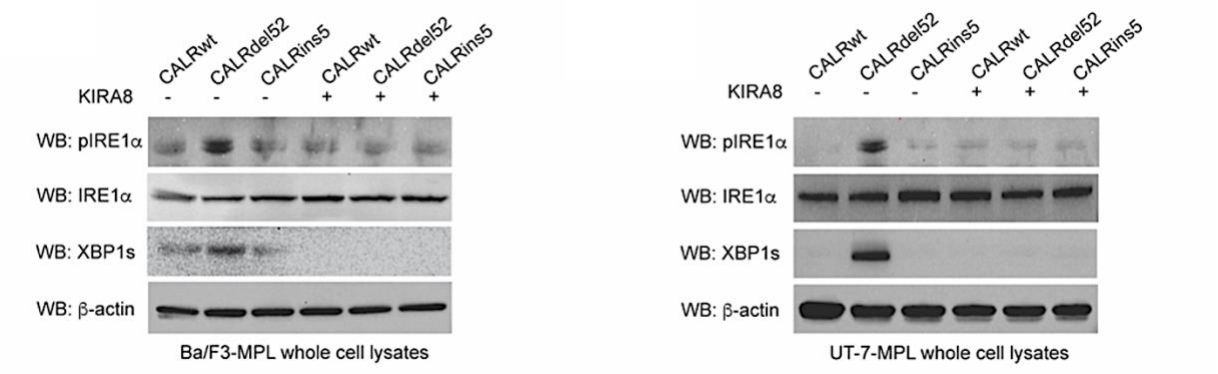

Figure 3.17 Western blot for phospho-IRE1α, total IRE1α and XBP1s in Ba/F3-MPL (left) cells expressing CALR variants treated with or without KIRA8 (5 μM for 4 hours). β-actin was used as a loading control. Western blot for phospho-IRE1α, total IRE1α and XBP1s in UT-7-MPL (right) cells expressing CALR variants treated with or without KIRA8 (5 μM for 4 hours). β-actin was used as a loading control. (Contributors: J.I.).

We found that KIRA8 specifically inhibited viability of and induced apoptosis in CALRdel52-expressing Ba/F3-MPL cells (**Figure 3.18: Left and Right**), UT-7-MPL cells (**Figure 3.19: Left and Right**), without affecting cells expressing CALRwt or CALRins5. This suggests that inhibiting IRE1α may have minimal off-target effects on cells not expressing CALRdel52. Finally, to assess the effects of KIRA8 treatment on XBP1 targets BCL-2 and IP3R, we performed western blot in KIRA8-treated Ba/F3-MPL-CALR cells.

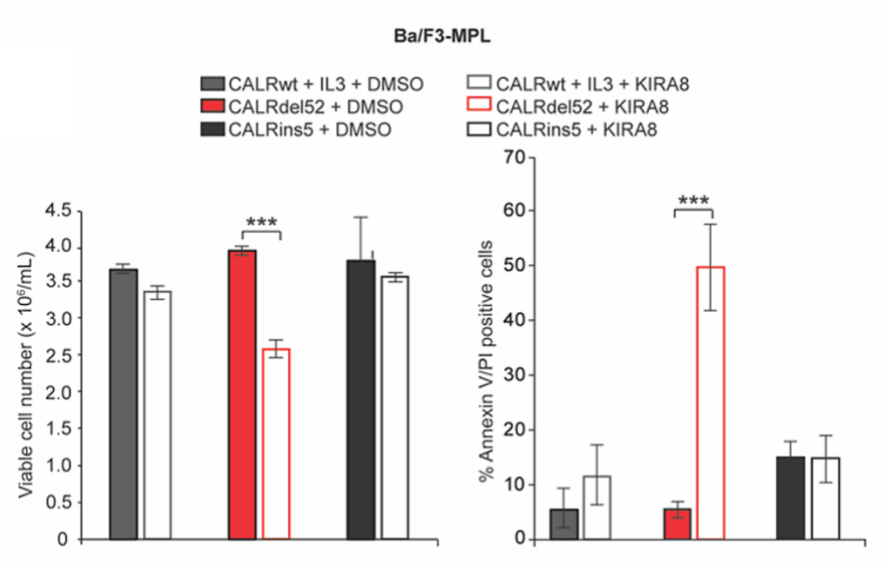

Figure 3.18 Left: total viable cell number at 72 hours post IL-3 withdrawal in Ba/F3-MPL cells expressing CALR variants treated with or without KIRA8 (5 μM). Right: Quantification of flow cytometric analysis for Annexin V/PI double positivity in Ba/F3-MPL cells expressing CALR variants and treated with or without KIRA8 (5 μM for 48 hours). Each bar represents the average of 3 independent replicates. Error bars denote standard deviation (SD). Significance was determined by 2-tailed Student's t-test (***$p<0.001$). (Contributors: J.I.).

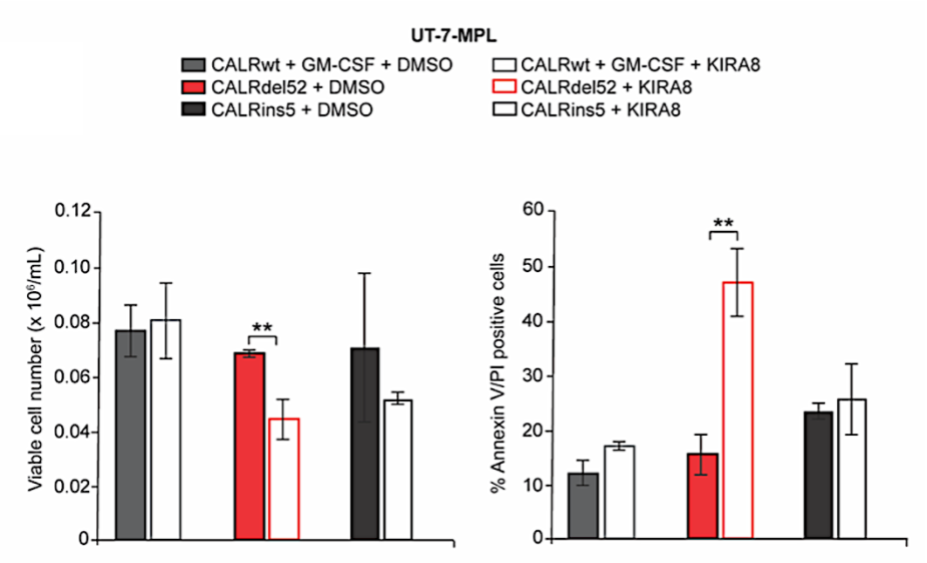

Figure 3.19 Left: total viable cell number at 72 hours post IL-3 withdrawal in Ba/F3-MPL cells expressing CALR variants treated with or without KIRA8 (5 μM). Right: quantification of flow cytometric analysis for Annexin V/PI double positivity in Ba/F3-MPL cells expressing CALR variants and treated with or without KIRA8 (5 μM for 48 hours). Each bar represents the average of 3 independent replicates. Error bars denote standard deviation (SD). Significance was determined by 2-tailed Student's t-test (***$p<0.001$). (Contributors: J.I.).

We found that KIRA8 treatment led to down-regulation of BCL-2 (**Figure 3.20: Left**), phospho-IP3R, and total IP3R expression levels (**Figure 3.20: Right**) in CALRdel52 cells, confirming that KIRA8 treatment is able to mitigate the expression and activity of these critical targets that drive CALRdel52 cell survival.

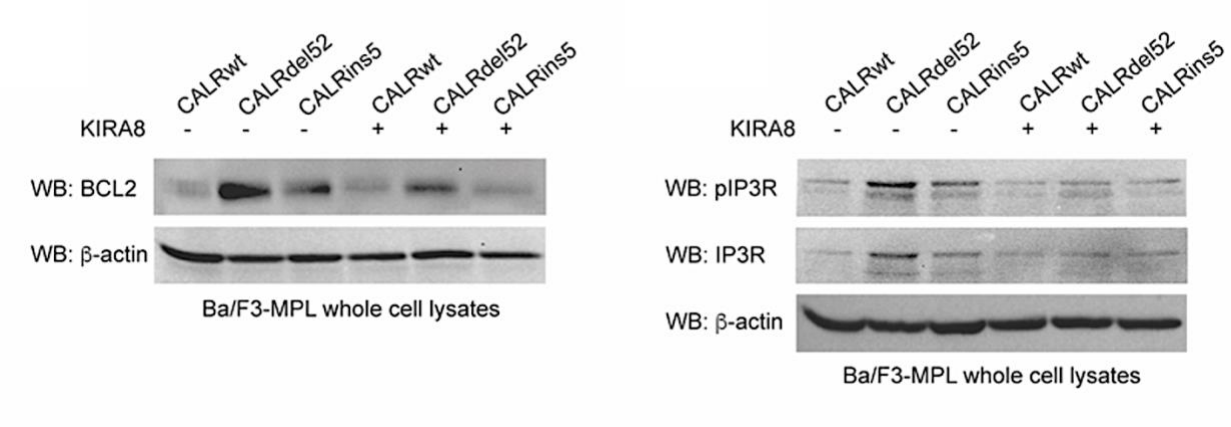

Figure 3.20 Left: Western blot for BCL-2 in Ba/F3-MPL cells expressing CALR variants treated with or without KIRA8 (5 μM for 24 hours). β-actin was used as a loading control. Right: Western blot for IP3R in Ba/F3-MPL cells expressing CALR variants treated with or without KIRA8 (5 μM for 24 hours). β-actin was used as a loading control. (Contributors: J.I.).

3.1.6 Inhibition of IRE1α signaling abrogates MPNs disease progression *in vivo*

Finally, to study the effects of IRE1α inhibition *in vivo*, we used a bone marrow transplantation (BMT) model of mutant CALR-driven ET as previously described (250, 287). Briefly, c-KIT–enriched primary mouse bone marrow cells were transduced with retroviruses expressing CALRwt, CALRdel52, or CALRins5, and transplanted into lethally irradiated recipient mice. 10 weeks post-transplantation, mice were bled retro-orbitally to confirm onset of thrombocytosis in CALRdel52 mice, then randomly divided into two groups per genotype (n=5 per group). Mice from each group were treated with intraperitoneal injection of either vehicle or 50 mg/kg KIRA8 on a 7 day on/7 day off dose schedule for a total of 6 weeks (**Figure 3.21**).

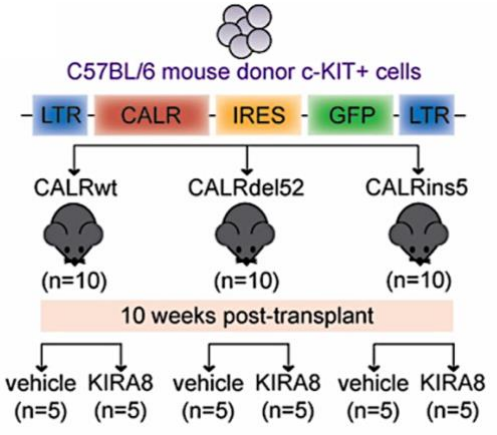

Figure 3.21 Schematic of retroviral bone marrow transplantation assay (BMT). c-KIT–enriched primary mouse bone marrow cells were transduced with retroviruses expressing CALRwt, CALRdel52, or CALRins5, and transplanted into lethally irradiated recipient mice. 10 weeks post-transplantation, mice were bled retro-orbitally to confirm onset of thrombocytosis in CALRdel52 mice, then randomly divided into two groups per genotype. Mice from each group were treated daily with intraperitoneal injection of either vehicle or 50 mg/kg KIRA8 for 7 days. At 16 weeks post-transplantation, mice were sacrificed for endpoint analysis.

At 16 weeks post-transplantation, mice were sacrificed for endpoint analysis, which included complete blood counts (CBC) and histopathological analysis. CBC analysis revealed that, as expected, mice receiving CALRdel52-expressing cells demonstrated significantly increased platelet (PLT) counts at 16 weeks, compared to mice receiving CALRwt and CALRins5-expressing cells. Notably, although CALRins5 mutations are associated with ET in human patients, this oncogene has been shown to be a weaker driver of ET in mice, with no detectable thrombocytosis at 16 weeks in a BMT model (293). Likewise, we saw no evidence of thrombocytosis in CALRins5 mice at this time point. Remarkably, we found that just 7 days of KIRA8 treatment in CALRdel52 mice was sufficient to induce a significant decrease in platelet counts (**Figure 3.22: Top**). Hematocrit (HCT) (**Figure 3.22: Center**) and white blood cell (WBC) counts (**Figure 3.22: Bottom**) were generally consistent across all genotypes, as previously reported (256), and unaffected by KIRA8 treatment.

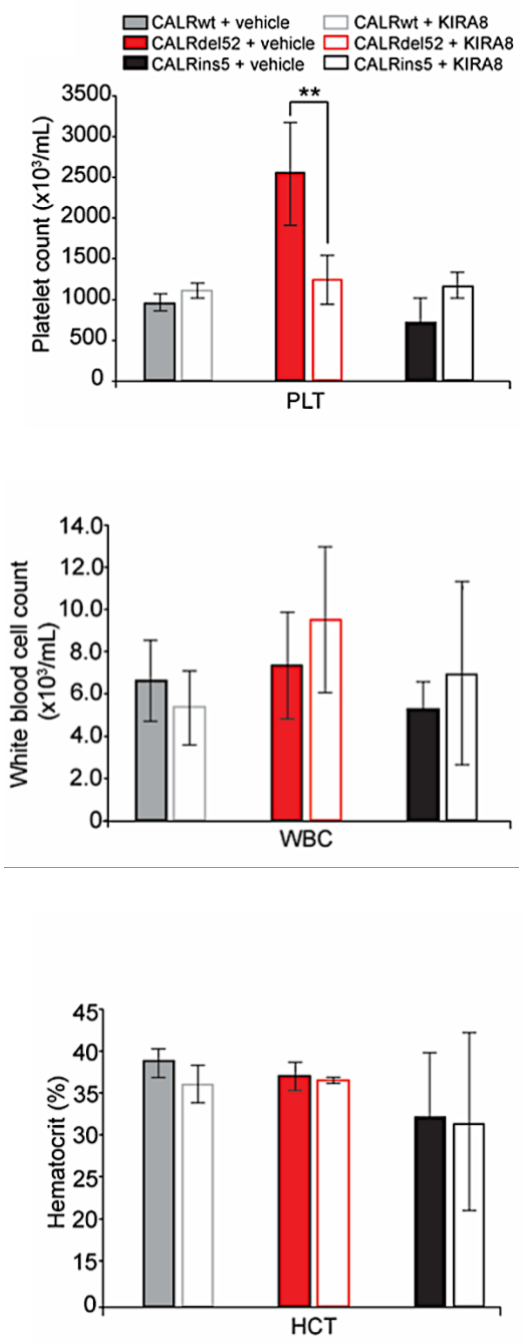

Figure 3.22 Platelet counts (PLT; top), white blood cell counts (WBC; middle) and hematocrit (HCT; bottom) at 16 weeks post-transplantation in the peripheral blood of recipient mice receiving CALRwt, CALRdel52, or CALRins5-expressing c-KIT+ bone marrow cells treated with KIRA8 as indicated (n=10 in each group). Each bar represents the average of 5 mice. Error bars denote standard deviation (SD). Significance was determined by 2-tailed Student's t-test (** $p<0.01$). (Contributors: J.I, Y.E., K.K.).

Histopathological analysis of mouse bone marrow sections further revealed that CALRdel52 mice displayed hallmark characteristics of ET, which were abrogated following 7 days of KIRA8 treatment. Bone marrow from vehicle-treated CALRdel52 mice displayed hypercellularity with enlarged, hyperlobulated megakaryocytes that demonstrated a tendency towards clustering and signs of emperipolesis. In contrast, bone marrow from KIRA8-treated CALRdel52 mice show mostly normocellularity with megakaryocytes that are decreased in size, frequency, clustering, and numbers (**Figure 3.23 and 3.24**).

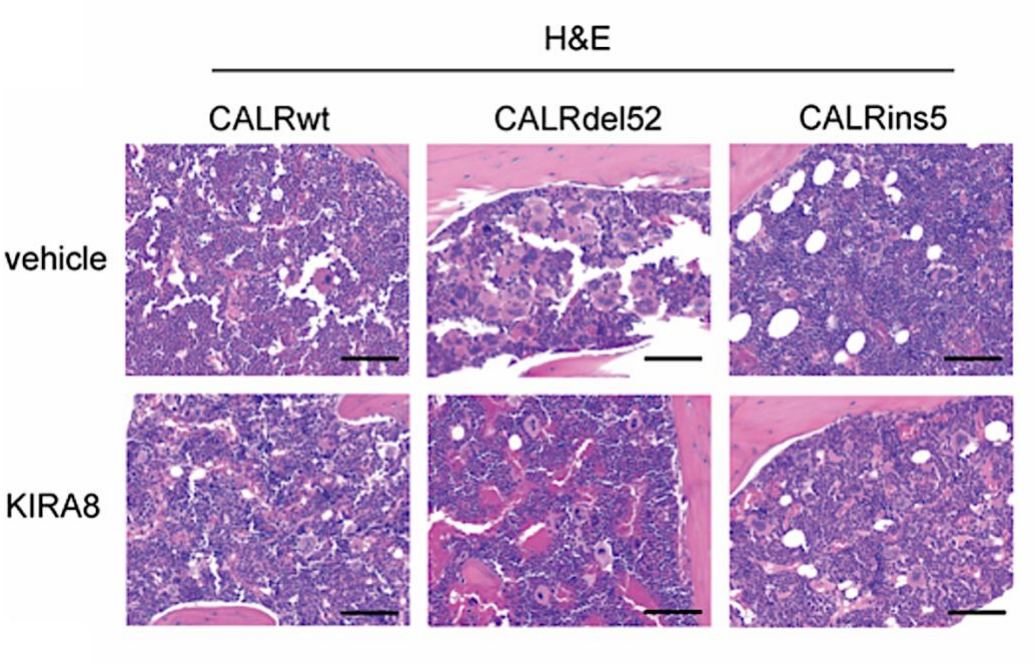

Figure 3.23 Histopathologic hematoxylin and eosin (H&E) sections of bone marrow from representative CALRwt, CALRdel52 and CALRins5 mice treated with vehicle or 50 mg/kg/day KIRA8 (20x magnification, black scale bars = 100 μm). (Contributors: J.I, Y.E., K.K.).

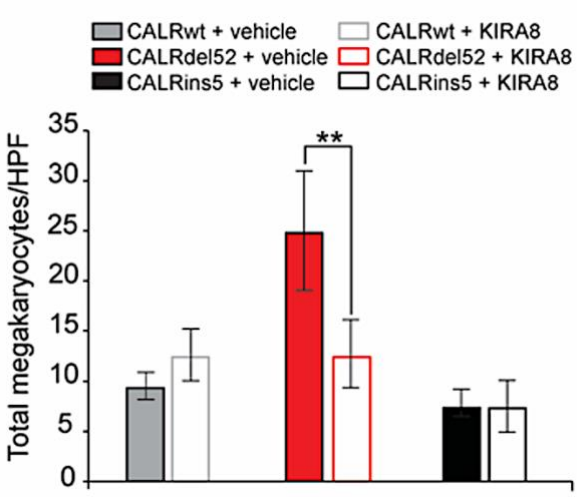

Figure 3.24 Megakaryocyte counts per high power field (HPF) in bone marrow of CALRwt, CALRdel52 or CALRins5 mice treated with vehicle or 50 mg/kg/day KIRA8. Each bar represents the average of 5 mice. Error bars denote standard deviation (SD). Significance was determined by 2-tailed Student's t-test (** $p<0.01$). (Contributors: J.I, Y.E., K.K.).

Lastly, to validate that the effects of KIRA8 on CALRdel52-driven disease attenuation were indeed mediated through inhibition of IRE1α/XBP1 signaling, we performed immunohistochemistry for total XBP1 on mouse bone marrow sections (**Figure 3.25**). In vehicle treated CALRdel52 mouse bone marrow, we saw prominent positive staining for XBP1, including nuclear expression in megakaryocytes. Importantly, KIRA8 treatment led markedly decreased expression of XBP1 in CALRdel52 mouse bone marrow.

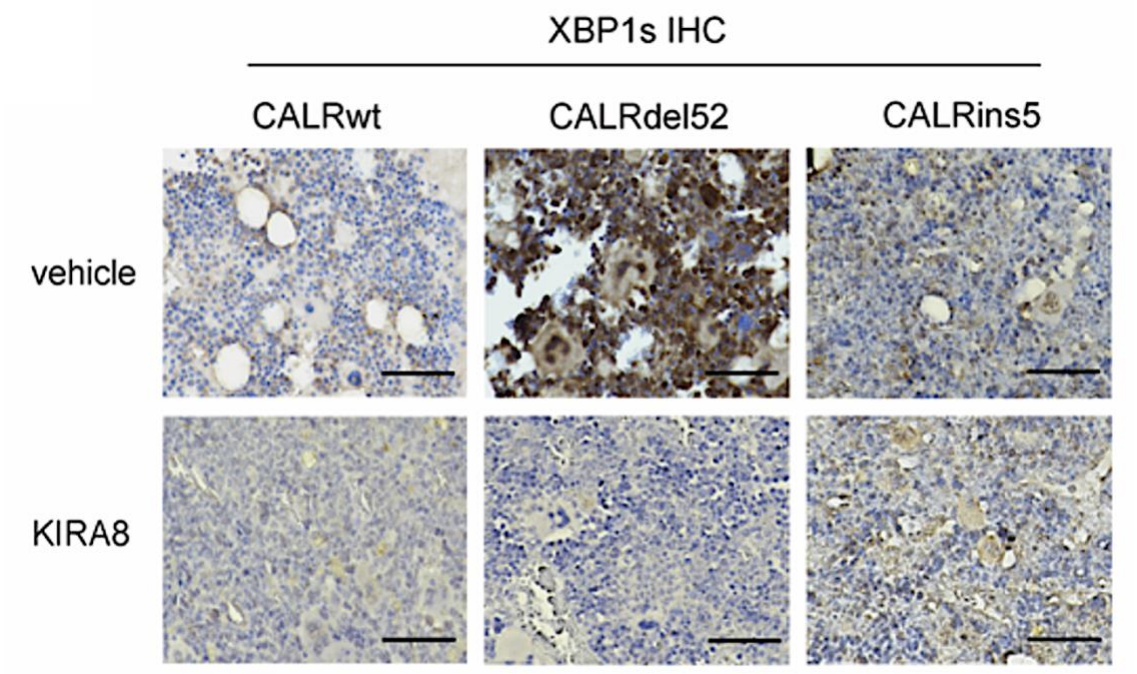

Figure 3.25 Immunohistochemical analysis for XBP1 in bone marrow from representative CALRwt, CALRdel52 and CALRins5 mice treated with vehicle or 50 mg/kg/day KIRA8 (40x magnification, black scale bars = 25 μm). (Contributors: J.I, Y.E., K.K.).

Finally, given the up-regulation of BCL-2 in CALRdel52-expressing cells, and the ability of BCL-2 inhibitor Venetoclax to induce apoptosis and reduce cell viability specifically in CALRdel52 cell lines, we tested Venetoclax in our BMT model to determine its efficacy in abrogating disease compared to KIRA8. The BMT was performed as above, and 10 weeks post-transplantation, mice were bled retro-orbitally to confirm onset of thrombocytosis in CALRdel52 mice, then randomly divided into two groups per genotype (n=10 per group). Mice from each group were treated for 5 days with vehicle, 50 mg/kg KIRA8 as described above, or 25 mg/kg Venetoclax administered by oral gavage (**Figure 3.26**). At 11 weeks post-transplantation, CBC analysis revealed that, as expected, mice receiving CALRdel52-expressing cells demonstrated significantly increased platelet (PLT) counts compared to mice receiving CALRwt and CALRins5-expressing cells. KIRA8 and Venetoclax treatment both led to significant PLT reduction in CALRdel52 mice, with KIRA8 showing slightly more efficacy than Venetoclax.

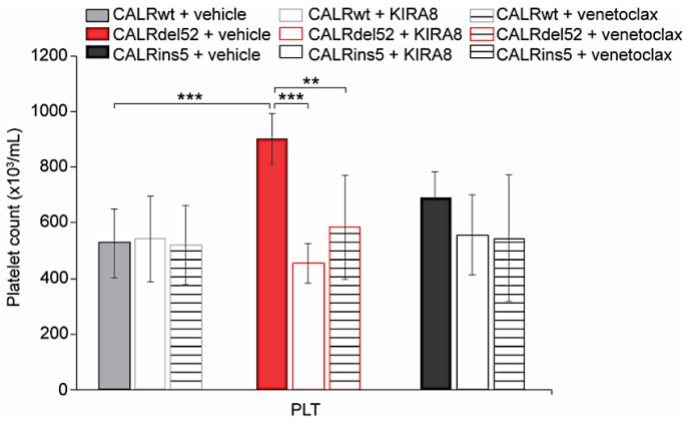

Figure 3.26 Platelet counts (PLT) at 11 weeks post-transplantation and 5 weeks post-treatment in the peripheral blood of recipient mice receiving CALRwt, CALRdel52, or CALRins5-expressing c-KIT+ bone marrow cells treated as indicated (n=30 in each group). Each bar represents the average of 10 mice. Error bars denote standard deviation (SD). Significance was determined by 2-tailed Student's t-test (** $p<0.01$). (Contributors: J.I., H.G., D.R., M.C.).

Together, these results demonstrate that pharmacological inhibition IRE1α signaling, where targets include IRE1α itself as well as BCL-2, leads to substantial abrogation of CALRdel52-driven MPNs disease progression *in vivo*. Further studies are warranted to test BCL-2 inhibition more thoroughly in this model (including treating mice until at least the 16-week endpoint). In addition, we conducted preliminary studies to test the efficacy of combined IRE1α and BCL-2 inhibition on CALRdel52-driven disease but found that the combination at the doses used (50 mg/kg/day KIRA8 + 25 mg/kg/day Venetoclax for 7 days) was lethal for all animals tested. Thus, additional studies are warranted to identify a therapeutic window for this combination that may result in synergistic inhibition of CALRdel52-driven disease.

CHAPTER 4: INVESTIGATING THE ROLE OF THE RTCB LIGASE IN CALR MUTANT MYELOPROLIFERATIVE NEOPLASMS

Building from our findings where type 1 CALR mutant cells rely on the IRE1α/XBP1 arm of the unfolded protein response for survival in MPNs, we decided to further interrogate components of this pathway and ask whether these represent a further therapeutic target for MPNs malignancy. To this end, we aimed at exploring the role of RTCB in CALR mutant MPNs. As the ligase responsible for catalyzing the splicing of XBP1 mRNA upon IRE1α cleavage (187-192, 208, 140, 152), we hypothesized that RTCB targeting could perhaps represent a further improvement in targeting IRE1α/XBP1 in type 1 CALR del52 mutant MPN, given the XBP1 independent function IRE1α exerts, such as RIDD activation, which can promote apoptosis. Notably, current IRE1α /XBP1 pathway inhibitors are limited to IRE1α inhibition, while XBP1 as a transcription factor remains yet challenging to target due its structural disorder and the lack of small-molecule binding pockets. Therefore, identifying and targeting components specific to XBP1 activation such as RTCB, can help separate IRE1α/XBP1 therapeutic functions and their relevance to cancer and biology.

4.2.1 RTCB protein expression in CALR mutant variant UT7-MPL MPNs in vitro cell model

Given the overexpression and activation of the IRE1α/XBP1 arm of the unfolded protein response in type 1 CALRdel52 mutant MPNs cells, we first aimed at examining RTCB expression in our UT7-MPL cells model overexpressing the CALR variants. Indeed, RTCB was expressed across all cells including CALRwt, CALRdel52 and CALRins5. Notably, we observed elevated RTCB expression in both CALRde52 and CALRins5 cells (**Figure 4.1**). Given this result, we then moved on to interrogating whether RTCB expression was required for the survival of both CALR mutant (CALRdel52 and CALRins5) cells.

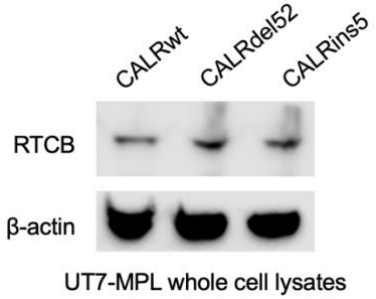

Figure 4.1 Western blot for RTCB in UT-MPL cells expressing CALRwt, CALRde52 or CALRins5 variants. β-actin was used as a loading control. (Contributors: J.I.)

4.2.2 Knockdown validation of RTCB in UT7-MPL cells expressing CALR mutant variants

First to interrogate the specific requirement of RTCB for the survival of CALRdel52 and/or CALRins5 expressing cells, we generated shRNA knockdowns against human RTCB in UT-7 MPL cells. From the 3 shRNAs tested, only one of these was able to achieve significant knockdown across all cell lines as validated via qPCR (**Figure 4.2**). We then moved forward with this set of CALR variants cells with successful RTCB shRNA knockdown, while considering the limitations and further need to include additional shRNAs to validate any preliminary observations. In addition, validation of knockdown efficiency at protein level for RTCB needs to follow up.

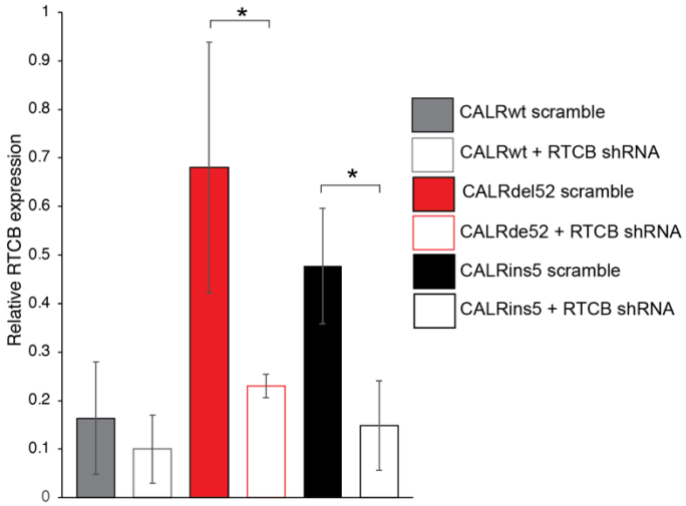

Figure 4.2 Validation of RTCB expression via in UT-7-MPL cells expressing CALR variants transduced with shRNA against RTCB (TRCN0000296541) or scramble control. Each bar represents the average of 3 independent replicates. Error bars denote standard deviation (SD). Significance was determined by 2-tailed Student's t-test (** $p<0.01$.) (Contributors: J.I.)

4.2.3 RTCB knockdown alters growth in CALR mutant expressing UT7-MPL cells

To examine the effect of RTCB knockdown on cell growth, we performed trypan blue exclusion cell counting assays. While RTCB knockdown did not attenuate the growth in CALRwt expressing UT7-MPL cells, we observed a significant decrease in cell growth in CALRdel52 expressing cells. However, surprisingly, we observed a drastic and even more significant attenuation of growth in CALRins5 expressing UT7-MPL cells, suggesting that this pathway might not be only significant for the growth of CALRde52 cells but also even more necessary for CALRins5 mutant cells. Notably, these experiments need to be further validated and followed up with additional shRNAs knockdown and/or RTCB deletion via CRISPR/Cas9.

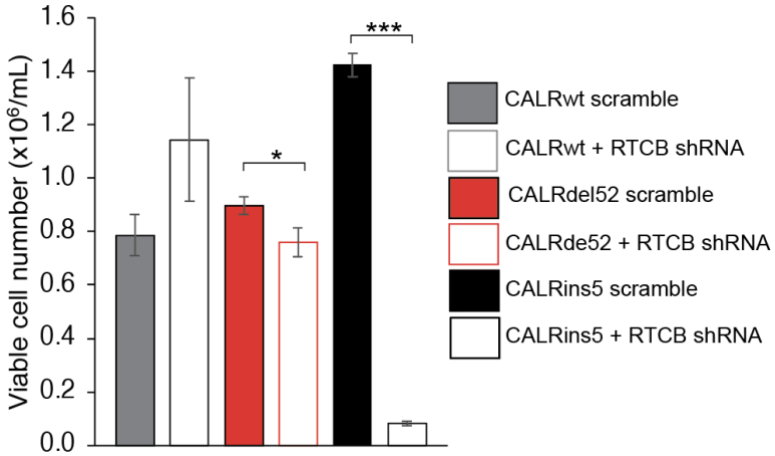

Figure 4.3 Total viable cell number at 72 hours post GM-CSF withdrawal in UT7-MPL cells expressing CALR variants and either a scrambled shRNA or shRNA against RTCB. UT7-MPL-CALRwt cells grown in the presence of GM-CSF was included as a control. Each bar represents the average of 3 independent replicates. Error bars denote standard deviation (SD). Significance was determined by 2-tailed Student's t-test (** $p<0.01$; ***$p<0.001$). (Contributors: J.I.)

CHAPTER 5: MODELING MYELOFIBROSIS IN AN IN-VITRO CELL SYSTEM

The bone marrow is a highly complex site, that houses a diverse population of cells with a multitude of functions. When it comes to studying the specific crosstalk functions among cells in this context, it can be quite challenging given signaling noise that can arise across the variety of cells at play. In the setting of myelofibrosis, which is characterized by the accumulation and excessive deposition of reticulin and collagen fibers (235), there is a major interplay between malignant clones and the bone marrow stromal cells (BMSCs) that promote fibrosis transformation (296-302). Notably, it has been proposed that fibrosis in MPNs results from abnormal growth factors and cytokine availability from mutant hematopoietic progenitors (236). Therefore, given the importance of cell-cross talk between mutant hematopoietic progenitors and the BMSCs in bone marrow fibrosis development, it is then critical to develop cell systems that recapitulate and yet facilitate the study of such specific cellular interactions and dynamics in order to isolate the mechanisms driving such fibrotic processes and enable molecular target discovery. Given this reasoning, we aimed at developing a cell *in vitro* system where we could study the specific contributions of CALR mutant MPNs cells to the bone marrow stroma in fibrosis development.

5.2.1 UT-7-MPL CALR mutant cell conditioned media leads to fibrotic markers upregulation in bone marrow stromal cells

First, we established a cell conditioned media system (**Figure 5.1**), where we took conditioned media from wild type, type 1 and type 2 CALR mutant expressing UT-7 cells and treated human bone marrow stroma cells (in this case use HS5, a human bone marrow derived stromal cell line) with that conditioned media to ask whether under these conditions we can recapitulate fibrotic transformation phenotype observed *in vivo*.

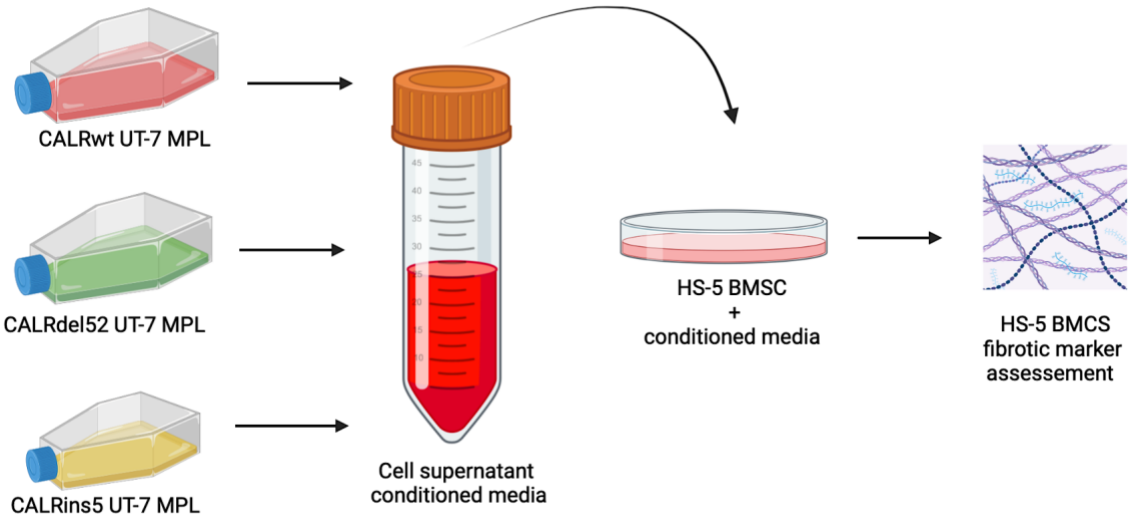

Figure 5.1 Development of media for myelofibrosis *in vitro* cell model. Supernatant conditioned media from UT7-MPL cells expressing either CALRwt, type 1 CALR de52, or type 2 CALRins5 was taken to treat HS-5 bone marrow stromal cells (BMSCs) followed by fibrotic marker (COL1A1 and fibronectin) expression assessment via western blot and immunofluorescence. (Generated in BioRender)

Notably, upon establishment of this system, we observed that treatment of HS-5 cells with conditioned media from CALR transformed UT7-MPL cells led to increase in fibrotic markers, particularly we observed upregulation of fibronectin via immunoblot in both CALRdel52 and CALRins5 conditioned media treated HS-5 cells after 7 days of treatment (**Figure 5.2**). In addition, we also observed upregulation of COL1A1 in CALRdel52 cells at this timepoint (**Figure 5.2**).

In an alternative approach, using immunofluorescence we also saw upregulation of fibronectin in CALRdel52 cells conditioned media treated HS-5 cells after 72hrs of treatment (**Figure 5.3**) Overall, these results show that via this *in vitro* system we are able to recapitulate a fibrotic phenotype that mimics CALR mutant transformed cells crosstalk with the bone marrow stroma, and propose the use of this isolated system to study the mechanisms involved in MF fibrogenesis in the future.

5.2.2 Type 1 CALR mutant UT7-MPL cells show elevated TGF-β secretion levels

To gain mechanistic insights, we proposed to start by studying TGF-β, a master regulator of fibrogenesis, which has been shown to play a role in myelofibrosis transformation. Notably, UPR signaling has been shown to modulate cytokine and growth factors downstream, and thus we hypothesize that perhaps there might be a contribution from the IRE1α/XBP1 pathway into TGF-β modulation. To this end, we assessed for TGF-β1 secretion levels in our *in-vitro* UT7-MPL CALR mutant transformed cell system. Based on this, we surprisingly found increased TGF-β1 levels in type 1 CALRdel52 UT7-MPL cells conditioned media compared to CALRwt or CALRins5 expressing cells (**Figure 5.4**).

5.2.3 TGF-β as a plausible myelofibrosis driver in type 1 CALR mutant myelofibrosis

Finally, to validate the already existing data supporting TGF-β1 modulation in fibrotic collagen deposition, we took our HS-5 cells and treated them with human recombinant TGFB-1; and indeed, we observed increase in COL1A1 expression via immunofluorescence (**Figure 5.5**). Overall, these preliminary data encourage future studies into whether a link exists between IRE1α/XBP1 activity and TGF-β modulation in fibrogenesis development in the context of myelofibrosis.

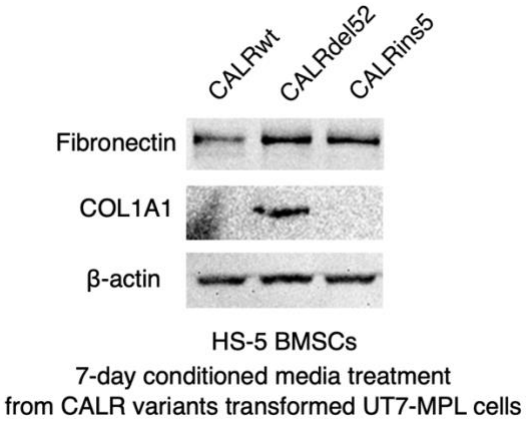

Figure 5.2 Western blot for fibronectin and COL1A1 in HS-5 BMSCs treated for 7 days with conditioned media from UT7-MPL cells expressing CALR variants. β-actin was used as a loading control. (Contributors: J.I.).

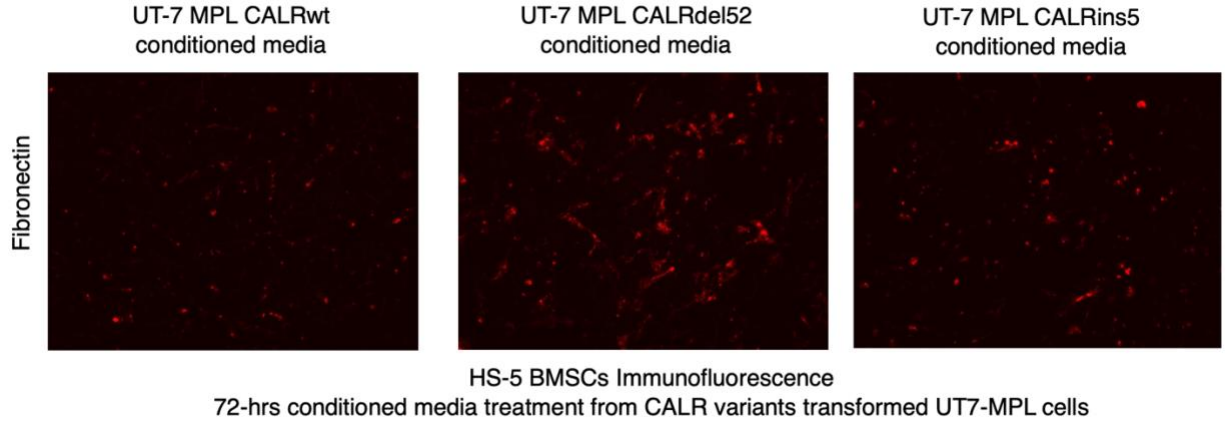

Figure 5.3 Immunofluorescence for fibronectin (red) in HS-5 BMSCs treated for 72 hours with days with conditioned media from UT7-MPL cells expressing CALR variants. (Contributors: J.I.).

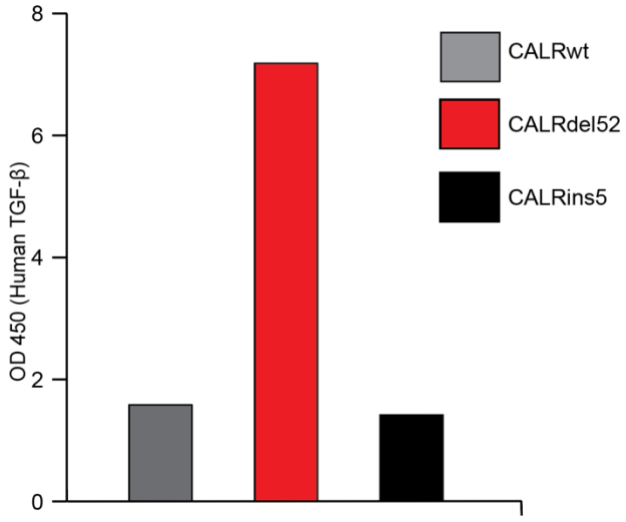

Figure 5.4 Relative TGF-β1 levels as quantified via enzyme-linked immunosorbent assay (ELISA) in the conditioned media from wild type, type 1 del52, and type 2 ins5 CALR mutant variants expressing UT7-MPL cells (1x replicate per condition). (Contributors: J.I.).

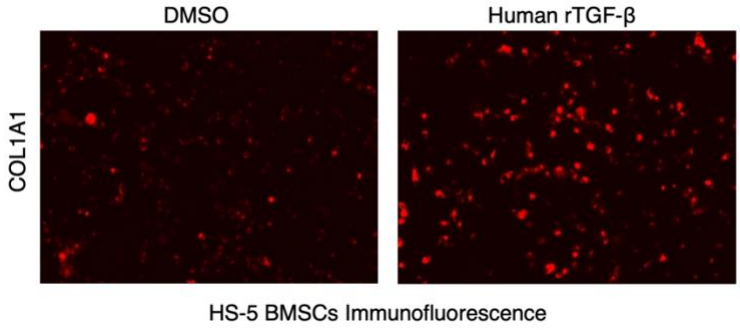

Figure 5.5 Immunofluorescence for COL1A1 (red) in HS-5 BMSCs treated with human recombinant TGF-β1 (2.5 ng/ml) for 48 hours. (Contributors: J.I).

CHAPTER 6: DISCUSSION

Chapter 6 consist in part of the discussion section from Ibarra and Elbanna et al., *Blood Cancer Discovery* (2022); see publications section.

The identification of the distinct phenotypic and prognostic outcomes of type 1 versus type 2 CALR mutations has provided important insight into how these mutations differ clinically, despite their shared mutant C-terminus (251,252). However, since this finding, there has been little in the way of understanding how these mutations differ in cellular consequence, and what their differential molecular dependencies may be. Here, we show the first evidence of a unique molecular dependency in type 1 versus type 2 CALR mutations and demonstrate that this novel dependency is a functional consequence of the molecular difference between type 1 and type 2 CALR mutations.

Because CALR mutations are classified based on extent of homology with the C-terminal Ca2+ binding domain of wild type protein, we sought to investigate pathways that would be most influenced by the loss of Ca2+ binding sites in the type 1 versus type 2 protein. This, together with the fact that CALR is an ER chaperone that is heavily implicated in the regulation of ER stress, led us to focus on the UPR as a potential differential dependency between type 1 and type 2 mutant CALR-expressing cells. In so doing, we found that type 1, but not type 2 CALR mutations lead to activation of the most ancient and conserved arm of the UPR, the IRE1α/XBP1 pathway. We hypothesized that type 1 CALR mutations may lead to depleted ER calcium due to the inability of the type 1 mutant protein to bind and store Ca2+ in the ER. Indeed, we found that type 1 CALR mutant proteins demonstrate significantly impaired Ca2+ binding ability, and that this results in chronically depleted ER Ca2+ levels. Further, we found that this ER Ca2+ depletion directly activates the IRE1α/XBP1 pathway of the UPR, and that the ER calcium efflux receptor IP3R is

up-regulated downstream of XBP1 to sustain a state of depleted ER calcium, which in turn creates a positive feedback loop to maintain IRE1α/XBP1 activation. We further show that this pathway represents a unique molecular dependency for type 1- compared to type 2-mutant CALR expressing cells or wild type cells, in part through up-regulation of BCL-2 and can be pharmacologically targeted both in vitro and in vivo to specifically induce death of type 1 mutant CALR-expressing cells and abrogate type 1 mutant CALR-driven disease (**Figure 6.1**).

One major outstanding question from this work is how and why the endogenous copy of wild type CALR in our over-expression cell line models fails to compensate for the loss of CALRdel52 Ca2+ binding that precipitates activation of the IRE1α/XBP1-BCL2/IP3R signaling network. Because CALR mutations are nearly always heterozygous, we hypothesize that mutant CALR may exert a dominant negative effect over the wild type copy and therefore not require homozygosity to engender a phenotype. Though outside the scope of this work, we are currently exploring this as a possibility for how CALR mutations may cause loss of total protein function even in a heterozygous background.

Additional remaining questions relate to the mechanisms underlying BCL2 and IP3R in this model. BCL2 has been shown to bind to the IP3 receptor in order to inhibit Ca2+ release from the ER, which in turn prevents apoptosis. In contrast, we show that although BCL2 is up-regulated by XBP1, IP3R is also up-regulated and activated by this pathway, and in fact serves to sustain IRE1α/XBP1 survival signaling. Further investigation into this paradoxical rewiring of BCL2-mediated regulation of IP3R and its underlying mechanisms in the context of type 1 CALR mutations is certainly warranted. Moreover, our data show that BCL2 is up-regulated downstream of XBP1, and that BCL2 promotes survival in type 1 CALR-mutated cells. This suggests that

targeting BCL2 by Venetoclax or Navitoclax may represent an additional therapeutic avenue for type 1 CALR+ patients.

Taken together, this work is the first to demonstrate that type 1 and type 2 mutant CALR-expressing cells display differential molecular dependencies, and that those differential dependencies can be targeted for therapeutic gain in type 1 versus type 2-driven MPNs. Moreover, this study answers an enduring question regarding the functional consequence of the loss of calcium binding sites on the type 1 mutant CALR protein and demonstrates how type 1 CALR mutant-expressing cells rewire the UPR and downstream calcium signaling and apoptotic pathways to drive MPNs.

In addition, our preliminary data indicate that RTCB knockdown attenuates survival of both CALRde52 and CALRins5, with more significant effects on CALRins5 expressing cells. This came as surprise to us given the dependency of CALRdel52 expressing cells on IRE1α/XBP1 activation. However, given RTCB also exerts functions independent of IRE1α/XBP1 activation as part of the TSEN tRNA splicing complex, there might be alternative functions that might contribute to CALRins5 dependency on RTCB. Yet, further validation of these findings in cell models, as well as *in vivo* and patient samples is required to provide more concrete evidence of RTCB relevance to CALR mutant MPNs

Moreover, our establishment of an *in vitro* cell system to model myelofibrosis is promising in the context of studying CALR mutant myelofibrosis. This system will not only serve to identify specific molecular players contributing to MF fibrotic transformation, but most importantly, it will further facilitate the dissection of cell-specific crosstalk mechanisms. Thus far based on our preliminary data, TGF-β1 appears as a contributor candidate for CALRdel52 driven MF. This system will allow further interrogation the role for TGF-β1 in this process, as well as that of the

IRE1α/XBP1 pathway. Finally, whether IRE1α/XBP1 and the UPR as a whole contribute to the transformation and progression of AML is also part of this larger open question and needs further study. We currently know that IRE1α/XBP1 pathway activation is necessary for the survival of type 1 CALRdel52 ET, but whether this pathway is relevant to MF and AML transformation in the context of this mutation remains to be explored. Further, given the therapeutic gain observed from IRE1a/XBP1 and BCL2 inhibition via KIRA8 and Venetoclax, respectively, it is then critical to compare the efficacy of these therapies against MPN first-line therapy, Ruxolitinib, and hydroxyurea in type 1 CALRdel52 mutant MPN disease. Finally, the mutant cell crosstalk contributions to myelofibrosis onset remain to be explored, and further define whether these are dependent or independent of TGF-β1 and/or IRE1α/XBP1.

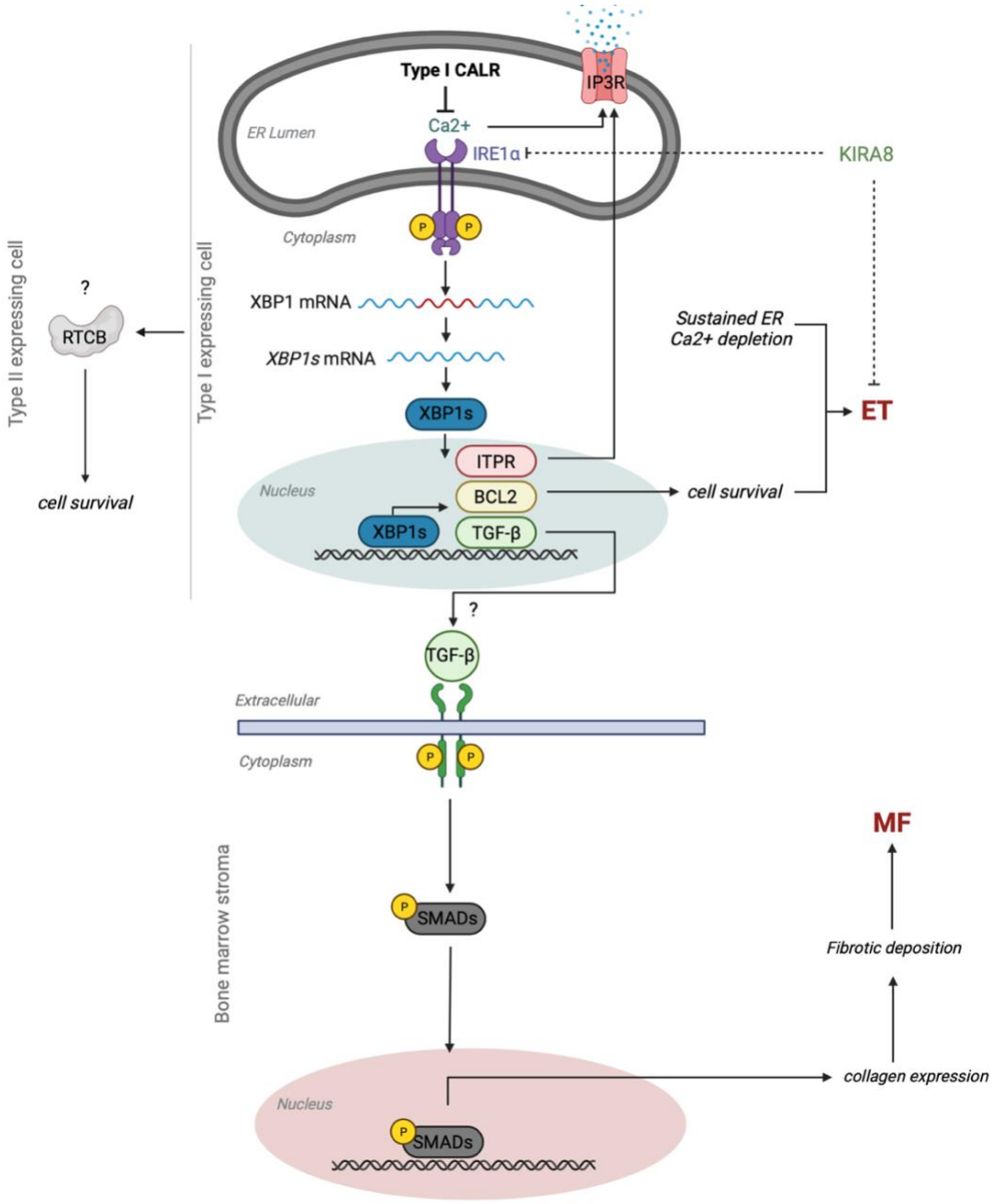

Figure 6.1. Summary. Type 1 CALRdel52 proteins exhibit loss of Ca2+ binding function. This leads to depleted ER Ca2+, which in turn activates the IRE1α/XBP1 pathway. XBP1 mediates up-regulation of BCL-2, which promotes cell survival, and IP3R, which facilitates continued ER Ca2+ efflux to sustain ER Ca2+ depletion and activation of IRE1α/XBP1, ultimately driving MPN. Further, preliminary data suggest that RTCB ligase could be promoting type 2 CALRins5 cell survival, while TGF- β might represent a contributor to MF fibrotic transformation downstream of IRE1α/XBP1 through crosstalk with the bone marrow stroma. (Generated in BioRender)

REFERENCES

1. Enciso J, Mendoza L, Pelayo R. Normal vs. Malignant hematopoiesis: the complexity of acute leukemia through systems biology. *Front Genet*. 2015;6:290. Published 2015 Sep 11. doi:10.3389/fgene.2015.00290

2. Robb L. Cytokine receptors and hematopoietic differentiation. *Oncogene*. 2007;26(47):6715-6723. doi:10.1038/sj.onc.1210756.

3. Boulais PE, Frenette PS. Making sense of hematopoietic stem cell niches. *Blood*. 2015;125(17):2621-2629. doi:10.1182/blood-2014-09-570192.

4. Metcalf D. On hematopoietic stem cell fate. *Immunity*. 2007;26(6):669-673. doi:10.1016/j.immuni.2007.05.012.

5. Jagannathan-Bogdan M, Zon LI. Hematopoiesis. *Development*. 2013;140(12):2463-2467. doi:10.1242/dev.083147.

6. Pinho S, Frenette PS. Haematopoietic stem cell activity and interactions with the niche. *Nat Rev Mol Cell Biol*. 2019;20(5):303-320. doi:10.1038/s41580-019-0103-9.

7. Kaushansky K. Lineage-specific hematopoietic growth factors. *N Engl J Med*. 2006;354(19):2034-2045. doi:10.1056/NEJMra052706

8. Orkin SH. Diversification of haematopoietic stem cells to specific lineages. *Nat Rev Genet*. 2000;1(1):57-64. doi:10.1038/35049577.

9. Ng AP, Alexander WS. Haematopoietic stem cells: past, present, and future. *Cell Death Discov*. 2017;3:17002. Published 2017 Feb 6. doi:10.1038/cddiscovery.2017.2

10. Metcalf D. Hematopoietic cytokines. *Blood*. 2008;111(2):485-491. doi:10.1182/blood-2007-03-079681

11. Robb L. Cytokine receptors and hematopoietic differentiation. *Oncogene*. 2007;26(47):6715-6723. doi:10.1038/sj.onc.1210756

12. Kuter DJ. Milestones in understanding platelet production: a historical overview. *Br J Haematol*. 2014;165(2):248-258. doi:10.1111/bjh.12781

13. Hitchcock IS, Hafer M, Sangkhae V, Tucker JA. The thrombopoietin receptor: revisiting the master regulator of platelet production. *Platelets*. 2021;32(6):770-778. doi:10.1080/09537104.2021.1925102

14. Lodish H, Flygare J, Chou S. From stem cell to erythroblast: regulation of red cell production at multiple levels by multiple hormones. *IUBMB Life*. 2010;62(7):492-496. doi:10.1002/iub.322

15. Rodriguez-Abreu D, Bordoni A, Zucca E. Epidemiology of hematological malignancies. *Ann Oncol*. 2007;18 Suppl 1:i3-i8. doi:10.1093/annonc/mdl443

16. Tietsche de Moraes Hungria V, Chiattone C, Pavlovsky M, et al. Epidemiology of Hematologic Malignancies in Real-World Settings: Findings From the Hemato-Oncology Latin America Observational Registry Study. *J Glob Oncol*. 2019;5:1-19. doi:10.1200/JGO.19.00025

17. Auberger P, Tamburini-Bonnefoy J, Puissant A. Drug Resistance in Hematological Malignancies. *Int J Mol Sci*. 2020;21(17):6091. Published 2020 Aug 24. doi:10.3390/ijms21176091

18. Fend F, Dogan A, Cook JR. Plasma cell neoplasms and related entities-evolution in diagnosis and classification. *Virchows Arch*. 2023;482(1):163-177. doi:10.1007/s00428-022-03431-3

19. Jiang M, Bennani NN, Feldman AL. Lymphoma classification update: T-cell lymphomas, Hodgkin lymphomas, and histiocytic/dendritic cell neoplasms. *Expert Rev Hematol*. 2017;10(3):239-249. doi:10.1080/17474086.2017.1281122

20. Murati A, Brecqueville M, Devillier R, Mozziconacci MJ, Gelsi-Boyer V, Birnbaum D. Myeloid malignancies: mutations, models, and management. *BMC Cancer*. 2012;12:304. Published 2012 Jul 23. doi:10.1186/1471-2407-12-304

21. Anderson LA, McMullin MF. Epidemiology of MPN: what do we know?. *Curr Hematol Malig Rep*. 2014;9(4):340-349. doi:10.1007/s11899-014-0228-z

22. Pizzi M, Croci GA, Ruggeri M, et al. The Classification of Myeloproliferative Neoplasms: Rationale, Historical Background and Future Perspectives with Focus on Unclassifiable Cases. *Cancers (Basel)*. 2021;13(22):5666. Published 2021 Nov 12. doi:10.3390/cancers13225666

23. Campo, Elias, et al. *WHO classification of tumours of haematopoietic and lymphoid tissues*. Ed. Steven H. Swerdlow. Vol. 2. Lyon: International agency for research on cancer, 2008.

24. Ren R. Mechanisms of BCR-ABL in the pathogenesis of chronic myelogenous leukaemia. *Nat Rev Cancer*. 2005;5(3):172-183. doi:10.1038/nrc1567

25. Barcelos MM, Santos-Silva MC. Molecular approach to diagnose BCR/ABL negative chronic myeloproliferative neoplasms. *Rev Bras Hematol Hemoter*. 2011;33(4):290-296. doi:10.5581/1516-8484.20110079

26. Barcelos MM, Santos-Silva MC. Molecular approach to diagnose BCR/ABL negative chronic myeloproliferative neoplasms. *Rev Bras Hematol Hemoter*. 2011;33(4):290-296. doi:10.5581/1516-8484.20110079
27. Arber DA, Orazi A, Hasserjian R, et al. The 2016 revision to the World Health Organization classification of myeloid neoplasms and acute leukemia. *Blood*. 2016;127(20):2391-2405. doi:10.1182/blood-2016-03-643544

28. Zahr AA, Salama ME, Carreau N, et al. Bone marrow fibrosis in myelofibrosis: pathogenesis, prognosis, and targeted strategies. *Haematologica*. 2016;101(6):660-671. doi:10.3324/haematol.2015.141283

29. Szuber N, Mudireddy M, Nicolosi M, et al. 3023 Mayo Clinic Patients With Myeloproliferative Neoplasms: Risk-Stratified Comparison of Survival and Outcomes Data Among Disease Subgroups. *Mayo Clin Proc*. 2019;94(4):599-610. doi:10.1016/j.mayocp.2018.08.022

30. Mesa RA, Li CY, Ketterling RP, Schroeder GS, Knudson RA, Tefferi A. Leukemic transformation in myelofibrosis with myeloid metaplasia: a single-institution experience with 91 cases. *Blood*. 2005;105(3):973-977. doi:10.1182/blood-2004-07-2864

31. Okamura T, Kinukawa N, Niho Y, Mizoguchi H. Primary chronic myelofibrosis: clinical and prognostic evaluation in 336 Japanese patients. *Int J Hematol*. 2001;73(2):194-198. doi:10.1007/BF02981937

32. Okamura T, Kinukawa N, Niho Y, Mizoguchi H. Primary chronic myelofibrosis: clinical and prognostic evaluation in 336 Japanese patients. *Int J Hematol*. 2001;73(2):194-198. doi:10.1007/BF02981937

33. Björkholm M, Derolf AR, Hultcrantz M, et al. Treatment-related risk factors for transformation to acute myeloid leukemia and myelodysplastic syndromes in myeloproliferative neoplasms. *J Clin Oncol*. 2011;29(17):2410-2415. doi:10.1200/JCO.2011.34.7542

34. Thepot S, Itzykson R, Seegers V, et al. Treatment of progression of Philadelphia-negative myeloproliferative neoplasms to myelodysplastic syndrome or acute myeloid leukemia by azacitidine: a report on 54 cases on the behalf of the Groupe Francophone des Myelodysplasies (GFM). *Blood*. 2010;116(19):3735-3742. doi:10.1182/blood-2010-03-274811

35. Quintás-Cardama A, Kantarjian H, Pierce S, Cortes J, Verstovsek S. Prognostic model to identify patients with myelofibrosis at the highest risk of transformation to acute myeloid leukemia. *Clin Lymphoma Myeloma Leuk*. 2013;13(3):315-318.e2. doi:10.1016/j.clml.2013.01.001

36. Marneth AE, Mullally A. The Molecular Genetics of Myeloproliferative Neoplasms. *Cold Spring Harb Perspect Med*. 2020;10(2):a034876. Published 2020 Feb 3. doi:10.1101/cshperspect.a034876

37. Tefferi A. Myeloproliferative neoplasms: A decade of discoveries and treatment advances. *Am J Hematol*. 2016;91(1):50-58. doi:10.1002/ajh.24221

38. Hochman MJ, Smith BD, Karantanos T, et al. Chronic myeloid leukemia (CML) evolves from Philadelphia chromosome-negative myeloproliferative neoplasms (MPNs) with unexpected frequency. *Int J Hematol*. 2023;117(3):456-462. doi:10.1007/s12185-022-03463-0

39. Bonnet D. Haematopoietic stem cells. *J Pathol*. 2002;197(4):430-440. doi:10.1002/path.1153

40. McCulloch EA, Till JE. Perspectives on the properties of stem cells. *Nat Med*. 2005;11(10):1026-1028. doi:10.1038/nm1005-1026

41. Zwicker JI, Paranagama D, Lessen DS, Colucci PM, Grunwald MR. Hemorrhage in patients with polycythemia vera receiving aspirin with an anticoagulant: a prospective, observational study. *Haematologica*. 2022;107(5):1106-1110. Published 2022 May 1. doi:10.3324/haematol.2021.279032

42. Silver RT, Erdos K, Taylor E 3rd, Scandura JM, Abu-Zeinah G. Splenomegaly (SPML) in polycythemia vera (PV): its clinical significance and its relation to symptoms, post-polycythemic myelofibrosis (PPMF) and survival. *Leukemia*. 2023;37(3):691-694. doi:10.1038/s41375-022-01793-w

43. Benevolo G, Vassallo F, Urbino I, Giai V. Polycythemia Vera (PV): Update on Emerging Treatment Options. *Ther Clin Risk Manag*. 2021;17:209-221. Published 2021 Mar 16. doi:10.2147/TCRM.S213020

44. Zwicker JI, Paranagama D, Lessen DS, Colucci PM, Grunwald MR. Hemorrhage in patients with polycythemia vera receiving aspirin with an anticoagulant: a prospective, observational study. *Haematologica*. 2022;107(5):1106-1110. Published 2022 May 1. doi:10.3324/haematol.2021.279032

45. Tefferi A, Vannucchi AM, Barbui T. Essential thrombocythemia treatment algorithm 2018. *Blood Cancer J*. 2018;8(1):2. Published 2018 Jan 10. doi:10.1038/s41408-017-0041-8

46. Accurso V, Santoro M, Mancuso S, et al. The Essential Thrombocythemia in 2020: What We Know and Where We Still Have to Dig Deep. *Clin Med Insights Blood Disord*. 2020;13:2634853520978210. Published 2020 Dec 28. doi:10.1177/2634853520978210

47. Tremblay D, Mascarenhas J. Next Generation Therapeutics for the Treatment of Myelofibrosis. *Cells*. 2021;10(5):1034. Published 2021 Apr 27. doi:10.3390/cells10051034

48. Tefferi A. Primary myelofibrosis: 2021 update on diagnosis, risk-stratification, and management. *Am J Hematol*. 2021;96(1):145-162. doi:10.1002/ajh.26050

49. Mannelli L, Guglielmelli P, Vannucchi AM. Stem cell transplant for the treatment of myelofibrosis. *Expert Rev Hematol*. 2020;13(4):363-374. doi:10.1080/17474086.2020.1733406

50. Tefferi A, Vannucchi AM, Barbui T. Polycythemia vera: historical oversights, diagnostic details, and therapeutic views. *Leukemia*. 2021;35(12):3339-3351. doi:10.1038/s41375-021-01401-3

51. Levine RL, Wadleigh M, Cools J, et al. Activating mutation in the tyrosine kinase JAK2 in polycythemia vera, essential thrombocythemia, and myeloid metaplasia with myelofibrosis. *Cancer Cell*. 2005;7(4):387-397. doi:10.1016/j.ccr.2005.03.023

52. James C, Ugo V, Le Couédic JP, et al. A unique clonal JAK2 mutation leading to constitutive signalling causes polycythaemia vera. *Nature*. 2005;434(7037):1144-1148. doi:10.1038/nature03546

53. Kralovics R, Passamonti F, Buser AS, et al. A gain-of-function mutation of JAK2 in myeloproliferative disorders. *N Engl J Med*. 2005;352(17):1779-1790. doi:10.1056/NEJMoa051113

54. Baxter EJ, Scott LM, Campbell PJ, et al. Acquired mutation of the tyrosine kinase JAK2 in human myeloproliferative disorders [published correction appears in Lancet. 2005 Jul 9-15;366(9480):122]. *Lancet*. 2005;365(9464):1054-1061. doi:10.1016/S0140-6736(05)71142-9

55. Mead AJ, Mullally A. Myeloproliferative neoplasm stem cells. *Blood*. 2017;129(12):1607-1616. doi:10.1182/blood-2016-10-696005

56. Morsia E, Torre E, Poloni A, Olivieri A, Rupoli S. Molecular Pathogenesis of Myeloproliferative Neoplasms: From Molecular Landscape to Therapeutic Implications. *Int J Mol Sci*. 2022;23(9):4573. Published 2022 Apr 20. doi:10.3390/ijms23094573

57. Pardanani AD, Levine RL, Lasho T, et al. MPL515 mutations in myeloproliferative and other myeloid disorders: a study of 1182 patients. *Blood*. 2006;108(10):3472-3476. doi:10.1182/blood-2006-04-018879

58. Tiedt R, Coers J, Ziegler S, et al. Pronounced thrombocytosis in transgenic mice expressing reduced levels of Mpl in platelets and terminally differentiated megakaryocytes. *Blood*. 2009;113(8):1768-1777. doi:10.1182/blood-2008-03-146084

59. Machlus KR, Italiano JE Jr. The incredible journey: From megakaryocyte development to platelet formation. *J Cell Biol*. 2013;201(6):785-796. doi:10.1083/jcb.201304054

60. Ng AP, Kauppi M, Metcalf D, et al. Mpl expression on megakaryocytes and platelets is dispensable for thrombopoiesis but essential to prevent myeloproliferation. *Proc Natl Acad Sci U S A*. 2014;111(16):5884-5889. doi:10.1073/pnas.1404354111

61. Pikman Y, Lee BH, Mercher T, et al. MPLW515L is a novel somatic activating mutation in myelofibrosis with myeloid metaplasia. *PLoS Med*. 2006;3(7):e270. doi:10.1371/journal.pmed.0030270

62. Beer PA, Campbell PJ, Scott LM, et al. MPL mutations in myeloproliferative disorders: analysis of the PT-1 cohort. *Blood*. 2008;112(1):141-149. doi:10.1182/blood-2008-01-131664

63. Milosevic Feenstra JD, Nivarthi H, Gisslinger H, et al. Whole-exome sequencing identifies novel MPL and JAK2 mutations in triple-negative myeloproliferative neoplasms. *Blood*. 2016;127(3):325-332. doi:10.1182/blood-2015-07-661835

64. Lannutti BJ, Epp A, Roy J, Chen J, Josephson NC. Incomplete restoration of Mpl expression in the mpl-/- mouse produces partial correction of the stem cell-repopulating defect and paradoxical thrombocytosis. *Blood*. 2009;113(8):1778-1785. doi:10.1182/blood-2007-11-124859

65. Pikman Y, Lee BH, Mercher T, et al. MPLW515L is a novel somatic activating mutation in myelofibrosis with myeloid metaplasia. *PLoS Med*. 2006;3(7):e270. doi:10.1371/journal.pmed.0030270

66. Rumi E, Pietra D, Guglielmelli P, et al. Acquired copy-neutral loss of heterozygosity of chromosome 1p as a molecular event associated with marrow fibrosis in MPL-mutated myeloproliferative neoplasms. *Blood*. 2013;121(21):4388-4395. doi:10.1182/blood-2013-02-486050

67. Nangalia J, Massie CE, Baxter EJ, et al. Somatic CALR mutations in myeloproliferative neoplasms with nonmutated JAK2. *N Engl J Med*. 2013;369(25):2391-2405. doi:10.1056/NEJMoa1312542

68. Klampfl T, Gisslinger H, Harutyunyan AS, et al. Somatic mutations of calreticulin in myeloproliferative neoplasms. *N Engl J Med*. 2013;369(25):2379-2390. doi:10.1056/NEJMoa1311347

69. Peterson JR, Ora A, Van PN, Helenius A. Transient, lectin-like association of calreticulin with folding intermediates of cellular and viral glycoproteins. *Mol Biol Cell*. 1995;6(9):1173-1184. doi:10.1091/mbc.6.9.1173

70. High S, Lecomte FJ, Russell SJ, Abell BM, Oliver JD. Glycoprotein folding in the endoplasmic reticulum: a tale of three chaperones?. *FEBS Lett*. 2000;476(1-2):38-41. doi:10.1016/s0014-5793(00)01666-5

71. Stubbins RJ, Francis A, Kuchenbauer F, Sanford D. Management of Acute Myeloid Leukemia: A Review for General Practitioners in Oncology. *Curr Oncol*. 2022;29(9):6245-6259. Published 2022 Aug 30. doi:10.3390/curroncol29090491

72. Saultz JN, Garzon R. Acute Myeloid Leukemia: A Concise Review. *J Clin Med*. 2016;5(3):33. Published 2016 Mar 5. doi:10.3390/jcm5030033

73. Oran B, Weisdorf DJ. Survival for older patients with acute myeloid leukemia: a population-based study. *Haematologica*. 2012;97(12):1916-1924. doi:10.3324/haematol.2012.066100

74. Menzin J, Lang K, Earle CC, Kerney D, Mallick R. The Outcomes and Costs of Acute Myeloid Leukemia Among the Elderly. *Arch Intern Med.* 2002;162(14):1597–1603. doi:10.1001/archinte.162.14.1597

75. De Kouchkovsky I, Abdul-Hay M. 'Acute myeloid leukemia: a comprehensive review and 2016 update'. *Blood Cancer J*. 2016;6(7):e441. Published 2016 Jul 1. doi:10.1038/bcj.2016.50

76. McNerney ME, Godley LA, Le Beau MM. Therapy-related myeloid neoplasms: when genetics and environment collide. *Nat Rev Cancer*. 2017;17(9):513-527. doi:10.1038/nrc.2017.60

77. Godley LA, Larson RA. Therapy-related myeloid leukemia. *Semin Oncol*. 2008;35(4):418-429. doi:10.1053/j.seminoncol.2008.04.012

78. Grabek J, Straube J, Bywater M, Lane SW. MPN: The Molecular Drivers of Disease Initiation, Progression and Transformation and their Effect on Treatment. *Cells*. 2020;9(8):1901. Published 2020 Aug 14. doi:10.3390/cells9081901

79. Bywater M, Lane SW. Paving the way to improve therapy for Myeloproliferative Neoplasms. *Nat Commun*. 2022;13(1):5025. Published 2022 Aug 26. doi:10.1038/s41467-022-32694-2

80. Tefferi A, Barbui T. Polycythemia vera and essential thrombocythemia: 2017 update on diagnosis, risk-stratification, and management. *Am J Hematol*. 2017;92(1):94-108. doi:10.1002/ajh.24607

81. Salit RB, Deeg HJ. Transplant Decisions in Patients with Myelofibrosis: Should Mutations Be the Judge?. *Biol Blood Marrow Transplant*. 2018;24(4):649-658. doi:10.1016/j.bbmt.2017.10.037

82. Devlin R, Gupta V. Myelofibrosis: to transplant or not to transplant?. *Hematology Am Soc Hematol Educ Program*. 2016;2016(1):543-551. doi:10.1182/asheducation-2016.1.543

83. Tefferi A, Partain DK, Palmer JM, et al. Allogeneic hematopoietic stem cell transplant overcomes the adverse survival effect of very high risk and unfavorable karyotype in myelofibrosis. *Am J Hematol*. 2018;93(5):649-654. doi:10.1002/ajh.25053

84. Gupta V, Kennedy JA, Capo-Chichi JM, et al. Genetic factors rather than blast reduction determine outcomes of allogeneic HCT in BCR-ABL-negative MPN in blast phase [published correction appears in Blood Adv. 2021 Jun 8;5(11):2518]. *Blood Adv*. 2020;4(21):5562-5573. doi:10.1182/bloodadvances.2020002727

85. Gangat N, Tefferi A. Myelofibrosis biology and contemporary management. *Br J Haematol*. 2020;191(2):152-170. doi:10.1111/bjh.16576

86. Szuber N, Mudireddy M, Nicolosi M, et al. 3023 Mayo Clinic Patients With Myeloproliferative Neoplasms: Risk-Stratified Comparison of Survival and Outcomes Data Among Disease Subgroups. *Mayo Clin Proc*. 2019;94(4):599-610. doi:10.1016/j.mayocp.2018.08.022

87. McLornan DP, Yakoub-Agha I, Robin M, Chalandon Y, Harrison CN, Kroger N. State-of-the-art review: allogeneic stem cell transplantation for myelofibrosis in 2019. *Haematologica*. 2019;104(4):659-668. doi:10.3324/haematol.2018.206151

88. Kerbauy DM, Gooley TA, Sale GE, et al. Hematopoietic cell transplantation as curative therapy for idiopathic myelofibrosis, advanced polycythemia vera, and essential thrombocythemia. *Biol Blood Marrow Transplant*. 2007;13(3):355-365. doi:10.1016/j.bbmt.2006.11.004

89. Deeg HJ, Gooley TA, Flowers ME, et al. Allogeneic hematopoietic stem cell transplantation for myelofibrosis. *Blood*. 2003;102(12):3912-3918. doi:10.1182/blood-2003-06-1856

90. Guardiola P, Anderson JE, Bandini G, et al. Allogeneic stem cell transplantation for agnogenic myeloid metaplasia: a European Group for Blood and Marrow Transplantation, Société Française de Greffe de Moelle, Gruppo Italiano per il Trapianto del Midollo Osseo, and Fred Hutchinson Cancer Research Center Collaborative Study. *Blood*. 1999;93(9):2831-2838.

91. Lussana F, Rambaldi A, Finazzi MC, et al. Allogeneic hematopoietic stem cell transplantation in patients with polycythemia vera or essential thrombocythemia transformed to myelofibrosis or acute myeloid leukemia: a report from the MPN Subcommittee of the Chronic Malignancies Working Party of the European Group for Blood and Marrow Transplantation. *Haematologica*. 2014;99(5):916-921. doi:10.3324/haematol.2013.094284

92. Barbui T, Barosi G, Birgegard G, et al. Philadelphia-negative classical myeloproliferative neoplasms: critical concepts and management recommendations from European LeukemiaNet. *J Clin Oncol*. 2011;29(6):761-770. doi:10.1200/JCO.2010.31.8436

93. Tefferi A, Barbui T. Polycythemia vera and essential thrombocythemia: 2017 update on diagnosis, risk-stratification, and management. *Am J Hematol*. 2017;92(1):94-108. doi:10.1002/ajh.24607

94. Martínez-Trillos A, Gaya A, Maffioli M, et al. Efficacy and tolerability of hydroxyurea in the treatment of the hyperproliferative manifestations of myelofibrosis: results in 40 patients. *Ann Hematol*. 2010;89(12):1233-1237. doi:10.1007/s00277-010-1019-9

95. Kim SY, Bae SH, Bang SM, et al. The 2020 revision of the guidelines for the management of myeloproliferative neoplasms. *Korean J Intern Med*. 2021;36(1):45-62. doi:10.3904/kjim.2020.319

96. Odenike O, Tefferi A. Conventional and new treatment options for myelofibrosis with myeloid metaplasia. *Semin Oncol*. 2005;32(4):422-431. doi:10.1053/j.seminoncol.2005.06.014

97. Tefferi A. Primary myelofibrosis: 2013 update on diagnosis, risk-stratification, and management [published correction appears in Am J Hematol. 2013 May;88(5):437-45]. *Am J Hematol*. 2013;88(2):141-150. doi:10.1002/ajh.23384

98. Mesa RA. The evolving treatment paradigm in myelofibrosis. *Leuk Lymphoma*. 2013;54(2):242-251. doi:10.3109/10428194.2012.710905

99. Alvarez-Larrán A, Kerguelen A, Hernández-Boluda JC, et al. Frequency and prognostic value of resistance/intolerance to hydroxycarbamide in 890 patients with polycythaemia vera. *Br J Haematol*. 2016;172(5):786-793. doi:10.1111/bjh.13886

100. Alvarez-Larrán A, Kerguelen A, Hernández-Boluda JC, et al. Frequency and prognostic value of resistance/intolerance to hydroxycarbamide in 890 patients with polycythaemia vera. *Br J Haematol*. 2016;172(5):786-793. doi:10.1111/bjh.13886

101. Antar A, Ishak RS, Otrock ZK, et al. Successful treatment of hydroxyurea-associated chronic leg ulcers associated with squamous cell carcinoma. *Hematol Oncol Stem Cell Ther*. 2014;7(4):166-169. doi:10.1016/j.hemonc.2014.09.008

102. Landolfi R, Marchioli R, Kutti J, et al. Efficacy and safety of low-dose aspirin in polycythemia vera. *N Engl J Med*. 2004;350(2):114-124. doi:10.1056/NEJMoa035572

103. Cortelazzo S, Finazzi G, Ruggeri M, et al. Hydroxyurea for patients with essential thrombocythemia and a high risk of thrombosis. *N Engl J Med*. 1995;332(17):1132-1136. doi:10.1056/NEJM199504273321704

104. Harrison CN, Campbell PJ, Buck G, et al. Hydroxyurea compared with anagrelide in high-risk essential thrombocythemia. *N Engl J Med*. 2005;353(1):33-45. doi:10.1056/NEJMoa043800

105. Li B, Rampal RK, Xiao Z. Targeted therapies for myeloproliferative neoplasms. *Biomark Res*. 2019;7:15. Published 2019 Jul 16. doi:10.1186/s40364-019-0166-y

106. Deisseroth A, Kaminskas E, Grillo J, et al. U.S. Food and Drug Administration approval: ruxolitinib for the treatment of patients with intermediate and high-risk myelofibrosis. *Clin Cancer Res*. 2012;18(12):3212-3217. doi:10.1158/1078-0432.CCR-12-0653

107. Penna D. New Horizons in Myeloproliferative Neoplasms Treatment: A Review of Current and Future Therapeutic Options. *Medicina (Kaunas)*. 2021;57(11):1181. Published 2021 Oct 31. doi:10.3390/medicina57111181

108. Arana Yi C, Tam CS, Verstovsek S. Efficacy, and safety of ruxolitinib in the treatment of patients with myelofibrosis. *Future Oncol*. 2015;11(5):719-733. doi:10.2217/fon.14.272

109. Ostojic A, Vrhovac R, Verstovsek S. Ruxolitinib for the treatment of myelofibrosis: its clinical potential. *Ther Clin Risk Manag*. 2012;8:95-103. doi:10.2147/TCRM.S23277

110. Austin RJ, Straube J, Bruedigam C, et al. Distinct effects of ruxolitinib and interferon-alpha on murine JAK2V617F myeloproliferative neoplasm hematopoietic stem cell populations. *Leukemia*. 2020;34(4):1075-1089. doi:10.1038/s41375-019-0638-y

111. Verstovsek S, Mesa RA, Gotlib J, et al. A double-blind, placebo-controlled trial of ruxolitinib for myelofibrosis. *N Engl J Med*. 2012;366(9):799-807. doi:10.1056/NEJMoa1110557

112. Harrison C, Kiladjian JJ, Al-Ali HK, et al. JAK inhibition with ruxolitinib versus best available therapy for myelofibrosis. *N Engl J Med*. 2012;366(9):787-798. doi:10.1056/NEJMoa1110556

113. Mesa R, Verstovsek S, Kiladjian JJ, et al. Changes in quality of life and disease-related symptoms in patients with polycythemia vera receiving ruxolitinib or standard therapy. *Eur J Haematol*. 2016;97(2):192-200. doi:10.1111/ejh.12707

114. Harrison CN, Vannucchi AM, Kiladjian JJ, et al. Long-term findings from COMFORT-II, a phase 3 study of ruxolitinib vs best available therapy for myelofibrosis [published correction appears in Leukemia. 2017 Mar;31(3):775]. *Leukemia*. 2016;30(8):1701-1707. doi:10.1038/leu.2016.148

115. Cervantes F, Vannucchi AM, Kiladjian J-J, et al. Three-year efficacy, safety, and survival findings from COMFORT-II, a phase 3 study comparing ruxolitinib with best available therapy for myelofibrosis. Blood. 2013;122(25):4047-4053. *Blood*. 2016;128(25):3013. doi:10.1182/blood-2016-11-750505

116. Verstovsek S, Gotlib J, Mesa RA, et al. Long-term survival in patients treated with ruxolitinib for myelofibrosis: COMFORT-I and -II pooled analyses. *J Hematol Oncol*. 2017;10(1):156. Published 2017 Sep 29. doi:10.1186/s13045-017-0527-7

117. Gupta V, Cerquozzi S, Foltz L, et al. Patterns of Ruxolitinib Therapy Failure and Its Management in Myelofibrosis: Perspectives of the Canadian Myeloproliferative Neoplasm Group. *JCO Oncol Pract*. 2020;16(7):351-359. doi:10.1200/JOP.19.00506

118. Rumi E, Pietra D, Ferretti V, et al. JAK2 or CALR mutation status defines subtypes of essential thrombocythemia with substantially different clinical course and outcomes. *Blood*. 2014;123(10):1544-1551. doi:10.1182/blood-2013-11-539098

119. Tefferi A, Lasho TL, Finke CM, et al. CALR vs JAK2 vs MPL-mutated or triple-negative myelofibrosis: clinical, cytogenetic, and molecular comparisons. *Leukemia*. 2014;28(7):1472-1477. doi:10.1038/leu.2014.3

120. Klampfl T, Gisslinger H, Harutyunyan AS, et al. Somatic mutations of calreticulin in myeloproliferative neoplasms. *N Engl J Med*. 2013;369(25):2379-2390. doi:10.1056/NEJMoa1311347

121. Almanza A, Carlesso A, Chintha C, et al. Endoplasmic reticulum stress signalling - from basic mechanisms to clinical applications. FEBS J. 2019;286(2):241-278. doi:10.1111/febs.14608

122. Schwarz DS, Blower MD. The endoplasmic reticulum: structure, function, and response to cellular signaling. *Cell Mol Life Sci*. 2016;73(1):79-94. doi:10.1007/s00018-015-2052-6

123. Reid DW, Nicchitta CV. Diversity, and selectivity in mRNA translation on the endoplasmic reticulum. *Nat Rev Mol Cell Biol*. 2015;16(4):221-231. doi:10.1038/nrm3958

124. Rapoport TA. Protein translocation across the eukaryotic endoplasmic reticulum and bacterial plasma membranes. *Nature*. 2007;450(7170):663-669. doi:10.1038/nature06384

125. Braakman I, Hebert DN. Protein folding in the endoplasmic reticulum. *Cold Spring Harb Perspect Biol*. 2013;5(5):a013201. Published 2013 May 1. doi:10.1101/cshperspect.a013201

126. Fagone P, Jackowski S. Membrane phospholipid synthesis and endoplasmic reticulum function. *J Lipid Res*. 2009;50 Suppl(Suppl):S311-S316. doi:10.1194/jlr.R800049-JLR200

127. Hebert DN, Garman SC, Molinari M. The glycan code of the endoplasmic reticulum: asparagine-linked carbohydrates as protein maturation and quality-control tags. *Trends Cell Biol*. 2005;15(7):364-370. doi:10.1016/j.tcb.2005.05.007

128. Clapham DE. Calcium signaling. *Cell*. 2007;131(6):1047-1058. doi:10.1016/j.cell.2007.11.028

129. Westrate LM, Lee JE, Prinz WA, Voeltz GK. Form follows function: the importance of endoplasmic reticulum shape. *Annu Rev Biochem*. 2015;84:791-811. doi:10.1146/annurev-biochem-072711-163501

130. Stefan CJ, Manford AG, Baird D, Yamada-Hanff J, Mao Y, Emr SD. Osh proteins regulate phosphoinositide metabolism at ER-plasma membrane contact sites. *Cell*. 2011;144(3):389-401. doi:10.1016/j.cell.2010.12.034

131. Smith MH, Ploegh HL, Weissman JS. Road to ruin: targeting proteins for degradation in the endoplasmic reticulum. *Science*. 2011;334(6059):1086-1090. doi:10.1126/science.1209235

132. Meusser B, Hirsch C, Jarosch E, Sommer T. ERAD: the long road to destruction. *Nat Cell Biol*. 2005;7(8):766-772. doi:10.1038/ncb0805-766

133. Christianson JC, Carvalho P. Order through destruction: how ER-associated protein degradation contributes to organelle homeostasis. *EMBO J*. 2022;41(6):e109845. doi:10.15252/embj.2021109845

134. Braakman I, Bulleid NJ. Protein folding and modification in the mammalian endoplasmic reticulum. *Annu Rev Biochem*. 2011;80:71-99. doi:10.1146/annurev-biochem-062209-093836

135. Lodish HF, Kong N, Snider M, Strous GJ. Hepatoma secretory proteins migrate from rough endoplasmic reticulum to Golgi at characteristic rates. *Nature*. 1983;304(5921):80-83. doi:10.1038/304080a0

136. Ellgaard L, McCaul N, Chatsisvili A, Braakman I. Co- and Post-Translational Protein Folding in the ER. *Traffic*. 2016;17(6):615-638. doi:10.1111/tra.12392

137. Ruggiano A, Foresti O, Carvalho P. Quality control: ER-associated degradation: protein quality control and beyond. *J Cell Biol*. 2014;204(6):869-879. doi:10.1083/jcb.201312042

138. Hetz C. The unfolded protein response: controlling cell fate decisions under ER stress and beyond. *Nat Rev Mol Cell Biol*. 2012;13(2):89-102. Published 2012 Jan 18. doi:10.1038/nrm3270

139. Walter P, Ron D. The unfolded protein response: from stress pathway to homeostatic regulation. *Science*. 2011;334(6059):1081-1086. doi:10.1126/science.1209038

140. Oakes SA. Endoplasmic Reticulum Stress Signaling in Cancer Cells. *Am J Pathol*. 2020;190(5):934-946. doi:10.1016/j.ajpath.2020.01.010

141. Soto C. Protein misfolding and disease; protein refolding and therapy. *FEBS Lett*. 2001;498(2-3):204-207. doi:10.1016/s0014-5793(01)02486-3

142. Kelly JW. Alternative conformations of amyloidogenic proteins govern their behavior. *Curr Opin Struct Biol*. 1996;6(1):11-17. doi:10.1016/s0959-440x(96)80089-3

143. Moreno-Gonzalez I, Soto C. Misfolded protein aggregates: mechanisms, structures, and potential for disease transmission. *Semin Cell Dev Biol*. 2011;22(5):482-487. doi:10.1016/j.semcdb.2011.04.002

144. Cheng Y, Yang JM. Survival, and death of endoplasmic-reticulum-stressed cells: Role of autophagy. *World J Biol Chem*. 2011;2(10):226-231. doi:10.4331/wjbc.v2.i10.226

145. Szegezdi E, Logue SE, Gorman AM, Samali A. Mediators of endoplasmic reticulum stress-induced apoptosis. *EMBO Rep*. 2006;7(9):880-885. doi:10.1038/sj.embor.7400779

146. Boyce M, Yuan J. Cellular response to endoplasmic reticulum stress: a matter of life or death. *Cell Death Differ*. 2006;13(3):363-373. doi:10.1038/sj.cdd.4401817

147. Wang S, Kaufman RJ. The impact of the unfolded protein response on human disease. *J Cell Biol*. 2012;197(7):857-867. doi:10.1083/jcb.201110131

148. Gardner BM, Walter P. Unfolded proteins are Ire1-activating ligands that directly induce the unfolded protein response. *Science*. 2011;333(6051):1891-1894. doi:10.1126/science.1209126

149. Bertolotti A, Zhang Y, Hendershot LM, Harding HP, Ron D. Dynamic interaction of BiP and ER stress transducers in the unfolded-protein response. *Nat Cell Biol*. 2000;2(6):326-332. doi:10.1038/35014014

150. Shen J, Chen X, Hendershot L, Prywes R. ER stress regulation of ATF6 localization by dissociation of BiP/GRP78 binding and unmasking of Golgi localization signals. *Dev Cell*. 2002;3(1):99-111. doi:10.1016/s1534-5807(02)00203-4

151. Shore GC, Papa FR, Oakes SA. Signaling cell death from the endoplasmic reticulum stress response. *Curr Opin Cell Biol*. 2011;23(2):143-149. doi:10.1016/j.ceb.2010.11.003

152. Oakes SA, Papa FR. The role of endoplasmic reticulum stress in human pathology. *Annu Rev Pathol*. 2015;10:173-194. doi:10.1146/annurev-pathol-012513-104649

153. Koopman M, Hetz C, Nollen EAA. Saved by the Matrix: UPR Independent Survival under ER Stress. *Cell*. 2019;179(6):1246-1248. doi:10.1016/j.cell.2019.11.012

154. Hotamisligil GS, Davis RJ. Cell Signaling and Stress Responses. *Cold Spring Harb Perspect Biol*. 2016;8(10):a006072. Published 2016 Oct 3. doi:10.1101/cshperspect.a006072

155. Tirasophon W, Welihinda AA, Kaufman RJ. A stress response pathway from the endoplasmic reticulum to the nucleus requires a novel bifunctional protein kinase/endoribonuclease (Ire1p) in mammalian cells. *Genes Dev*. 1998;12(12):1812-1824. doi:10.1101/gad.12.12.1812

156. Harding HP, Zhang Y, Ron D. Protein translation and folding are coupled by an endoplasmic-reticulum-resident kinase [published correction appears in Nature 1999 Mar 4;398(6722):90]. *Nature*. 1999;397(6716):271-274. doi:10.1038/16729

157. Haze K, Yoshida H, Yanagi H, Yura T, Mori K. Mammalian transcription factor ATF6 is synthesized as a transmembrane protein and activated by proteolysis in response to endoplasmic reticulum stress. *Mol Biol Cell*. 1999;10(11):3787-3799. doi:10.1091/mbc.10.11.3787

158. Ghosh R, Wang L, Wang ES, et al. Allosteric inhibition of the IRE1α RNase preserves cell viability and function during endoplasmic reticulum stress. *Cell*. 2014;158(3):534-548. doi:10.1016/j.cell.2014.07.002

159. Han D, Lerner AG, Vande Walle L, et al. IRE1alpha kinase activation modes control alternate endoribonuclease outputs to determine divergent cell fates. *Cell*. 2009;138(3):562-575. doi:10.1016/j.cell.2009.07.017

160. Calfon M, Zeng H, Urano F, et al. IRE1 couples endoplasmic reticulum load to secretory capacity by processing the XBP-1 mRNA [published correction appears in Nature 2002 Nov 14;420(6912):202]. *Nature*. 2002;415(6867):92-96. doi:10.1038/415092a

161. Yoshida H, Matsui T, Yamamoto A, Okada T, Mori K. XBP1 mRNA is induced by ATF6 and spliced by IRE1 in response to ER stress to produce a highly active transcription factor. *Cell*. 2001;107(7):881-891. doi:10.1016/s0092-8674(01)00611-0

162. Wang XZ, Harding HP, Zhang Y, Jolicoeur EM, Kuroda M, Ron D. Cloning of mammalian Ire1 reveals diversity in the ER stress responses. *EMBO J*. 1998;17(19):5708-5717. doi:10.1093/emboj/17.19.5708

163. Iwawaki T, Hosoda A, Okuda T, et al. Translational control by the ER transmembrane kinase/ribonuclease IRE1 under ER stress. *Nat Cell Biol*. 2001;3(2):158-164. doi:10.1038/35055065

164. Mori K, Ma W, Gething MJ, Sambrook J. A transmembrane protein with a cdc2+/CDC28-related kinase activity is required for signaling from the ER to the nucleus. *Cell*. 1993;74(4):743-756. doi:10.1016/0092-8674(93)90521-q

165. Nikawa J, Yamashita S. IRE1 encodes a putative protein kinase containing a membrane-spanning domain and is required for inositol phototrophy in Saccharomyces cerevisiae. *Mol Microbiol*. 1992;6(11):1441-1446. doi:10.1111/j.1365-2958.1992.tb00864.x

166. Zinszner H, Kuroda M, Wang X, et al. CHOP is implicated in programmed cell death in response to impaired function of the endoplasmic reticulum. *Genes Dev*. 1998;12(7):982-995. doi:10.1101/gad.12.7.982

167. Bouchecareilh M, Higa A, Fribourg S, Moenner M, Chevet E. Peptides derived from the bifunctional kinase/RNase enzyme IRE1α modulate IRE1α activity and protect cells from endoplasmic reticulum stress. *FASEB J*. 2011;25(9):3115-3129. doi:10.1096/fj.11-182931

168. Sanches M, Duffy NM, Talukdar M, et al. Structure and mechanism of action of the hydroxy-aryl-aldehyde class of IRE1 endoribonuclease inhibitors. *Nat Commun*. 2014;5:4202. Published 2014 Aug 28. doi:10.1038/ncomms5202

169. Iwawaki T, Akai R, Yamanaka S, Kohno K. Function of IRE1 alpha in the placenta is essential for placental development and embryonic viability. *Proc Natl Acad Sci U S A*. 2009;106(39):16657-16662. doi:10.1073/pnas.0903775106

170. Sidrauski C, Walter P. The transmembrane kinase Ire1p is a site-specific endonuclease that initiates mRNA splicing in the unfolded protein response. *Cell*. 1997;90(6):1031-1039. doi:10.1016/s0092-8674(00)80369-4

171. Greer CL, Peebles CL, Gegenheimer P, Abelson J. Mechanism of action of a yeast RNA ligase in tRNA splicing. *Cell*. 1983;32(2):537-546. doi:10.1016/0092-8674(83)90473-7

172. Sidrauski C, Cox JS, Walter P. tRNA ligase is required for regulated mRNA splicing in the unfolded protein response. *Cell*. 1996;87(3):405-413. doi:10.1016/s0092-8674(00)81361-6

173. Schwer B, Sawaya R, Ho CK, Shuman S. Portability and fidelity of RNA-repair systems. *Proc Natl Acad Sci U S A*. 2004;101(9):2788-2793. doi:10.1073/pnas.0305859101

174. Tanaka N, Meineke B, Shuman S. RtcB, a novel RNA ligase, can catalyze tRNA splicing and HAC1 mRNA splicing in vivo. *J Biol Chem*. 2011;286(35):30253-30257. doi:10.1074/jbc.C111.274597

175. Baltz AG, Munschauer M, Schwanhäusser B, et al. The mRNA-bound proteome and its global occupancy profile on protein-coding transcripts. *Mol Cell*. 2012;46(5):674-690. doi:10.1016/j.molcel.2012.05.021

176. Lu Y, Liang FX, Wang X. A synthetic biology approach identifies the mammalian UPR RNA ligase RtcB. *Mol Cell*. 2014;55(5):758-770. doi:10.1016/j.molcel.2014.06.032

177. Travers KJ, Patil CK, Wodicka L, Lockhart DJ, Weissman JS, Walter P. Functional and genomic analyses reveal an essential coordination between the unfolded protein response and ER-associated degradation. *Cell*. 2000;101(3):249-258. doi:10.1016/s0092-8674(00)80835-1

178. Iwakoshi NN, Lee AH, Glimcher LH. The X-box binding protein-1 transcription factor is required for plasma cell differentiation and the unfolded protein response. *Immunol Rev*. 2003;194:29-38. doi:10.1034/j.1600-065x.2003.00057.x

179. Lee AH, Iwakoshi NN, Glimcher LH. XBP-1 regulates a subset of endoplasmic reticulum resident chaperone genes in the unfolded protein response. *Mol Cell Biol*. 2003;23(21):7448-7459. doi:10.1128/MCB.23.21.7448-7459.2003

180. Han D, Lerner AG, Vande Walle L, et al. IRE1alpha kinase activation modes control alternate endoribonuclease outputs to determine divergent cell fates. *Cell*. 2009;138(3):562-575. doi:10.1016/j.cell.2009.07.017

181. Ghosh R, Wang L, Wang ES, et al. Allosteric inhibition of the IRE1α RNase preserves cell viability and function during endoplasmic reticulum stress. *Cell*. 2014;158(3):534-548. doi:10.1016/j.cell.2014.07.002

182. Hollien J, Lin JH, Li H, Stevens N, Walter P, Weissman JS. Regulated Ire1-dependent decay of messenger RNAs in mammalian cells. *J Cell Biol*. 2009;186(3):323-331. doi:10.1083/jcb.200903014

183. Coelho DS, Domingos PM. Physiological roles of regulated Ire1 dependent decay. *Front Genet*. 2014;5:76. Published 2014 Apr 16. doi:10.3389/fgene.2014.00076

184. Sano R, Reed JC. ER stress-induced cell death mechanisms. *Biochim Biophys Acta*. 2013;1833(12):3460-3470. doi:10.1016/j.bbamcr.2013.06.028

185. Gómora-García JC, Gerónimo-Olvera C, Pérez-Martínez X, Massieu L. IRE1α RIDD activity induced under ER stress drives neuronal death by the degradation of 14-3-3 θ mRNA in cortical neurons during glucose deprivation. *Cell Death Discov*. 2021;7(1):131. Published 2021 Jun 3. doi:10.1038/s41420-021-00518-9

186. Maurel M, Chevet E, Tavernier J, Gerlo S. Getting RIDD of RNA: IRE1 in cell fate regulation. *Trends Biochem Sci*. 2014;39(5):245-254. doi:10.1016/j.tibs.2014.02.008

187. Hirata A. Recent Insights Into the Structure, Function, and Evolution of the RNA-Splicing Endonucleases. *Front Genet*. 2019;10:103. Published 2019 Feb 12. doi:10.3389/fgene.2019.00103

188. Abelson J, Trotta CR, Li H. tRNA splicing. *J Biol Chem*. 1998;273(21):12685-12688. doi:10.1074/jbc.273.21.12685

189. Yoshihisa T. Handling tRNA introns, archaeal way, and eukaryotic way. *Front Genet*. 2014;5:213. Published 2014 Jul 10. doi:10.3389/fgene.2014.00213

190. Lopes RR, Kessler AC, Polycarpo C, Alfonzo JD. Cutting, dicing, healing, and sealing: the molecular surgery of tRNA. *Wiley Interdiscip Rev RNA*. 2015;6(3):337-349. doi:10.1002/wrna.1279

191. Calvin K, Li H. RNA-splicing endonuclease structure and function. *Cell Mol Life Sci*. 2008;65(7-8):1176-1185. doi:10.1007/s00018-008-7393-y

192. Hayne CK, Schmidt CA, Haque MI, Matera AG, Stanley RE. Reconstitution of the human tRNA splicing endonuclease complex: insight into the regulation of pre-tRNA cleavage. *Nucleic Acids Res*. 2020;48(14):7609-7622. doi:10.1093/nar/gkaa438

193. Hopper AK, Nostramo RT. tRNA Processing and Subcellular Trafficking Proteins Multitask in Pathways for Other RNAs. *Front Genet*. 2019;10:96. Published 2019 Feb 20. doi:10.3389/fgene.2019.00096

194. Dixit S, Henderson JC, Alfonzo JD. Multi-Substrate Specificity and the Evolutionary Basis for Interdependence in tRNA Editing and Methylation Enzymes. *Front Genet*. 2019;10:104. Published 2019 Feb 14. doi:10.3389/fgene.2019.00104

195. Chatterjee K, Nostramo RT, Wan Y, Hopper AK. tRNA dynamics between the nucleus, cytoplasm, and mitochondrial surface: Location, location, location. *Biochim Biophys Acta Gene Regul Mech*. 2018;1861(4):373-386. doi:10.1016/j.bbagrm.2017.11.007

196. Swinehart WE, Jackman JE. Diversity in mechanism and function of tRNA methyltransferases. *RNA Biol*. 2015;12(4):398-411. doi:10.1080/15476286.2015.1008358

197. Jackman JE, Alfonzo JD. Transfer RNA modifications: nature's combinatorial chemistry playground. *Wiley Interdiscip Rev RNA*. 2013;4(1):35-48. doi:10.1002/wrna.1144

198. Fujishima K, Kanai A. tRNA gene diversity in the three domains of life. *Front Genet*. 2014;5:142. Published 2014 May 26. doi:10.3389/fgene.2014.00142

199. Abelson J, Trotta CR, Li H. tRNA splicing. *J Biol Chem*. 1998;273(21):12685-12688. doi:10.1074/jbc.273.21.12685

200. Friedel M, Nikolajewa S, Sühnel J, Wilhelm T. DiProDB: a database for dinucleotide properties. *Nucleic Acids Res*. 2009;37(Database issue):D37-D40. doi:10.1093/nar/gkn597

201. Trotta CR, Miao F, Arn EA, et al. The yeast tRNA splicing endonuclease: a tetrameric enzyme with two active site subunits homologous to the archaeal tRNA endonucleases. *Cell*. 1997;89(6):849-858. doi:10.1016/s0092-8674(00)80270-6

202. Paushkin SV, Patel M, Furia BS, Peltz SW, Trotta CR. Identification of a human endonuclease complex reveals a link between tRNA splicing and pre-mRNA 3' end formation. *Cell*. 2004;117(3):311-321. doi:10.1016/s0092-8674(04)00342-3

203. Trotta CR, Paushkin SV, Patel M, Li H, Peltz SW. Cleavage of pre-tRNAs by the splicing endonuclease requires a composite active site. *Nature*. 2006;441(7091):375-377. doi:10.1038/nature04741

204. Reyes VM, Abelson J. Substrate recognition and splice site determination in yeast tRNA splicing. *Cell*. 1988;55(4):719-730. doi:10.1016/0092-8674(88)90230-9

205. Yoshihisa T. Handling tRNA introns, archaeal way, and eukaryotic way. *Front Genet*. 2014;5:213. Published 2014 Jul 10. doi:10.3389/fgene.2014.00213

206. Popow J, Englert M, Weitzer S, et al. HSPC117 is the essential subunit of a human tRNA splicing ligase complex. *Science*. 2011;331(6018):760-764. doi:10.1126/science.1197847

207. Cherry PD, White LK, York K, Hesselberth JR. Genetic bypass of essential RNA repair enzymes in budding yeast. *RNA*. 2018;24(3):313-323. doi:10.1261/rna.061788.117

208. Lu Y, Liang FX, Wang X. A synthetic biology approach identifies the mammalian UPR RNA ligase RtcB. *Mol Cell*. 2014;55(5):758-770. doi:10.1016/j.molcel.2014.06.032

209. Schmidt CA, Giusto JD, Bao A, Hopper AK, Matera AG. Molecular determinants of metazoan tricRNA biogenesis. *Nucleic Acids Res*. 2019;47(12):6452-6465. doi:10.1093/nar/gkz311

210. Tanaka N, Chakravarty AK, Maughan B, Shuman S. Novel mechanism of RNA repair by RtcB via sequential 2',3'-cyclic phosphodiesterase and 3'-Phosphate/5'-hydroxyl ligation reactions. *J Biol Chem*. 2011;286(50):43134-43143. doi:10.1074/jbc.M111.302133

211. Kroupova A, Ackle F, Asanović I, et al. Molecular architecture of the human tRNA ligase complex. *Elife*. 2021;10:e71656. Published 2021 Dec 2. doi:10.7554/eLife.71656

212. Jaffe LF. Sources of calcium in egg activation: a review and hypothesis. *Dev Biol*. 1983;99(2):265-276. doi:10.1016/0012-1606(83)90276-2

213. Eisen A, Reynolds GT. Source and sinks for the calcium released during fertilization of single sea urchin eggs. *J Cell Biol*. 1985;100(5):1522-1527. doi:10.1083/jcb.100.5.1522

214. Koch GL. The endoplasmic reticulum and calcium storage. *Bioessays*. 1990;12(11):527-531. doi:10.1002/bies.950121105

215. Clapham DE. Calcium signaling. *Cell*. 2007;131(6):1047-1058. doi:10.1016/j.cell.2007.11.028

216. Samtleben S, Jaepel J, Fecher C, Andreska T, Rehberg M, Blum R. Direct imaging of ER calcium with targeted-esterase induced dye loading (TED). *J Vis Exp*. 2013;(75):e50317. Published 2013 May 7. doi:10.3791/50317

217. Putney JW Jr. Capacitative calcium entry: sensing the calcium stores. *J Cell Biol*. 2005;169(3):381-382. doi:10.1083/jcb.200503161

218. Carreras-Sureda A, Pihán P, Hetz C. Calcium signaling at the endoplasmic reticulum: fine-tuning stress responses. *Cell Calcium*. 2018;70:24-31. doi:10.1016/j.ceca.2017.08.004

219. Groenendyk J, Agellon LB, Michalak M. Calcium signaling and endoplasmic reticulum stress. *Int Rev Cell Mol Biol*. 2021;363:1-20. doi:10.1016/bs.ircmb.2021.03.003

220. Braakman I, Bulleid NJ. Protein folding and modification in the mammalian endoplasmic reticulum. *Annu Rev Biochem*. 2011;80:71-99. doi:10.1146/annurev-biochem-062209-093836

221. Shore GC, Papa FR, Oakes SA. Signaling cell death from the endoplasmic reticulum stress response. *Curr Opin Cell Biol*. 2011;23(2):143-149. doi:10.1016/j.ceb.2010.11.003

222. Urra H, Dufey E, Lisbona F, Rojas-Rivera D, Hetz C. When ER stress reaches a dead end. *Biochim Biophys Acta*. 2013;1833(12):3507-3517. doi:10.1016/j.bbamcr.2013.07.024

223. Chonghaile TN, Gupta S, John M, Szegezdi E, Logue SE, Samali A. BCL-2 modulates the unfolded protein response by enhancing splicing of X-box binding protein-1. *Biochem Biophys Res Commun*. 2015;466(1):40-45. doi:10.1016/j.bbrc.2015.08.100

224. Tsujimoto Y, Finger LR, Yunis J, Nowell PC, Croce CM. Cloning of the chromosome breakpoint of neoplastic B cells with the t(14;18) chromosome translocation. *Science*. 1984;226(4678):1097-1099. doi:10.1126/science.6093263

225. Oltvai ZN, Milliman CL, Korsmeyer SJ. Bcl-2 heterodimerizes in vivo with a conserved homolog, Bax, that accelerates programmed cell death. *Cell*. 1993;74(4):609-619. doi:10.1016/0092-8674(93)90509-o

226. Szegezdi E, Macdonald DC, Ní Chonghaile T, Gupta S, Samali A. Bcl-2 family on guard at the ER. *Am J Physiol Cell Physiol*. 2009;296(5):C941-C953. doi:10.1152/ajpcell.00612.2008

227. Youle RJ, Strasser A. The BCL-2 protein family: opposing activities that mediate cell death. *Nat Rev Mol Cell Biol*. 2008;9(1):47-59. doi:10.1038/nrm2308

228. Tait SW, Green DR. Mitochondria, and cell death: outer membrane permeabilization and beyond. *Nat Rev Mol Cell Biol*. 2010;11(9):621-632. doi:10.1038/nrm2952

229. Pihán P, Carreras-Sureda A, Hetz C. BCL-2 family: integrating stress responses at the ER to control cell demise. *Cell Death Differ*. 2017;24(9):1478-1487. doi:10.1038/cdd.2017.82

230. Kuter DJ, Bain B, Mufti G, Bagg A, Hasserjian RP. Bone marrow fibrosis: pathophysiology and clinical significance of increased bone marrow stromal fibres. *Br J Haematol*. 2007;139(3):351-362. doi:10.1111/j.1365-2141.2007.06807.x

231. Bonnans C, Chou J, Werb Z. Remodelling the extracellular matrix in development and disease. *Nat Rev Mol Cell Biol*. 2014;15(12):786-801. doi:10.1038/nrm3904

232. Kröger N, Zabelina T, Alchalby H, et al. Dynamic of bone marrow fibrosis regression predicts survival after allogeneic stem cell transplantation for myelofibrosis. *Biol Blood Marrow Transplant*. 2014;20(6):812-815. doi:10.1016/j.bbmt.2014.02.019

233. Lekovic D, Gotic M, Perunicic-Jovanovic M, et al. Contribution of comorbidities and grade of bone marrow fibrosis to the prognosis of survival in patients with primary myelofibrosis. *Med Oncol*. 2014;31(3):869. doi:10.1007/s12032-014-0869-8

234. Gleitz HFE, Pritchard JE, Kramann R, Schneider RK. Fibrosis driving myofibroblast precursors in MPN and new therapeutic pathways. *Hemasphere*. 2019;3(Suppl):142-145. Published 2019 Jun 30. doi:10.1097/HS9.0000000000000216

235. Zahr AA, Salama ME, Carreau N, et al. Bone marrow fibrosis in myelofibrosis: pathogenesis, prognosis, and targeted strategies. *Haematologica*. 2016;101(6):660-671. doi:10.3324/haematol.2015.141283

236. Agarwal A, Morrone K, Bartenstein M, Zhao ZJ, Verma A, Goel S. Bone marrow fibrosis in primary myelofibrosis: pathogenic mechanisms and the role of TGF-β. *Stem Cell Investig*. 2016;3:5. Published 2016 Feb 26. doi:10.3978/j.issn.2306-9759.2016.02.03

237. Wong WJ, Baltay M, Getz A, et al. Gene expression profiling distinguishes prefibrotic from overtly fibrotic myeloproliferative neoplasms and identifies disease subsets with distinct inflammatory signatures. *PLoS One*. 2019;14(5):e0216810. Published 2019 May 9. doi:10.1371/journal.pone.0216810

238. Vukotić M, Kapor S, Dragojević T, et al. Inhibition of proinflammatory signaling impairs fibrosis of bone marrow mesenchymal stromal cells in myeloproliferative neoplasms. *Exp Mol Med*. 2022;54(3):273-284. doi:10.1038/s12276-022-00742-y

239. Arber DA, Orazi A, Hasserjian RP, et al. International Consensus Classification of Myeloid Neoplasms and Acute Leukemias: integrating morphologic, clinical, and genomic data. *Blood*. 2022;140(11):1200-1228. doi:10.1182/blood.2022015850

240. Klampfl T, Gisslinger H, Harutyunyan AS, et al. Somatic mutations of calreticulin in myeloproliferative neoplasms. *N Engl J Med*. 2013;369(25):2379-2390. doi:10.1056/NEJMoa1311347

241. Moore PC, Qi JY, Thamsen M, et al. Parallel Signaling through IRE1α and PERK Regulates Pancreatic Neuroendocrine Tumor Growth and Survival. *Cancer Res*. 2019;79(24):6190-6203. doi:10.1158/0008-5472.CAN-19-1116

242. Campbell PJ, Green AR. The myeloproliferative disorders. N Engl J Med 2006;355:2452–66.

243. Levine RL, Gilliland DG. Myeloproliferative disorders. Blood 2008;112:2190–8.

244. Spivak JL. Myeloproliferative Neoplasms. N Engl J Med 2017;376(22):2168-2181.

245. Klampfl T, Gisslinger H, Harutyunyan AS, Nivarthi H, Rumi E, Milosevic JD, et al. Somatic mutations of calreticulin in myeloproliferative neoplasms. N Engl J Med 2013;369:2379–90.

246. Nangalia J, Massie CE, Baxter EJ, Nice FL, Gundem G, Wedge DC, et al. Somatic CALR mutations in myeloproliferative neoplasms with nonmutated JAK2. N Engl J Med 2013;369:2391–405.

247. Michalak M, Corbett EF, Mesaeli N, Nakamura K, Opas M. calreticulin: one protein, one gene, many functions. Biochem J 1999;344 Pt2:281–92.

248. Chachoua I, Pecquet C, El-Khoury M, Nivarthi H, Albu RI, Marty C, et al. Thrombopoietin receptor activation by myeloproliferative neoplasm associated calreticulin mutants. Blood 2016;127:1325–35.

249. Araki M, Yang Y, Masubuchi N, Hironaka Y, Takei H, Morishita S, et al. Activation of the thrombopoietin receptor by mutant calreticulin in CALR-mutant myeloproliferative neoplasms. Blood 2016;127:1307–16.

250. Elf S, Abdelfattah NS, Chen E, Perales-Patôn J, Rosen EA, Ko A et al. Mutant calreticulin requires both its mutant C-terminus and the thrombopoietin receptor for oncogenic transformation. Cancer Discov 2016;6(4):368-81.

251. Tefferi A, Wassie EA, Guglielmelli P, Gangat N, Belachew AA, Lasho TL et al. Type 1 versus Type 2 calreticulin mutations in essential thrombocythemia: a collaborative study of 1027 patients. Am J Hematol 2014;89(8):E121-4.

252. Pietra D, Rumi E, Ferretti VV, Di Buduo CA, Milanesi C, Cavalloni C et al. Differential clinical effects of different mutation subtypes in CALR-mutant myeloproliferative neoplasms. Leukemia 2016;30(2): 431–438.

253. Guglielmelli P, Biamonte F, Rotunno G, Artusi V, Artuso L, Bernardis I, et al. Impact of mutational status on outcomes in myelofibrosis patients treated with ruxolitinib in the COMFORT-II study. Blood 2014;123(14):2157–60.

254. Wang X, Ye F, Tripodi J, Hu CS, Qiu J, Najfeld V et al. JAK2 inhibitors do not affect stem cells present in the spleens of patients with myelofibrosis. Blood 2014;124(19):2987-95.
255. Deininger M, Radich J, Burn TC, Huber R, Paranagama D, Verstovsek S. The effect of long-term ruxolitinib treatment on JAK2p.V617F allele burden in patients with myelofibrosis. Blood 2015;126(13):1551–4.

256. Vannucchi AM, Kantarjian HM, Kiladjian JJ, Gotlib J, Cervantes F, Mesa RA, et al. A pooled analysis of overall survival in COMFORT-I and COMFORT-II, 2 randomized phase III trials of ruxolitinib for the treatment of myelofibrosis. Haematologica 2015;100(9):1139–45.

257. Verstovsek S, Mesa RA, Gotlib J, Levy RS, Gupta V, DiPersio JF, et al. Efficacy, safety, and survival with ruxolitinib in patients with myelofibrosis: results of a median 3-year follow-up of COMFORT-I. Haematologica 2015;100(4):479–88.

258. Harrison CN, Vannucchi AM, Kiladjian JJ, Al-Ali HK, Gisslinger H, Knoops L, et al. Long-term findings from COMFORT-II, a phase 3 study of ruxolitinib vs best available therapy for myelofibrosis. Leukemia 2016;30(8):1701–7.

259. Verstovsek S, Mesa RA, Gotlib J, Gupta V, DiPersio JF, Catalano JV, et al. Long-term treatment with ruxolitinib for patients with myelofibrosis: 5-year update from the randomized, double-blind, placebo-controlled, phase 3 COMFORT-I trial. J Hematol Oncol 2017;10(1):55.

260. Vainchenker W, Leroy E, Gilles L, Marty C, Plo I, Constantinescu SN. JAK inhibitors for the treatment of myeloproliferative neoplasms and other disorders. F1000Res. 2018;7:82.

261. Di Buduo CA, Abbonante V, Marty C, Moccia F, Rumi E, Pietra D et al. Defective interaction of mutant calreticulin and SOCE in megakaryocytes from patients with myeloproliferative neoplasms. Blood 2020;135(2):133-144.

262. Liou J, Kim ML, Heo WD, Jones JT, Myers JW, Ferrell JE et al. STIM is a Ca2+ sensor essential for Ca2+-store-depletion-triggered Ca2+ influx. Curr Biol. 2005;15(13):1235-1241.

263. Walter P, Ron D. The unfolded protein response: from stress pathway to homeostatic regulation. Science 2011;334(6059):1081-6.

264. Wang M, Kaufman RJ. The impact of the endoplasmic reticulum protein-folding environment on cancer development. Nat Rev Cancer 2014;14(9):581-97.

265. Chevet E, Hetz C, Samali A. Endoplasmic reticulum stress--activated cell reprogramming in oncogenesis. Cancer Discov 2015;5(6):586-97.

266. Salati S, Genovese E, Carretta C, Zini R, Bartalucci N, Prudente Z et al. calreticulin Ins5 and Del52 mutations impair unfolded protein and oxidative stress responses in K562 cells expressing CALR mutants. Sci Rep 2019;9,10558.

267. Nam AS, Kim KT, Chaligne R, Izzo F, Ang C, Taylor J, et al. Somatic mutations, and cell identity linked by Genotyping of Transcriptomes. Nature 2019 Jul;571(7765):355-360.

268. Pronier E, Cifani P, Merlinsky TR, Berman KB, Somasundara AVH, Rampal RK et al. Targeting the CALR interactome in myeloproliferative neoplasms. JCI Insight 2018;3(22):e122703.

269. Elf S, Abdelfattah NS, Baral AJ, Beeson D, Rivera JF, Ko A. Defining the requirements for the pathogenic interaction between mutant calreticulin and MPL in MPN. Blood 2018;131(7):782–786.

270. Cox JS, Walter P. A novel mechanism for regulating activity of a transcription factor that controls the unfolded protein response. Cell 1996;87:391–404.

271. Yoshida H, Matsui T, Yamamoto A, Okada T, Mori K. XBP1 mRNA is induced by ATF6 and spliced by IRE1 in response to ER stress to produce a highly active transcription factor. Cell 2001;107:881–891.

272. Ghosh R, Wang L, Wang ES, Perera BG, Igbaria A, Morita S et al. Allosteric inhibition of the IRE1α RNase preserves cell viability and function during endoplasmic reticulum stress. Cell. 2014;158(3):534-48.

273. Campbell KP, MacLennan DH, Jorgensen AO. Staining of the Ca2+-binding proteins, calsequestrin, calmodulin, troponin C, and S-100, with the cationic carbocyanine dye "Stains-all". J Biol Chem. 1983;258(18):11267-73.

274. Suzuki J, Kanemaru K, Ishii K, Ohkura M, Okubo Y, Masamisu I. Imaging intraorganellar Ca2+ at subcellular resolution using CEPIA. Nat Commun 2014;5, 4153.

275. Weber K, Bartsch U, Stocking C, Fehse B. A multicolor panel of novel lentiviral "gene ontology" (LeGO) vectors for functional gene analysis. Mol Ther 2008;16(4):698-706.

276. Baksh S, Michalak M. Expression of calreticulin in Escherichia coli and identification of its Ca2+ binding domains. J Biol Chem 1991;266:21458–21465.

277. Oakes SA, Papa FR. The role of endoplasmic reticulum stress in human pathology. Annu Rev Pathol 2015;10:173-194.

278. Zhu W, Cowie A, Wasfy GW, Penn LZ, Leber B, Andrews DW. Bcl-2 mutants with restricted subcellular location reveal spatially distinct pathways for apoptosis in different cell types. EMBO J 1996;15(16):4130-4141.

279. Distelhorst CW, McCormick TS. Bcl-2 acts subsequent to and independent of Ca2+ fluxes to inhibit apoptosis in thapsigargin- and glucocorticoid-treated mouse lymphoma cells. Cell Calcium 1996;19(6):473-83.

280. Foyouzi-Youssefi R, Arnaudeau S, Borner C, Kelley WL, Tschopp J, Lew DP et al. Bcl-2 decreases the free Ca2+ concentration within the endoplasmic reticulum. Proc Natl Acad Sci U S A. 2000;97(11):5723-5728.

281. Oakes SA, Opferman JT, Pozzan T, Korsmeyer SJ, Scorrano L. Regulation of endoplasmic reticulum Ca2+ dynamics by proapoptotic BCL-2 family members. Biochem Pharmacol 2003;66(8):1335-40.

282. Chonghaile TN, Gupta S, John M, Szegezdi E, Logue SE, Samali A. BCL-2 modulates the unfolded protein response by enhancing splicing of X-box binding protein-1. Biochem Biophys Res Commun 2015;466(1):40-5.

283. Mak DO, Foskett JK. Inositol 1,4,5-trisphosphate receptors in the endoplasmic reticulum: A single-channel point of view. Cell Calcium 2015;58(1):67-78.

284. Chen R, Valencia I, Zhong F, McColl KS, Roderick HL, Bootman MD et al. Bcl-2 functionally interacts with inositol 1,4,5-trisphosphate receptors to regulate calcium release from the ER in response to inositol 1,4,5-trisphosphate. J Cell Biol 2004;166: 193–203.

285. Peppiatt CM, Collins TJ, Mackenzie L, Conway SJ, Holmes AB, Bootman MD et al. 2-Aminoethoxydiphenyl borate (2-APB) antagonises inositol 1,4,5-trisphosphate-induced calcium release, inhibits calcium pumps and has a use-dependent and slowly reversible action on store-operated calcium entry channels. Cell Calcium 2003;34(1):97-108.

286. Thamsen M, Ghosh R, Auyeung VC, Brumwell A, Chapman HA, Backes BJ et al. Small molecule inhibition of IRE1α kinase/RNase has anti-fibrotic effects in the lung. PLoS One 2019;14(1):e0209824.

287. Marty C, Pecquet C, Nivarthi H, El-Khoury M, Chachoua I, Tulliez M et al. calreticulin mutants in mice induce an MPL-dependent thrombocytosis with frequent progression to myelofibrosis. Blood 2016;127(10):1317-24.

288. Afgan E, Baker D, Batut B, van den Beek M, Bouvier D, Cech M et al. The Galaxy platform for accessible, reproducible, and collaborative biomedical analyses: 2018 update. Nucleic Acids Res 2018;46(W1):W537-W544.

289. Krueger, F. "Trim galore." A wrapper tool around Cutadapt and FastQC to consistently apply quality and adapter trimming to FastQ files 516 (2015): 517.

290. Dobin A, Davis CA, Schlesinger F, Drenkow J, Zaleski C, Jha S et al. STAR: ultrafast universal RNA-seq aligner. Bioinformatics 2013;29(1):15-21.

291. Liao Y, Smyth GK, Shi W. featureCounts: an efficient general purpose program for assigning sequence reads to genomic features. Bioinformatics 2014;30(7):923-30.

292. Love MI, Huber W, Anders S. Moderated estimation of fold change and dispersion for RNA-seq data with DESeq2. Genome Biol 2014;15(12):550.

293. Subramanian A, Tamayo P, Mootha VK, Mukherjee S, Ebert BL, Gillette MA et al. Gene set enrichment analysis: a knowledge-based approach for interpreting genome-wide expression profiles. Proc Natl Acad Sci U S A 2005;102(43):15545-50.

294. Ibarra J, Elbanna YA, Kurylowicz K, et al. Type I but Not Type II calreticulin Mutations Activate the IRE1α/XBP1 Pathway of the Unfolded Protein Response to Drive Myeloproliferative Neoplasms. *Blood Cancer Discov.* 2022 Jul 6;3(4):298-315. doi: 10.1158/2643-3230.BCD-21-0144. PMID: 35405004; PMCID: PMC9338758.

295. Austin RJ, Straube J, Bruedigam C, et al. Distinct effects of ruxolitinib and interferon-alpha on murine JAK2V617F myeloproliferative neoplasm hematopoietic stem cell populations. *Leukemia*. 2020;34(4):1075-1089. doi:10.1038/s41375-019-0638-y

296. Gleitz HFE, Benabid A, Schneider RK. Still a burning question: the interplay between inflammation and fibrosis in myeloproliferative neoplasms. *Curr Opin Hematol*. 2021;28(5):364-371. doi:10.1097/MOH.0000000000000669

297. Zahr AA, Salama ME, Carreau N, et al. Bone marrow fibrosis in myelofibrosis: pathogenesis, prognosis, and targeted strategies. *Haematologica*. 2016;101(6):660-671. doi:10.3324/haematol.2015.141283

298. Decker M, Martinez-Morentin L, Wang G, et al. Leptin-receptor-expressing bone marrow stromal cells are myofibroblasts in primary myelofibrosis. *Nat Cell Biol*. 2017;19(6):677-688. doi:10.1038/ncb3530

299. Schneider RK, Mullally A, Dugourd A, et al. Gli1^{+} Mesenchymal Stromal Cells Are a Key Driver of Bone Marrow Fibrosis and an Important Cellular Therapeutic Target [published correction appears in Cell Stem Cell. 2018 Aug 2;23(2):308-309]. *Cell Stem Cell*. 2017;20(6):785-800.e8. doi:10.1016/j.stem.2017.03.008

300. Leimkühler NB, Gleitz HFE, Ronghui L, et al. Heterogeneous bone-marrow stromal progenitors drive myelofibrosis via a druggable alarmin axis. *Cell Stem Cell*. 2021;28(4):637-652.e8. doi:10.1016/j.stem.2020.11.004

301. La Spina E, Giallongo S, Giallongo C, et al. Mesenchymal stromal cells in tumor microenvironment remodeling of BCR-ABL negative myeloproliferative diseases. *Front Oncol*. 2023;13:1141610. Published 2023 Feb 23. doi:10.3389/fonc.2023.1141610

302. Chatain N, Koschmieder S, Jost E. Role of Inflammatory Factors during Disease Pathogenesis and Stem Cell Transplantation in Myeloproliferative Neoplasms. *Cancers (Basel)*. 2020;12(8):2250. Published 2020 Aug 12. doi:10.3390/cancers12082250